EVALUATION OF MECHANICAL BEHAVIOUR OF FRICTION WELDED BIMETALLIC WELDS

A thesis submitted in partial fulfilment of the requirement for the award of degree

MASTER OF ENGINEERING
IN
PRODUCTION & INDUSTRIAL

Submitted By:
Yogesh Kumar Singla
Roll No. 800882012

Under the Guidance of

Dr. Rahul Chhibber
Assistant Professor,
Deptt. Of Mechanical Engg.
Thapar University,
Patiala-147004

Dr. Bijan Kumar Dutta
Distinguish Scientist
Head,
Computational Mech. Section
Sr. Professor, HBNI
Reactor Safety Division,
BARC, Mumbai-400085

DEPARTMENT OF MECHANICAL ENGINEERING
THAPAR UNIVERSITY
PATIALA-147004, INDIA

CERTIFICATE

This is to certify that the thesis titled, **"Evaluation of Mechanical Behaviour of Friction Welded Bimetallic Welds"**, being submitted by **Mr. Yogesh Kumar Singla**, in partial fulfilment of the requirement for the award of degree of **MASTER OF ENGINEERING (PRODUCTION & INDUSTRIAL) at THAPAR UNIVERSITY, PATIALA** is a bonafied work carried out by his under our guidance and supervision and no part of this thesis has been submitted for the award of any other degree.

Dr. Rahul Chhibber
Assistant Professor,
Deptt. Of Mechanical Engg.
Thapar University,
Patiala – 147004

Dr. Bijan Kumar Dutta
Distinguish Scientist,
Head,
Computational Mech. Section
Sr. Professor, HBNI
Reactor Safety Division
BARC, Mumbai – 400085

Dr. S.K. Mohapatra
Professor & Head,
Thapar University,
Patiala – 147004

Dr. R.K. Sharma
Dean, Academic Affairs
Thapar University,
Patiala – 147004

ACKNOWLEDGEMENT

I am highly grateful to the authorities of Thapar University, Patiala for providing this opportunity to carry out the Thesis work.

I would like to express a deep sense of gratitude and thank profusely to my thesis guide **Dr. Rahul Chhibber** & **Dr. Bijan Kumar Dutta** for their sincere & invaluable guidance, suggestions and attitude which inspired me to submit seminar report in the present form.

I am highly thankful to non teaching staff, Mr. Rajinder Kumar, Mr. Narender, Mr. Pardeep Kumar Singla, Mr. Surinder, Mr. Mohinder Suri, Mr. R.K Banerjee (attendant), Mr. Deshraj, Mr. A S Cheema, Mr. Purshotam and all the workshop staff who helped me in various aspects of my research.

I would also like to offer my sincere thanks to Dr. I P S Ahuja, H.O.D. (Mechanical), Punjabi University, Patiala and Mr. Tarun Nanda, Asstt. Prof., MED, TU, Patiala.

I am also highly thankful to my friends Aman Abrol, Rupesh Kaushik, Laxmi Shankar, Arminder Walia, Charanjit Singh, Ravinderpal Singh, Harvinder Singh, Harkamal Singh, Ashish Gupta, Harpreet Singh, Sukhbir Singh and all the members of team fateh.

I am also thankful to other faculty members of Mechanical Department, TU, Patiala for their intellectual support. My special thanks are due to my family members and friends who constantly encouraged me to complete this study.

Yogesh Kumar Singla

ABSTRACT

Friction welding is a solid state joining process that uses rotational motion and high axial pressure to convert rotational energy into frictional heat at a circular interface.

For this purpose a friction welding setup was designed. Vertical Milling Machine was used for friction welding. The materials used were Mild Steel and Stainless Steel - 304. The Piezoelectric Dynamometer was used to plot the graphs of forces & Pressure Gauge was used to control the friction force & forge force. Thermocouple & Digital thermometer were used to note down the temperature produced during friction welding. A Dial indicator was used to control the burn off length.

Four parameters were varied Friction force, Forge force, RPM & Burn off length at two different levels. Fixed parameters were length and diameter of the specimen. Total number of experiments conducted was sixteen. For each experiment four specimens were made.

After friction welding Macroscopic behaviour (Tensile Strength, Temperature produced during friction welding & Composition change) & Microscopic behaviour (Microstructure, Micro hardness, SEM & XRD) of the welded region was analyzed.

An attempt to relate the Microscopic and Macroscopic behaviour with the friction welding parameters was made in this work.

TABLE OF CONTENTS

LIST OF FIGURES

LIST OF TABLES

CHAPTER 1 INTRODUCTION

1.1 FRICTION WELDING

Friction welding is a solid state joining process that uses rotational motion and high axial pressure to convert rotational energy into frictional heat at a circular interface. The basic principle of friction welding is that one of the components being welded is rotated while the other is kept stationary. The two components are then brought together by an axially applied force. Rubbing the two surfaces together produces sufficient heat that local plastic zones are formed and axially applied force causes the plasticized metal to be extruded from the joint, carrying with it any contaminants, oxides etc. Thus two automatically clean surfaces are brought together under pressure and an intermettalic bond is formed. The heat generated is confined to the interface, heat input is low and the hot work applied to the weld area results in a grain refinement. This rapidly, easily controlled and easily mechanized process has been used extensively in the automotive industry for items such as differential casings, half shafts and bi-metallic valves.

One important characteristic of friction welding is its ability to weld alloys and combination of alloys previously regarded as unweldable. It is possible to make dissimilar metal joints, joining steel, copper and aluminium to themselves and to each other and to successfully weld alloys such as the 2.5% copper-Al 2618 and the Al Zn Mg Cu alloy 7075 without hot cracking. The primary reason for this is that no melting takes place and thus no brittle intermetallic phases are formed. [1, 2, 3, 9]

Initially parts are loaded by the welder: one is placed in a rotating spindle and the other is positioned in a stationary clamp. The process can be described best in the three stages as follows:

STAGE 1: Component in the spindle is brought up to pre-determined rotational speed and then a pre-determined axial force is applied. (Figure 1.1)

STAGE 2: These conditions are maintained for a pre-determined amount of time until desired temperatures and material conditions exist. (Figure 1.2)

STAGE 3: Rotational speed is then stopped and axial force is applied until desired upset is obtained. Then the components are unloaded and the cycle is repeated. (Figure 1.3)

Figure 1.1 Stage: 1[3]

Figure 1.2 Stage: 2[3]

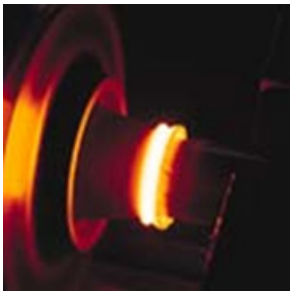

Figure 1.3 Stage: 3[3]

For more understanding:

- One component rotated rapidly, the other is stationary. (Figure 1.4)

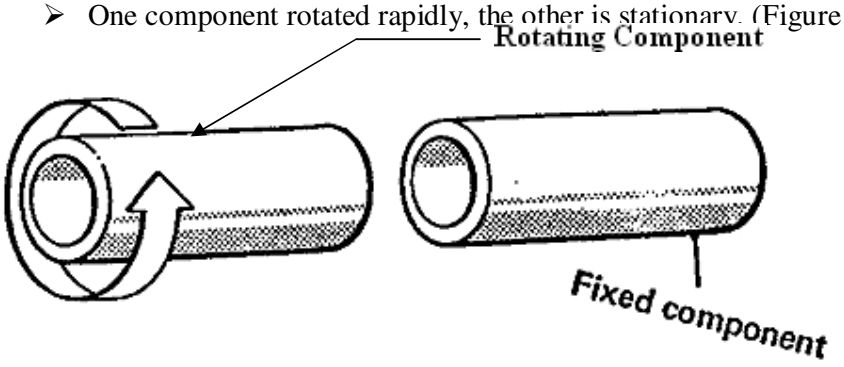

Figure 1.4 Showing rotating & fixed component [7]

- Rotating and stationary components brought together into contact and force applied. (Figure 1.5)

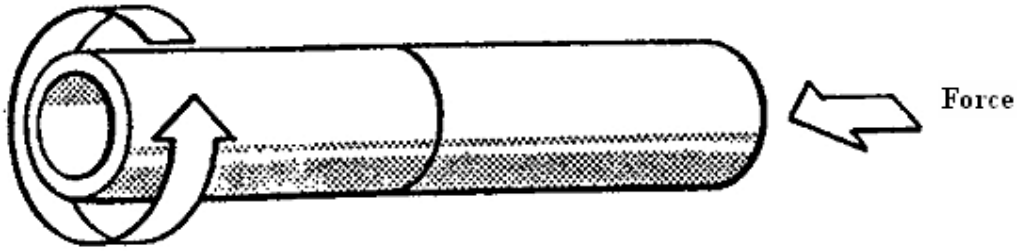

Figure 1.5 Both the components are in same axis [7]

- Axial force is increased to bring components into a plastic state at interface. (Figure-1.6)

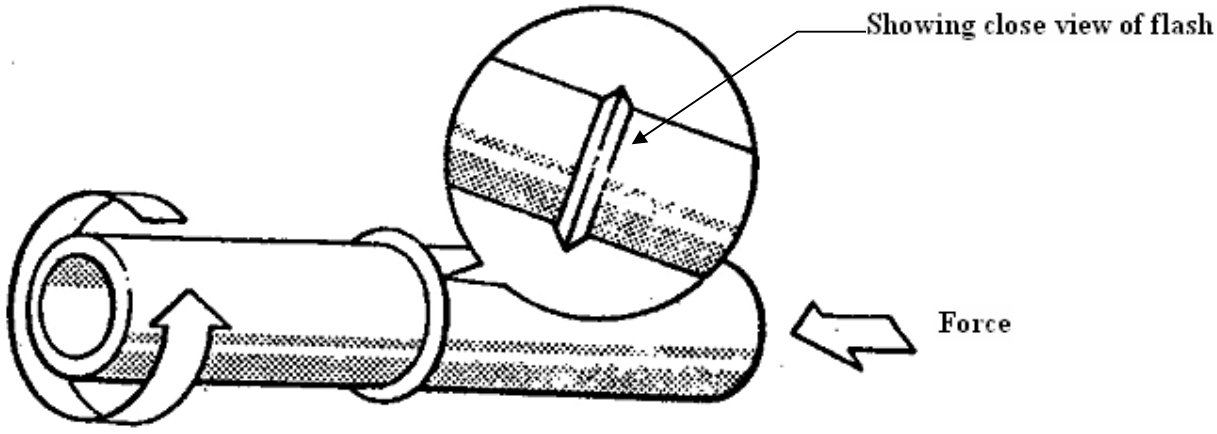

Figure 1.6 Flash formed by increasing force [7]

- Rotation is stopped and more axial force is applied known as forge force. (Figure-1.7)

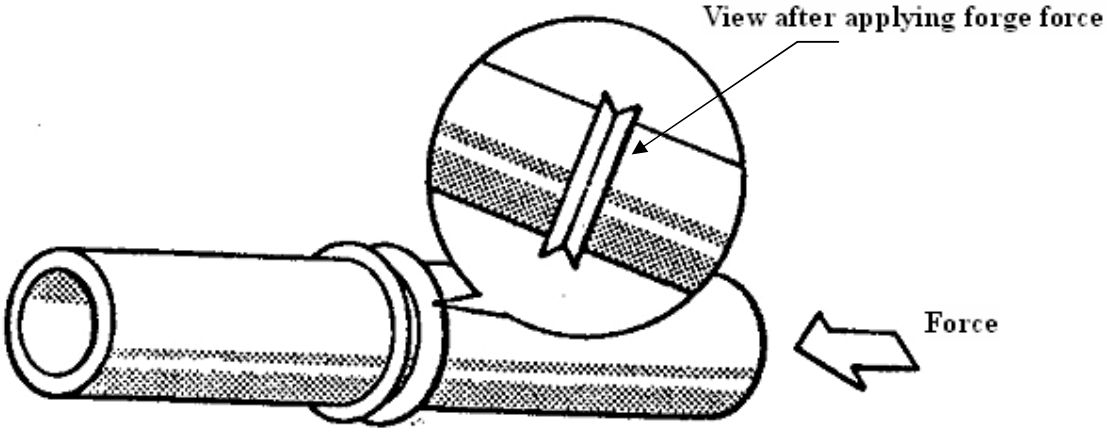

Figure 1.7 components after welding [7]

- Result - A full cross sectional weld in the parent material after machining operations. (Figure-1.8)

Figure 1.8 Single piece rod after machining operations [7]

1.2 PHASES OF FRICTION WELDING

The following are the main phases of friction welding.

1.2.1 FIRST FRICTION PHASE: The spindle begins to rotate and the parts are pressed in contact with each other with a force generally in range of 20.68-41.36 N/mm^2 of weld area. Typically pre-heating of the weld interface occurs with no material displacement at this point. Friction duration is controlled by time. The purpose of the first friction phase is to burn off any light oils or light oxides at the weld interface.

1.2.2 SECOND FRICTION PHASE: This phase controls the amount of material length loss. Approximately 2/3 of total material displacement occurs. Welding force of 41.36-82.73 N/mm^2 of weld area is applied generally. The three methods of controlling the amount of material length loss in this friction phase are *Time, Constant Distance* and *Position.*

With the Time method of controlling length loss, a simple timer is used to count the number of seconds when friction pressure is applied. When the pre-set time is achieved the machine rotation is stopped.

1.2.3 FORGE PHASE: The final phase in friction welding is the forge phase. The spindle is forced to a stop and both components are pressed against each other at extreme pressure and allowed to cool. Typically, approximately 1/3 of total material displacement occurs during this phase. There is no control as to how much material is displaced in the forge phase but it is dependent on the amount of heat generated in the Second Phase and the amount of pressure applied. Forge phase duration is controlled by time (typically only 5 to 15 seconds) and a forging force of 82.73-165.47 N/mm^2 of weld area is applied generally. [4]

1.3 TYPES / METHODS OF FRICTION WELDING

The following are the different methods or types of friction welding.

1.3.1 CONVENTIONAL / CONTINUOUS DRIVE FRICTION WELDING: This is the original method of friction welding. In this process mechanical energy is converted to heat energy by rotating one work piece while pressing it against a stationary work piece. After a specific period of time rotation is suddenly stopped and the pressure is increased and held for another specified time producing a weld. This method of welding is also referred to as the continuous drive friction welding. In conventional friction welding the variables to be controlled are:

- RPM
- Friction force
- Friction time or the burn off length
- Forge force

1.3.2 INERTIA / SPIN / ROTATIONAL WELDING: This system consists of two chucks for holding the materials to be welded, one of which is fixed and the other rotating. Before welding one of the work pieces is attached to the rotating chuck along with a flywheel of a given weight. The piece is then spun up to a high rate of rotation to store the required energy in the flywheel. Once spinning at the proper speed, the motor is removed and the pieces forced together under pressure. The force is kept on the pieces after the spinning stops to allow the weld to set. Three interrelated parameters control the character of the weld. These are:

- Initial sliding velocity at the faying surface
- Moment of the inertia of the flywheel
- Axial thrust force at the welding interface

All these depend upon the combination of materials and the configuration of the weld.

1.3.3 ORBITAL FRICTION WELDING: This method overcomes some of the major limitations of the other friction welding techniques viz; its application to circular

or nearly circular components, difficulty in attaining angular alignment and non uniform pattern of heat generation over the interface.

Here, one component is stationary and the other moves in a circular path with an orbit radius 'e' without rotating about its own axis. The two components are pressed together and when sufficient heat has been generated all that is done is to reduce the orbit radius 'e' to zero, i.e. to centre the moving component against the stationary one to achieve per feet alignment.

In practice such an orbital motion would result in very high centrifugal force at the work holder. A simple operating principle to achieve relative orbital motion involves rotating both the components in the same direction with their axes offset. Heating is affected by applying an axial friction force. When sufficient heat has been generated, the axes are realigned and a force is applied to the still rotating component.

1.3.4 LINEAR VIBRATION WELDING: In Linear vibration welding the materials are placed in contact and put under pressure. An external vibration force is then applied to slip the pieces relative to each other, perpendicular to the pressure being applied. The parts are vibrated through a relatively small displacement known as the amplitude, typically between 1.0 and 1.8 mm, for a frequency of vibration of 200 Hz (high frequency), or 2–4 mm at 100 Hz (low frequency), in the plane of the joint. In this way the temperature of parts rises due to relative motion. When the temperature of layers rises to the required degree, the vibration is stopped and axial pressure is increased. This technique is widely used in the automotive industry, among others. A minor modification is ANGULAR FRICTION WELDING, which vibrates the material by torquing them through a small angle.

1.4 MACHINE PARAMETERS

The controlled variables also called machine parameters in friction welding are the speed of rotation, the axial force and the amount of axial shortening or burn off length or weld time.

1.4.1 FRICTION / ROTATION / PERIPHERAL SPEED: The most widely used speed cycle is one where a constant speed is maintained during the friction heating phase followed by rapid heating. The rotation speed is often specified in terms of sliding speed at two third of the radius at the faying surface. In the welding of solid specimen, although the speed of rotation is kept constant, the rubbing speed across the interface varies linearly from zero at the centre to a maximum value at the outer radius.

It is an important parameter in determining the maximum interface temperature and hence the final joint metallurgy. High speeds produce overheated structures whereas low speeds can produce insufficient heating.

1.4.2 FRICTION PRESSURE / FRICTION FORCE: The friction pressure in conjunction with the peripheral speed determines the thermal conditions established in the weld region, and the rate at which metal is extruded radially to form an upset. For most materials, there is wide range of combinations of speed and pressure that may be used to give excellent mechanical and metallurgical integrity in the weld.

Low value of friction force results proportionately low unit thermal energy liberation, greater wet dissipation and consequently an increased width of heat affected zone (HAZ), where as if very high friction force is employed, the softer metal at the interface would be squeezed out leaving relatively cooler metal at the interface which again would be detrimental for weld formation and will result in lowering of strength of weld.

The axial force is normally set to a desired value before the test is carried out. However the axial force does not remain constant but varies with time.

1.4.3 BURN OFF LENGTH: Burn off length is the overall length loss of the components during the application of friction force & forge force.

The duration of the heating (Burn off) is selected so as to ensure that the faying surfaces are cleaned by friction and the weld zone temperature is raised to achieve the required plasticity for solid state pressure welding.

1.4.4 FORGE PRESSURE / FORGE FORCE: This is the longitudinal force applied to the faying surfaces at the time when relative movement between the components is ceasing and/or has ceased. This is usually higher than the friction force. [5]

1.5 MATERIALS WELDED BY FRICTION WELDING

Friction welding have the advantage of joining similar metal and bi-metallic combinations not normally considered bondable (or "incompatible"), such as aluminium to steel, copper to aluminium, titanium to copper, titanium to stainless and nickel alloys to steel. As a general rule, all metallic engineered materials which are forgeable can be friction welded, including automotive valve alloys, tool steel, alloy steels, and tantalum. Many castings, powder metals (PM), and metal matrix composites are weld able. Bi-metallic designs allow engineers to use expensive material only where needed. Forgings and castings can be replaced with less expensive forgings or castings. They can be welded to bar stocks, tubes, plates and endless applications. [5, 6, 8]

Materials that can be friction welded are listed below:

- Aluminium and its alloys
- Nickel alloys
- Brass and Bronze
- Alloy steels
- Magnesium alloys
- Carbon steel
- Stainless steel
- Tantalum
- Titanium alloys
- Tungsten
- Zirconium alloys
- Alloy steel to Carbon steel
- Copper to Carbon steel
- Super alloys to Carbon steel
- Stainless steel to Carbon steel
- Sintered steel to Carbon steel
- Aluminium to Stainless steel
- Copper to aluminium

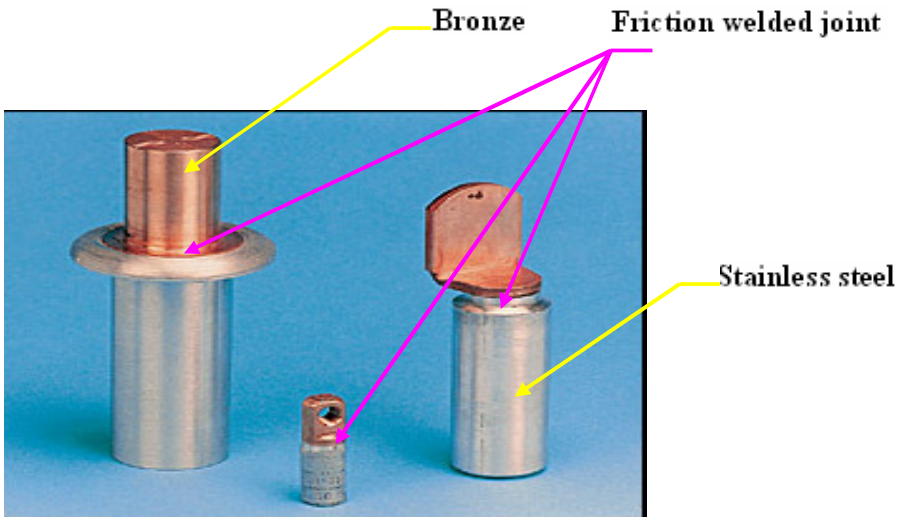

Figure 1.9 Friction welding of Bronze & Stainless steel [6]

1.5.1 MATERIAL COMBINATIONS FOR FRICTION WELDING: Many different materials can be welded by using friction welding. It is clear from the figure 1.10 given below.

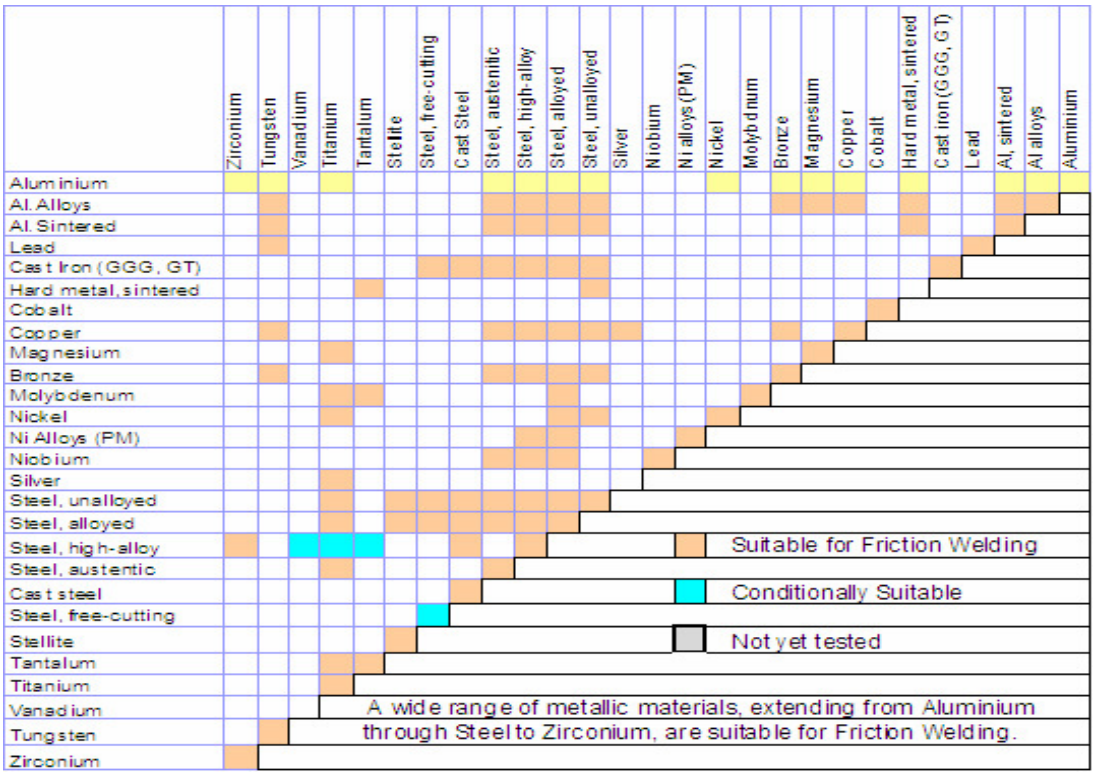

Figure 1.10 Showing the combination of materials that can be friction welded [9]

1.5.2 DESTRUCTIVE QUALITY CONTROL EXAMINATIONS: The following are the Destructive quality control examinations commonly used for friction weldments.

- Bending
- Tension
- Impact
- Fatigue
- Hardness
- Torsion
- Shear

1.5.3 NON-DESTRUCTIVE QUALITY CONTROL EXAMINATIONS: Non-destructive quality control examinations commonly used for friction welding includes the following:

- Ultrasonic flaw detection

- Dye Penetrant
- Leak test
- Visual inspection
- Surface etch
- Pressure test

1.6 APPLICATIONS OF FRICTION WELDING

Friction welders are versatile enough to join a wide range of part shapes, materials, and weld sizes. Friction welded applications typically include aircraft and aerospace components, cutting tools, agricultural machinery, automotive parts, oil field pieces, waste canisters, military equipment, spindle blanks and bimetallic materials. Production of bimetallic shafts, steering shafts and worm gears, control shafts, axle shafts, engine valves, transmission shafts etc., for automobile industry, joining of super alloy turbine wheels to steels shafts, joining of thin walled containers to bases etc. Production of cutting tools like drills, taps, reamers and some of the shanked milling cutters where HSS cutting body can weld to carbon steel shanks. Production of pump shafts and control valve shafts, involving joints between plain carbon and corrosion resistant alloy steel (Oil and Gas Industries). Joining together dissimilar steel in the manufacture of bimetal fasteners that are used to support insulation covers for use in nuclear plant construction. [3, 6, 8]

1.6.1 FRICTION WELDING OF BI-METALLIC MATERIALS: Friction welding with dissimilar materials produces the same strength properties as parent materials and allows you to maximize and conserve your material expenditures where needed most.

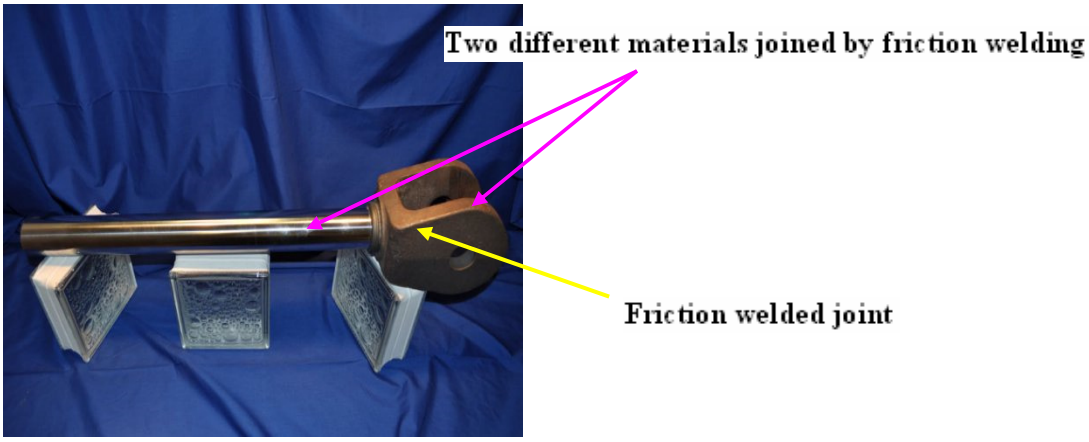

Figure 1.11 Hydraulic shaft is welded by using two different materials [8]

A hydraulic actuator shaft for the Forestry Industry is friction welded. This bimetal weld joins a large, odd shape casting to a long, finished chrome shaft.

1.6.2 MULTIPLE COMPONENTS FRICTION WELDING: Friction welding is not limited to two material types or sizes. Multiple materials and sizes are used for reduction in tooling costs and optimizing near final size.

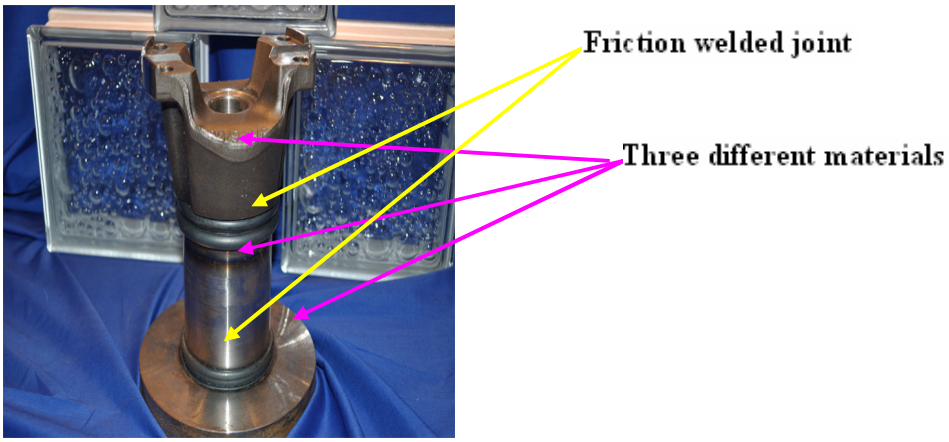

Figure 1.12 Three different materials joined by friction welding [8]

This part is used in the Agricultural Equipment Industry. This forged yoke is a semi-finished machined part, friction welded to a tube and then to a disc. The odd shape required special tooling for quality and to prevent flaws on semi-finished part. This is a multiple friction weld with bi-metal material.

1.6.3 THIN WALLED FRICTION WELDING: Applying friction welding techniques to thin wall materials provide higher strength properties and increased life over conventional joining processes.

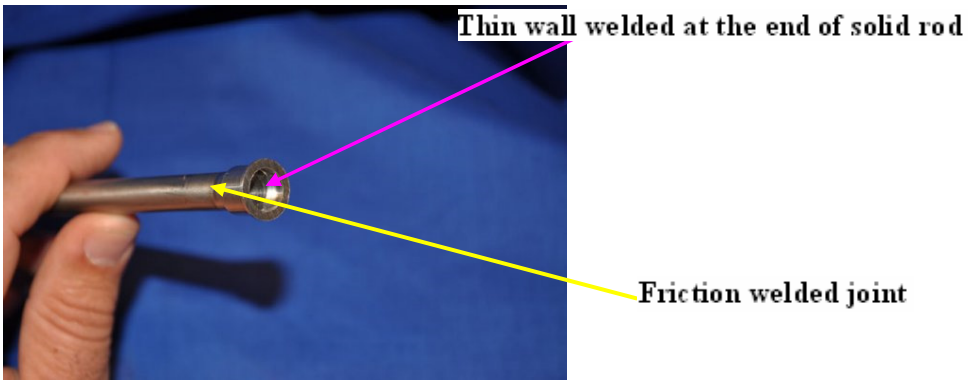

Figure 1.13 Friction welding of thin wall at the end of solid rod [8]

Used in the Recreational Industry, this thin wall, fuel line tube was friction welded to a solid end of similar material. CNC machining was performed to complete the part to print specification.

Following are some more examples of different parts joined by friction welding:

- Bimetal outboard motor shaft
- Brake 'S' cam
- Cluster gear
- Drive axle shaft
- Tubular photo coupler roll
- Gear hub
- Vice lead screw
- Conveyor roller
- Lathe spindle blank
- Sprocket hub
- Track roller
- Shift lever

1.7 ADVANTAGES OF FRICTION WELDING

The following are the advantages of friction welding:

1. Friction welding techniques are generally melt-free, which offers the advantage of avoiding grain growth in materials such as high-strength heat-treated steels.
2. Dissimilar materials normally not compatible for welding can be friction welded. This is particularly useful in the aerospace field, where it is used to join lightweight aluminum stock to high-strength steels.
3. Friction welding provides a "full strength" bond with no additional weight.
4. Bi-metallic friction welding is commonly used in Nuclear Industry, where copper-steel joints are common in the reactor cooling systems.
5. The elimination of tube machining, gas and consumable costs, combined with the higher production rates of friction welding, easily offset the high hourly cost of this process.
6. Suitable for quantities ranging from prototype to high production.

7. Environmental friendly process - no fumes, gases, or smoke generated.
8. Solid state process - no possibility of porosity or slag inclusions.
9. Reduces machining labour, thereby reducing perishable tooling costs while increasing capacity.
10. Simplicity of operation.
11. Low power requirements.
12. As compared to conventional flash or resistance butt welding, friction welding produces improved welds at higher speed and lower cost, less electric current is required, and costly copper fixtures to hold components are eliminated.
13. There is no flux, gas, filler metal present to cause imperfections in welds.
14. The Friction Welding process is at least twice - and up to 100 times - as fast as other welding techniques.
15. The machine controlled process eliminates human error, and weld quality is independent of operator skill or attitude.
16. Process parameters easily monitored.
17. Weld complex shapes or circular shapes at all stages of components: finished, semi-finished, and raw stock.
18. Surface impurities burn during friction welding process.
19. Reduced HAZ (heat affected zone). [1, 2, 3, 5, 6, 7, 8, 9]

1.8 DISADVANTAGES OF FRICTION WELDING

The following are the disadvantages of friction welding.

1) The use of this process is restricted to flat and angular butt welds, where one part is normal to the other part.
2) So far the process has been applied only to the joining of small pieces in the form of bar stock.
3) Sometimes, quite a heavy flash is forced out in friction welds.
4) If tubing is welded, flash may have to be removed from inside the joint.
5) Flash from medium and high carbon steels being hard, must either be removed while it is hot or annealed before it is machined.
6) Thrust pressures in inertia welding will range from 700 to 2800 kg/cm^2, which require a heavy rigid machine. [2, 5]

CHAPTER 2 LITERATURE REVIEW

1) A. A. Essa, A. S. Bahrani [1991]

Methods of solid phase bonding of metals to ceramics are reviewed with particular emphasis on friction welding. The results of experiments on the direct friction welding of an aluminium alloy to 94% alumina are reported in this study by A. A. Essa et. al. High strength bonds between the aluminium alloy and the alumina were achieved but there were problems with the cracking of the alumina. It was not possible to friction weld mild steel to alumina and copper to alumina. A mechanism was proposed for the friction welding of metals to ceramics.

2) Ahmet Hascalik, Nuri Orhan [2005]

The aim of this study was to investigate the feasibility of joining Al_2O_3 reinforced Al alloy composite to SAE 1020 steel by rotational friction welding. The aluminium based MMC material containing 5, 10 and 15 vol% Al_2O_3 particles with average particle sizes of 30 and 60 micro m was produced by powder metallurgy technique. The integrity of the joints has been investigated by optical and SEM, while the mechanical properties assessment included micro hardness and shear test. Results indicated that Al/ Al_2O_3 composite could be joined to SAE 1020 steel by friction welding. However, it was pointed out that the quality of the joint was affected negatively with the increase in particle size and volume % of the oxide particles in the MMC.

3) Ahmet Z. Sahin, Bekir S. Yibaş, M. Ahmed, J. Nickel [1997]

In this study by Ahmet Z. Sahin et. al. the heat-transfer mechanism initiating the friction welding process was examined and a transient two-dimensional heat conduction model for the welding of two dissimilar cylindrical metal bars was introduced. The bar materials consist of copper and steel. To relate the theoretical predictions with the resulting welds, experiments are conducted under different welding conditions by means of which metallurgical and microprobe analysis of the weld cross-sections was carried out. This provides visualization of the melted zones and of the diffusion depths. A statistical analysis was carried out for the affecting parameters on the mechanical properties of the resulting welds. The factors affecting the weld include the speed of rotation, the weld duration (burn-off time), and the friction load, while the mechanical properties include the tensile strength, the yield strength, the ultimate yield strength and the micro hardness of the weld cross-sections.

4) Antonio A. M. da Silva , Axel Meyer, Jorge F. dos Santos, Carlos Eduardo Fortis Kwietniewski and Telmo R. Strohaecker [2004]

The aim of this paper was to investigate the feasibility of joining particle-reinforced composites by rotational friction welding. The integrity of the joints has been investigated by optical and electron microscopy, while the mechanical properties assessment included micro hardness and tensile tests. The mechanical properties

assessment has indicated no detrimental effect of the joining process on the tensile properties. Titanium matrix composite (TMC) has been used. Titanium matrix composite (TMC) has demonstrated a high strength-to-weight ratio as well as good properties at high temperature. The successful application of TMC depends on a suitable joining technique. Rotational friction welding seems to be an ideal choice because it is a solid state joining process (TMCs have shown to be sensitive to fusion welding processes) achieving good mechanical properties.

5) A. Vairis, M. Frost [1998]

A. Vairis presented a new hysteresis free linear friction welding machine is described, capable of welding at variable frequencies and amplitudes of oscillation with adjustable friction and forging pressures. Experiments were performed with Ti 6AI 4V up to a frequency of 119 Hz and for two amplitudes of oscillation (3 and 0.92mm). The minimum power input required to achieve welding conditions is shown to depend on both frequency and amplitude of oscillation. Weld impact strength is shown to depend on the friction pressure applied for the large amplitude case. Also, it is shown that forging at the end of the process can help to improve weak welds in situations where the energy input is just below the minimum required to achieve optimum welding conditions.

6) D. Ananthapadmanaban, V. Seshagiri Rao, Nikhil Abraham and K. Prasad Rao [2009]

The aim of this work was to study mechanical property variation under different friction welding conditions for mild steel stainless steel joints by D. Ananthapadmanabam et. al. Yield strength, ultimate tensile strength, percentage elongation of the welded joints and hardness variations across the weld interface has been reported. The integrity of the joints has been investigated using optical microscopy and scanning electron microscopy.

7) Emel Taban, Jerry E. Gould, John C. lippold [2009]

Joining of dissimilar materials is of increasing interest for a wide range of industrial applications. The automotive industry, in particular, views dissimilar materials joining as a gateway for the implementation of light weight materials. Specifically, the introduction of aluminum alloy parts into a steel car body requires the development of reliable, efficient and economic joining processes. Since aluminum and steel demonstrate different physical, mechanical and metallurgical properties, identification of proper welding processes and practices can be problematic. In this work, inertia friction welding has been used to create joints between a 6061-T6 aluminum alloy and a AISI 1018 steel using various parameters. The joints were evaluated by mechanical testing and metallurgical analysis. Micro structural analyses was done using metallography, micro hardness testing, scanning electron microscopy (SEM), energy dispersive spectroscopy (EDS), X-ray elemental mapping, focused ion beam (FIB) with ultra high resolution SEM and transmission electron microscopy (TEM) in TEM and STEM modes. Results of these analysis suggested that joint strengths on the order of 250 MPa could be achieved. In addition, failures were seen in the plasticized layer on the aluminum side of the joint. Further, bond lines were

characterized by a thin layer of formed Al–Fe intermetallic. This intermetallic layer averaged roughly 250 nm thick and compositionally appears related to the Fe Al and Fe_2Al_5 phases.

8) F. Rotundo, L. Ceschini, A. Morri, T. S. Jun, A. M. Korsunsky [2010]

The aim of this study is to evaluate the possibility of using the linear friction welding (LFW) technique to produce sound joints on a 2124Al/25 vol.% SiC_p composite. The MMC joints were subjected to micro structural and mechanical characterization, including hardness, tensile and fatigue tests, without any post-weld heat treatment. The micro structural analyses showed substantially defect-free joints, with a uniform particle distribution in the central zone and a relevant plastic flow of the aluminium matrix alloy. The hardness decrease in the welded zone was approximately 10% in respect to the base material. The joint efficiency was higher than 80%, both in respect to the ultimate tensile strength and fatigue strength at 10^7 cycles. S-N probability curves were calculated using the maximum likelihood method. Generally the fracture occurred in the Thermo-Mechanically Affected Zone (TMAZ), with a relevant reduction in the elongation to failure.

9) Hakan Ates, Mehmet Turker and Adem Kurt [2007]

In this paper the Effect of friction pressure on the properties of friction hot rolled MA956 iron-based super alloy plate, produced by mechanical alloying, has been investigated. Joining processes were carried out by various friction welding parameters. Tensile strengths and hardness values of the weld interface were determined and the microstructure features of these samples were investigated. Optimum friction pressure for this material was determined.

10) Hazman Seli, Ahmad Izani Md. Ismail, Endri Rachman, Zainal Arifin Ahmad [2010]

In friction welding of two dissimilar materials, two rods are welded together by holding one of them still while rotating the other under the influence of an axial load which creates frictional heat in the interface. In this study, mechanical properties of mild steel and aluminium welded rods were evaluated to understand the thermal effects, and an explicit one-dimensional finite difference method was used to approximate the heating and cooling temperature distribution of the joint. The thermal effects of the friction welding were observed to have lowered the welded materials hardness compared to the parent materials. The tensile strength of the welded rods is lower than the parent rods due to incomplete welding. The preliminary predictions were compared to actual thermocouple data from welds conducted under identical conditions and were shown to be in fair agreement. The finite difference method proposed in this work will provide guidance in weld parameter development and will allow better understanding of the friction welding process.

11) H.C. Dey, M. Ashfaq, A.K. Bhaduri and K. Prasad Rao [2009]

This paper gives the details of mechanical tests, microstructure analysis using optical and scanning electron microscopy. The dissimilar metal joint of titanium (Ti) to 304L stainless steel (SS) is essential in the nuclear industry for the dissolution of spent fuel that is carried out in boiling nitric acid in the dissolver vessel (made of Ti) and the dissolved solution is transported through the 304L SS pipes to the other plant components made of 304L SS. Because of the radioactive environment, leak tightness and corrosion resistance of this dissimilar joint are important. In this work, friction welding process was attempted to join Ti to 304L SS. Direct friction welding of Ti to 304L SS results in a stronger weld in which failure occurs in the Ti base metal during tensile testing. However, the joints have almost zero bend ductility that has been attributed to the formation of intermetallics due to mechanical alloying, strain hardening of Ti near the joint interface and residual stresses. Post-weld heat treatment marginally increases the bend ductility to 5° because of relieving of the effects of strain hardening and of residual stresses at the joint interface. Corrosion test in boiling nitric acid is as per ASTM A-262 practice. The average corrosion rate is 10 mpy with the joints remaining intact after the corrosion test.

12) Hyung-Seop Shin, Jung-Soo Park, Yoon-Chul Jung, Jung-Ho Ahn, Yoshihiko Yokoyama, Akihisa Inoue [2008]

In this present study by Hyung-Seop Shin et. al. the friction welding of three kinds of Zr-Cu-Al bulk glassy alloys (BGAs) which show eutectic or hypoeutectic compositions to similar and dissimilar BGAs and crystalline metals has been tried. The shape and volume of the protrusion formed at the weld interface were investigated. In order to characterize the friction welded interface, micrographic observation and X-ray diffraction analysis on the weld cross-section were carried out. A successful joining of Zr-Cu-Al bulk glassy alloys to similar and dissimilar BGAs was achieved without occurrence of crystallizations at the weld interface through the precise control of friction conditions. In addition, the joining of Zr50 Cu40 Al10 BGA to crystalline alloys was tried, but it was only successful for specific material combinations. The residual strength after welding of dissimilar BGAs was evaluated by the four-point bending test.

13) Hyung-Seop Shin, Young-Jin Jeong, Ho- Yeon Choi, Hidemi, Kato, Akihisa Inoue [2006]

In this study by Hyung-Seop Shin et. al. friction welding of Zr based bulk metallic glass (Zr55 Al10 Ni5 Cu30 alloy) has been tried. Friction time and friction pressure were chosen as the control parameters for the friction welding process. Their influences on the shape and volume of the protrusion formed from the welded interface were investigated. Temperature distribution around the interface during friction was measured using an infrared thermal imager. Successful joining of Zr55 Al10 Ni5 Cu30BMG was accomplished through the precise control of friction time and friction pressure.

14) I. Mitelea, C.M. Craciunescu [2009]

In this paper the influence of the main friction welding parameters, such as the axial pressure, the friction stroke and the upsetting temperature on the compositional, structural and hardness gradient is shown for dissimilar joints made out of carburised and volume-hardened steels. The expulsion of the carbon-enriched layer in the burr as a qualitative factor is analyzed. Low axial pressure and long friction time favours to the presence of a carburized layer in the joint plane. A high axial pressure, as well as increase in the friction stroke favours the expulsion of the carbon-enriched layer from the joining area into the burr. A high upsetting pressure leads to an increase of the plasticized material expulsion in the burr.

15) J. Luo, Y. H. Ye, J. J. Xu, J. Y. Luo, S. M. Chen, X. C. Wang, K. W. Liu [2008]

The continuous drive friction welding technique is usually used to join damping-tube and gland. Generally, the inner friction welding flashes at the end of damping tube are very harmful to the assembly of damping device and the cleanness of damping liquid. These thin and natural formed inner friction welding flashes are very easy to crack, break and form a large of metal particles on the special vibrating working conditions of damping-tube. These metal particles increase wearing damage and reduce the safety coefficient of the damping-tube. It is very difficult to deal with these inner friction welding flashes of the damping-tube; especially the diameter of the damping tube is small. To address this problem, in this article, J. Luo et. al. proposed a mixed-integrated approach, which includes adjusting the size of the covering of damping-tube, designing a new structure, applying a controlling mould in friction welding and optimizing the parameters of the welding technology by friction torque-time method. This approach reduces the some of the inner welding flashes, controls the crimping direction of the friction welding flashes, and promotes the forming of the outer friction welding flashes. The macrostructure of welding flashes and friction welded are analyzed. The experimental results show that proposed mixed- integrated approach eliminates the problems of the inner friction welding flashes in the damping-tube friction welding.

16) Jolanta Zimmerman, Wladyslaw Wlosinski and Zdzislaw R. Lindemann [2009]

In this paper a modeling of friction welding of elastic materials with elastic–plastic metals is presented by Jolanta Zimmerman et. al. This model has been practically verified in the process of friction welding of corundum ceramic of 97.5% Al_2O_3 content and aluminium alloy 6061-T6 as well as in the same ceramic and electrolytic copper of 99.9% Cu content. Mechanical strength of the acquired welded joints was around 30 MPa.

A simulation of the process was performed by means of the finite element method using two FEM systems, namely ADINA-T and ADINA. The simulations made it possible to observe the temperature distribution and thermo-mechanical fields that take place during the process. The obtained results show that the temperature, pressure and the deformation distribution near the contact surface are non-homogeneous. It causes not even conditions to create the bond and internal stresses generation. The agreement between the numerical geometry prediction and the experimental data proves the validity of the proposed model.

The performed calculations and preliminary studies on the influence of the diffusion phenomena on the welding process showed that the diffusion depth is approximately 4 μm and the calculated diffusion coefficient of Al into Al_2O_3 is 1.8×10^{-13} m^2/s. Numerical simulation of the friction welding process allows better understanding of the whole process, final products shape prediction and can be helpful during design of the process using other materials.

17) Koen Faes, Alfred Dhooge, Patrick De Baets, Eric Van Der Donckt and Wim De Waele [2009]

A new welding method for fully automatic welding of pipelines has been developed by Keon Faes et. al. The proposed welding procedure, called Friex, is a new variant of the well-known friction welding process. An intermediate ring is rotated in between the pipes to be welded to generate the heat necessary to realize the weld. In the first part of this paper, the working principles of the Friex welding process are briefly described. The influence of the rotation speed on the weld properties is discussed for welding 3 in. pipes in the pipeline steel API-5L X52. Two normalized fine-grained steels were used for the welding ring. The optimization of the thickness of the welding ring is also discussed in this paper.

18) L. D'Alvise , E. Massoni and S.J. Walløe [2002]

In this study the development and experimental validation of a finite element code to simulate the inertia friction welding (IFW) process. The mechanical equations take into account, among others, the physics in terms of inertia, forces and friction. They are solved for velocity and pressure through the $P1^+/P1$ formulation. Due to the rotational movement of the work piece, a third nodal unknown V_θ, the rotational velocity, is added to the variables V_r and V_z. The thermal calculation influences the rheological and tribological parameters and is coupled to the mechanical solution. Powerful contact algorithm and automatic remeshing are implemented to model the flash formation at the joint interface, its self-contact with the work piece and the multi-body contact between dissimilar materials. A novel formulation for the friction law is implemented to suitably represent the physical phenomena in IFW. A residual stress analysis is carried out.

19) Mohamad Zaky Noh, Luay Bakir Hussain, Zainal Arifin Ahmad [2007]

The joining of ceramic–metal can be done using different techniques such as brazing diffusion bonding, and friction welding. However, the mechanism of ceramic–metal join ing has still not been fully understood. In this study, an alumina rod was bonded to a mild steel rod via the friction welding technique by using an Al 1100 sheet as an inter-layer. The diameters of the rods were both 10mm, respectively. A friction pressure of 20MPa and a forging pressure of 40 MPa were used. Rotational speed was maintained at 900rpm and friction times from 2 to 20 s were applied. The joining strength was determined through a four point bending test. The maximum bending strength, 240 MPa was obtained when the friction time of 20 s was used. Under optical microscope and scanning electron microscope observation, the bonding aluminum interface was clearly obtained. Mechanical interlocking and close contact between the alumina–aluminum and aluminum–mild steel were observed at magnifications of 3000×. The strength of alumina–steel bonding is much dependent on the wet ability of the alumina surface by

the partially molten aluminium interlayer and the existence of mechanical interlocking between the interlayer and mild steel.

20) M. Maalekian, E. Kozeschnik, H.P. Brantner, H. Cerjak [2008]

For the first time a comparative thermal analysis of the friction welding process using various heat generation models is presented by M. Maalekian et. al. The heat generation rate in orbital friction welding of steel bars is analyzed using four different methods; constant coulomb friction, sliding-sticking friction, the experimentally measured power data and an inverse heat conduction approach. A comparison between the calculated temperature profiles and the experimental data shows that the inverse heat conduction approach predicts the heat generation rate accurately, whereas the constant friction coefficient approach leads to the most inaccurate temperature profile. Moreover, a three dimensional thermo mechanical finite element analysis based on the calculated heat input data and the experimental axial shortening rate demonstrates that the process can be analyzed in a one-dimensional domain due to the short frictional heating cycle and the uniform heat generation rate across the interface. The FE analysis also indicates that the heat generation rate due to the plastic deformation in the work piece away from the interface is negligible compared to the heat generation rate by friction.

21) M.N. Ahmad Fauzi, M.B. Uday, H. Zuhailawati and A.B. Ismail [2010]

According to M.N. Ahmad Fauzi et. al., the study of the interface of ceramic/metal alloy friction welded components is essential for understanding of the quality of bonding between two dissimilar materials. In the present study, optical and electron microscopy as well as four-point bending strength and micro hardness measurements were used to evaluate the quality of bonding of alumina and 6061 aluminum alloy joints produced by friction welding. The joints were also examined with EDX (energy dispersive X-ray) in order to determine the phases formed during welding. The bonded alumina-6061 aluminum samples were produced by varying the rotational speed but keeping constant the friction pressure and friction time. The experimental results showed that the effect of rotation speed and degree of deformation appears to be high on the 6061 Al alloy than on the alumina part. It is discovered that the weld interface formed included three different regions: unaffected zone (UZ), deformed zone (DZ), as well as transformed and recrystallized fully deformed zone (FPDZ). Therefore, when rotational speed increases, the thickness of full plastic deformed zone (FPDZ) at the interface increases as a result of more mass discarded from the welding interface. It was also observed that rotational speed of 2500 rpm can produce a very good joint and micro hardness with good microstructure as compared to the other experimental rotational speeds.

22) Mumin Sahin [2005]

In this study, an experimental set-up was designed and produced to achieve the friction welding of components having equal diameter. The set-up was designed as continuous drive, and transition from friction to forging stage can be done automatically. In the experiments, high-speed steel (HSS—S 6-5-2) and medium-carbon steel (AISI 1040) were used. Post-weld annealing was applied to the joints at 650 °C for 4 h. First, the optimum welding parameters for the joints were obtained. Later, the strengths of the

joints were determined by tension, fatigue and notch-impact tests, and results were compared with the tensile strengths of materials. Then, hardness variations and microstructures in the post-weld of the joints were obtained and examined.

23) Mumin Sahin [2007]

The aim of this study was to investigate experimentally the micro-structural properties and welding strengths of the joints using austenitic-stainless steel (AISI 304) parts. The experiments were carried out using a beforehand designed and constructed experimental friction welding set-up, constructed as continuous-drive. Firstly, welding experiments under different friction time and friction pressure were carried out to obtain optimum parameters using statistical approach. Later, the strengths of the joints were determined by tension, fatigue and notch-impact tests, and results were compared with strengths of materials. Hardness variations and microstructures in the interfaces of the joints were also obtained and examined. Then, obtained results were compared with those of previous studies.

24) Mumin Sahin [2009]

An experimental set-up was designed in order to achieve friction welding of plastically deformed austenitic-stainless steels. AISI 304 austenitic-stainless steels having equal and different diameters were welded under different process parameters. Strengths of the joints having equal diameter were determined by using a statistical approach as a result of tension tests. Hardness variations and microstructures using scanning electron microscope (SEM) analysis in the welding zone were obtained and examined. Subsequently, the effect on the welding zone of plastic deformation was analyzed. It has been established that plastic deformation of AISI 304 austenitic-stainless steel has neither an effect on the process nor on the strength of the welding joint.

25) Muhim Sahin, H. Erol Akata [2003]

In the present study, an experimental setup was designed and realised in order to achieve the friction welding of plastically deformed steel bars. The parts having same and different diameters deformed plastically, but same material was welded with different process parameters. The strengths of the joints were determined by tension tests. Hardness variations and microstructures in the welding zone were obtained and the effects of welding parameters on the welding zone were investigated.

26) Muhim Sahin, H. Erol Akata, Kaan Ozel [2006]

In this study, 5083 aluminium alloys, which were exposed to severe plastic deformation, were joined with friction welding method and the variation in mechanical properties of the joist was experimentally investigated. Severe plastic deformation methods can be classified as equal channel angular pressing (ECAP) (in other words, equal cross section lateral extrusion-ECSLE) and cyclic extrusion compression. Aluminium alloy as test material 5083 and square cross-sectional equal channel angular pressing die for severe plastic deformation were used in this study. Firstly, 5083 alloys, as purchased, were joined with friction welding method. The optimum parameters for friction time, upset time, friction pressure and upset pressure, which are necessary for

welding, were obtained. Afterwards, 5083 aluminium materials as purchased were prepared as square cross-section and then 1-pass severe plastic deformation was applied to specimen by equal channel angular pressing die. The obtained parts as square formed were prepared as cylindrical form by machining and then the parts were joined by continuous drive friction welding equipment that was designed and produced in laboratory conditions before. Later, the tensile strength of parts, obtained at optimum conditions, was compared with those of the joined parts as purchased form. Then, hardness variations and microstructures of joints were examined.

27) Mumin Sahin, H. Erol Akata, Turgut Gulmez [2006]

This study deals with the importance of welding in manufacturing methods. There are various welding methods that have been developed to obtain suitable joints in various applications. However, friction welding, which is an alternative manufacturing method, is one of the methods that have been widely used for many years. Mumin Sahin et. al. present an experimental friction welding set-up, which is a continuous drive friction welding set-up, was used in the experiments. Firstly, optimum parameters were obtained to join parts having equal diameter. Secondly, the effect of welding parameters on welding strength was investigated. Later, the mechanical properties of joints were examined by using tensile tests, fatigue tests, notch-impact tests and hardness tests. Finally, the results obtained were shown and discussed.

28) N. Ozdemir, F. Sarsilmaz and A. Hascahk [2007]

The aim of this study is to investigate experimentally the interface properties in terms of rotational speed in friction-welded AISI 304L to AISI 4340 alloy steel. Friction welding was conducted with five different rotational speeds using a direct-drive type friction welding machine. Friction pressure, forging pressure, friction time and forging time are fixed. The integrity of joints was investigated by scanning electron microscopy, while the mechanical properties assessments included micro hardness and tensile tests. The experimental results showed that the thickness of full plastic deformed zone (FPDZ) formed at interface reduce as a result of more mass discarded from the welding interface with increase of the rotational speed. It was also observed that the width of the FPDZ has a important effect on the tensile strength of friction-welded samples and the tensile strength increases with increase of the rotational speed.

29) Niyazi Ozdemir and Nuri Orhan [2005]

In this study, joining characteristic of a fine-grained hypereutectoid ultra-high-carbon steel (UHCS) with thermo-mechanical cycle was investigated by the friction welding process. The joining performances of UHCS/UHCS friction welded joints were studied, and the influences of welding parameters (friction pressure, forging pressure, friction. time, forging time and rotational speed) on the microstructure and mechanical properties of the welded joints were also estimated. The microstructural properties of the heat-affected zone (HAZ) were examined by optical and scanning electron microscopy (SEM). The micro hardness across and perpendicular to the interface were measured and the strength of the joints was determined with tensile tests. The results were evaluated considering the microstructures formed during welding. The experimental results indicate that each parameter has a little individual effect on the

quality of the joint but the combined effect of the rotation speed, friction pressure and friction time has a significant effect on the mechanical and metallurgical properties. Especially, by choosing rotation speed, friction pressure and friction time properly, it is possible to increase the quality of joint.

30) P.D. Sketchley, P. L. Threadgill, I. G. Wright [2002]

An Fe_3Al based oxide dispersion strengthened (ODS) alloy is under consideration for possible use as tubes in advanced heat exchangers, and it is necessary to investigate methods of joining the alloy to itself, and to Haynes 230 alloy. Previous experience on iron aluminides has shown them to be weld able by several processes, but it is known that fusion processes invariably lead to a loss of the Y_2O_3 oxide dispersion which is an essential feature of ODS alloys. Therefore, solid state processes offer a potential advantage, and in this work continuous drive rotary friction welding has been investigated by P. D. Sketchley et. al.

31) P. Sathiya, S. Aravindan and A. Noorul Haq [2008]

This study emphasizes on joints of two types of industrially important stainless steels such as austenitic and ferritic stainless steels. The present study utilized a continuous drive friction welding machine to process similar joints. Cylindrical specimens of austenitic stainless steel and ferritic stainless steel of similar composition and shape (equal diameter and length) were used in this study. The processed joints were tested through uni axial tension test, impact test and hardness test. Microstructural studies were also carried out. The characteristics such as tensile strength, toughness, hardness across the joint zone and microstructural aspects exhibited by friction processed joints were compared to the respective parent materials. Joints processed by this method exhibited better properties when compared to the fusion processed joints.

32) R Chhibber, N Arora, S. R. Gupta, B K Dutta [2006]

The present paper is an effort towards identifying and understanding the problems affecting the bimetallic welds (BMWs) and is as well an attempt to highlight the current issues in the structural integrity assessment of structures having these welds. The basic aim of this work is to provide a clear understanding of the current structural safety issues and their importance in underpinning the use of BMWs in modern nuclear reactors.

33) R. E. Craine, A. Francis [1986]

In all types of friction welding the joining process is started by the generation at the rubbing interface of frictional heat arising from the relative motion of the components. In one form of orbital friction welding the two components to be joined are rotated about their longitudinal axes in the same sense with the same constant angular speed. The two longitudinal axes are being parallel but offset by a small distance. The interface rubbing velocity so created is particularly simple and in this paper a general expression for the rate of heat generation at the rubbing interface during the early stages of the orbital friction welding process is presented. The particular cases of a pair of rods of circular cross-section and two rods of square cross-section are considered in some detail.

34) S.D. Meshram, T. Mohandas and G. Madhusudhan Reddy [2007]

By S.D. Meshram et. al., dissimilar metal combinations Fe–Ti, Cu–Ti, Fe–Cu, Fe–Ni and Cu–Ni has been investigated. As Fe, Cu, Ti and Ni are the most extensively used materials in engineering application in the alloyed form. Metals are taken in commercially pure form so as to understand the basic mechanism of joining, which can be then employed to complex alloy systems. Influence of interaction time in continuous drive friction welding on microstructure and tensile properties is studied. Increased interaction time led to decrease in strength and insoluble systems and improved strength in soluble systems. Mechanical transport of the material is predominant at the peripheral region of the weld.

35) V. V. Satyanarayana, G. Madhusudhan Reddy and T. Mohandas [2005]

Continuous drive friction welding studies on austenitic–ferritic stainless steel combination has been attempted in this investigation by V.V. Satyanarayana et. al. Parameter optimization, microstructure–mechanical property correlation and fracture behaviour is a major contribution of the study. Sound welds are obtained at certain weld parameter combinations only. The mechanical properties of dissimilar metal welds are comparable to those of ferritic stainless steel welds. Evaluation of the joints for resistance to pitting corrosion revealed that the dissimilar welds exhibit lower resistance to pitting corrosion compared to the ferritic and austenitic stainless steel welds. Interface on the austenitic stainless steel side exhibited higher residual stress possibly due to its higher flow stress and higher coefficient of thermal expansion.

36) Yuanzhi Zhu, Zhe Zhu, Zhidong Xiang, Zhimin Yin, Zhifang Wu, Wenging Yan [2008]

In this present study, the microstructure evolution in 4Cr10 Si2 Mo at the weld joint of 4Cr10 Si2Mo/Nimonic 80A formed by inertia friction welding was studied. It is discovered that the welds formed included three zones: thermo-mechanically affected zone (TMAZ); heat-affected zone and the matrix. The TMAZ compromised two regions: a chemical composition mixture zone (CMZ) and a pure shearing zone (PSZ). The austenite grain of the matrix in the CMZ sizing in 3-5m contains large numbers of carbides with a size smaller than 50 nm. However, the grain size in PSZ is about 8–10m. The dislocation density in this zone is much lower than that in CMZ. The carbides in PSZ were mainly distributed at grain boundaries or on shear band. In some locations of high dislocation density, clusters of pearlite of hundreds of nanometres precipitated from the dislocation networks. Grain size in the heat-affected zone is similar to that in the as-received 4Cr10 Si2 Mo

CHAPTER 3 PROBLEM FORMULATION

The use of Mild Steel and Stainless Steel weld joints is in Nuclear Reactors. These bimetallic welds impose a safety issue for the structural engineers. The bimetallic welds present a heterogeneous interface, which results in variation of micro-structural and mechanical properties across a very narrow zone. These welds also show thermal fatigue and residual stresses. The joining of Mild Steel and Stainless Steel is done by using Conventional welding procedure. This procedure generally uses a filler metal of similar nature as of stainless steel to weld the two pieces of mild steel and stainless steel using conventional arc welding processes such as Gas Tungsten Arc Welding, Shielded Metal Arc Welding, and Submerged Arc Welding. The joining of Mild Steel and Stainless Steel should be done in such a way so as to reduce the Residual stresses produced during joining process.

Friction welding provides a solid state approach for joining the steels without adding any external filler material. This approach is particularly useful in joining of dissimilar welds. The reason being the absence of any external filler material which may be further add in the heterogeneity of the weld structure.

From the literature survey, following gaps have been identified.

(i) Limited data related to friction welding of mild steel and stainless steel weld joints has been reported.

(ii) Not much studies have been reported on the microstructural evolution in friction welded joints and their relationship with variation of friction welding parameters.

In this thesis an attempt was made to fulfil the gaps observed from the literature survey by attempting to carry out joining of mild steel and stainless steel bars using friction welding and to understand the micro-structural evolution and mechanical behaviour of the friction welded joints. The friction welding parameters were to be varied and their effect was to be evaluated on the microscopic and macroscopic behaviour.

For the achievement of the above objective an experimental setup was to be designed. The four parameters Friction force, Forge force, Burn off length & Revolutions per Minute were to be varied.

CHAPTER 4 EXPERIMENTATION

4.1 EXPERIMENTAL SETUP DESIGN

For doing friction welding Vertical Milling Machine was used. Two different materials were used, Stainless Steel – 304 and Mild Steel.

The setup basically consists of following main elements:

1 **Vertical Milling Machine –** Vertical Milling Machine & Lathe both can be used for friction welding. Vertical Milling Machine (Figure 4.1) was used for this purpose because of its stability & less vibration as compared to Lathe machine.

Figure 4.1 Vertical Milling Machine used for friction welding

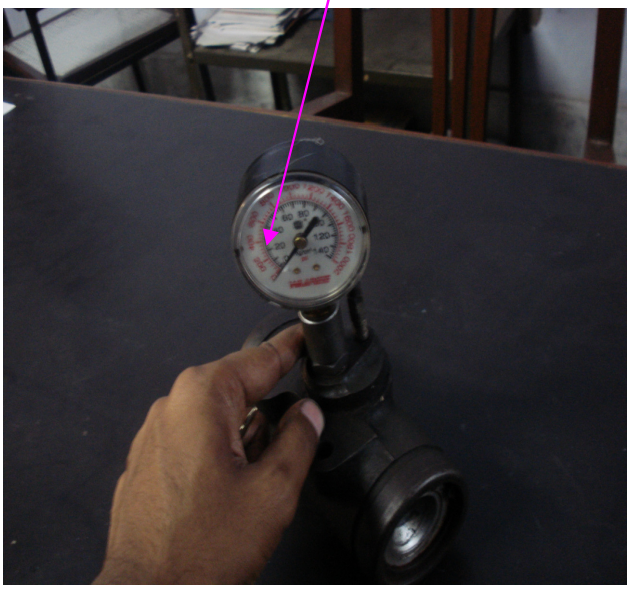

Figure 4.2 Pressure gauge used during friction welding to control the force

2 **Pressure gauge –** Pressure Gauge (Figure 4.2) was used to control the friction force and forge force during friction welding. It consists of a hydraulic cylinder and a dial gauge.

3 **Piezoelectric Dynamometer –** piezoelectric Dynamometer (Figure 4.4) was used to plot the graph of forces produced during friction welding.

4 **Dial Indicator –** A Dial Indicator with magnetic stand (Figure 4.5) was used to note down burn off length during friction welding process.

5 **Digital Thermometer –** Digital Thermometer (Figure 4.3) was used to note down the temperature during friction welding process.

6 **Computer & Display of piezoelectric Dynamometer –** Computer and Display (Figure 4.6) was attached with Piezoelectric Dynamometer to plot the graphs of forces.

Figure 4.3 Digital Thermometer used to note temperature

Figure 4.4 Piezoelectric Load Cell used to plot graphs

Figure 4.5 Dial indicator used to control the burn off length

Figure 4.6 Computer and Display of Piezoelectric Dynamometer

4.2 SPECIMEN SPECIFICATIONS

The following are the specifications which will be used:

- Length of specimen : 70mm (each)
- Diameter of specimen : 12mm

Two cylindrical specimens of same size 70 mm lengths & 12mm diameter were used shown in Figure 4.7

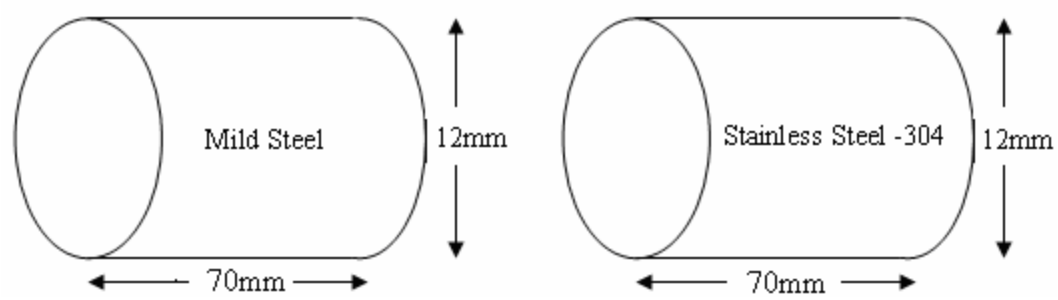

Figure 4.7 Dimensions of cylindrical pieces

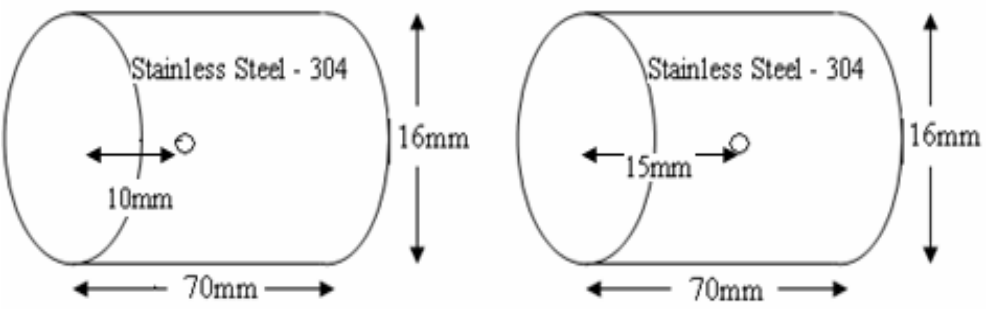

Figure 4.8 Dimensions of holes

In stainless Steel – 304 specimens a hole of 2mm depth and 3mm diameter was made at a height of 10mm on 16 specimens and 15mm on another 16 specimens from the top surface which was being welded. (Figure 4.8)

4.3 SPECIMEN PREPARATION

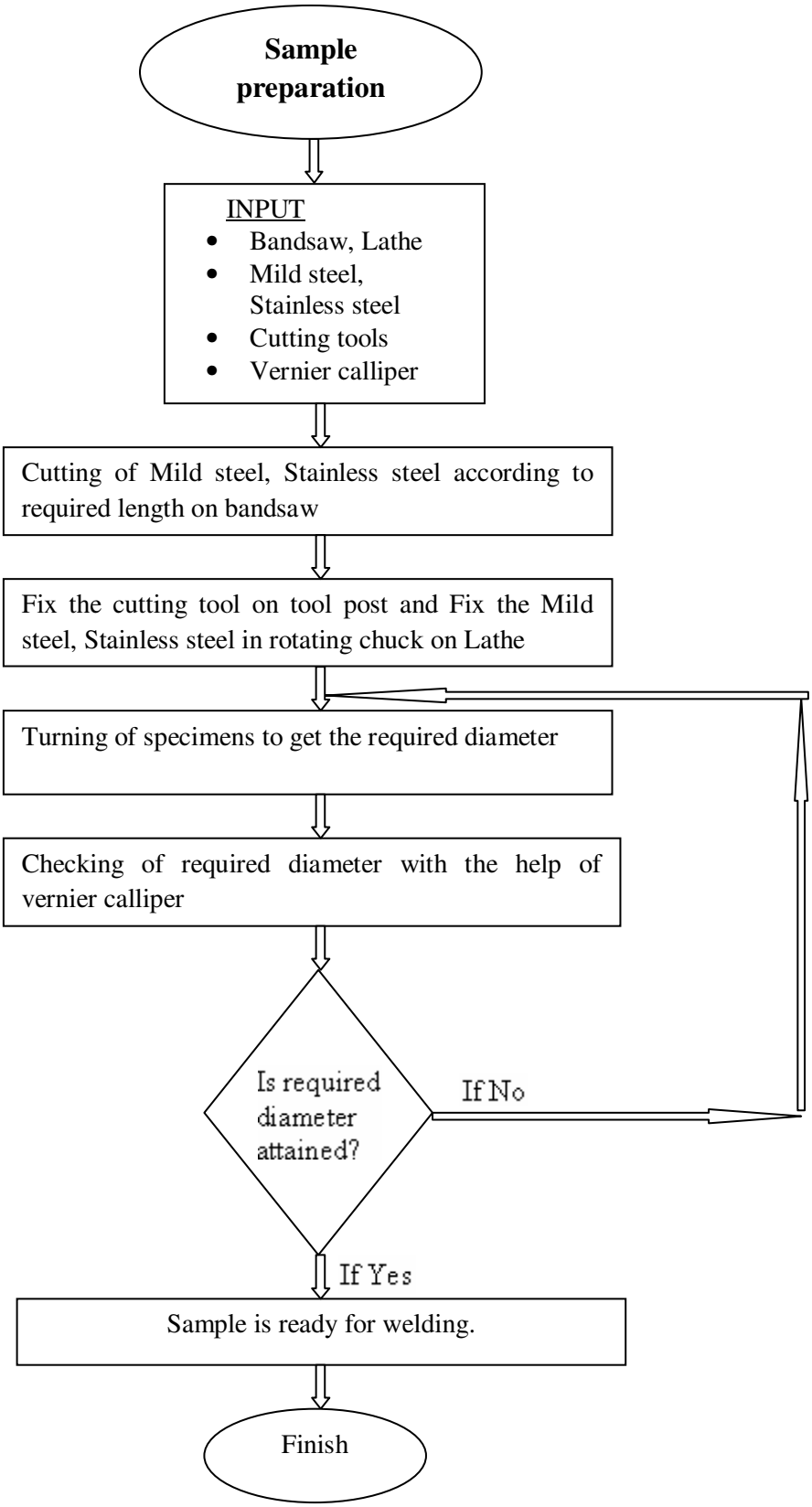

Figure 4.9 Flow chart for sample preparation

Firstly a rod of 16 mm diameter of Mild Steel & Stainless Steel was cut into pieces of 70 mm length (each) on Bandsaw (Figure 4.10).

Figure 4.10 Bandsaw used for cutting of specimens

Figure 4.11 Pieces after cutting, turning and drilling operation

After cutting operation 16 mm diameter of Mild Steel and Stainless Steel having length 70mm each was to be joined. It was found that the pieces did not join even after running the setup for 6 minutes. So the pieces of 16 mm diameter were turned on Lathe and made 14 mm diameter. It was found that still the pieces could not be joined. Then the pieces of Mild Steel and Stainless Steel was turned and made 12 mm diameter on Lathe. A hole of 2 mm depth and 3 mm diameter was made on 16 pieces of SS at a height of 10mm and on another 16 pieces of SS at a height of 15 mm from the top surface which was being welded on Drilling machine (Figure 4.11).

4.4 VARIED PARAMETERS

The following are the four parameters which have been varied up to two levels.

- **Friction Force:** The friction pressure in conjunction with the peripheral speed determines the thermal conditions established in the weld region, and the rate at which metal is extruded radially to form an upset.
- **Burn off Length:** Burn off length is the overall length loss of the specimens during the application of friction force & forge force. It can be original length minus length of welded component.
- **Forge Force:** This is the longitudinal force applied to the faying surfaces at the time when relative movement between the specimens is ceasing and/or has ceased. This is usually higher than the friction force.
- **Revolutions per Minute:** It is the revolutions of the rotating chuck in a minute. Revolutions can be set according to the requirement.

Total of sixteen experiments were done. 4 parameters, 2 levels = 2^4 = 16.

4.5 FIXED PARAMATERS

The following are the parameters that were kept constant throughout the experiment.

- **Diameter of the specimen:** 12mm
- **Total length of the specimen:** 140mm (70mm each)

4.6 TEST MATRIX

Four parameters Friction Force, Forge Force, Burn off Length, RPM which have been varied at two levels and total number of specimens made for each experiment as shown in Table 4.1.

No. of Experiments	Parameters				
	Friction Force (F) in Newton (N)	Forge Force (f) in Newton (N)	Burn off Length (L) in mm	RPM (R)	No. of samples for each experiment
1	5650	11300	1.5	1400	1,2,3,4
2	7910	11300	1.5	1400	5,6,7,8
3	5650	11300	2.5	1400	9,10,11,12
4	5650	11300	1.5	1800	13,14,15,16
5	7910	11300	2.5	1400	17,18,19,20
6	5650	11300	2.5	1800	21,22,23,24
7	7910	11300	1.5	1800	25,26,27,28
8	7910	11300	2.5	1800	29,30,31,32
9	7910	13560	2.5	1800	33,34,35,36
10	5650	13560	2.5	1800	37,38,39,40
11	7910	13560	1.5	1800	41,42,43,44
12	7910	13560	2.5	1400	45,46,47,48
13	5650	13560	1.5	1800	49,50,51,52
14	7910	13560	1.5	1400	53,54,55,56
15	5650	13560	2.5	1400	57,58,59,60
16	5650	13560	1.5	1400	61,62,63,64

Table 4.1 Test matrix showing parameters varied at different levels and no. of specimens for each experiment

4.7 COMPLETE SETUP & WELDING PROCEDURE

One of the two specimens being welded (Mild Steel) was fixed in a collet which was rotating at a given RPM while the other component (Stainless Steel - 304) was fixed which was tightened in a cast iron rectangular block with the help of a bolt. The rectangular block was welded with a cast iron circular plate which was further tightened on a Piezoelectric Dynamometer. The function of cast iron material was to absorb vibration during friction welding.

After setting the specimens in proper alignment machine was started and a vertical upward force was applied. Within 2 to 7 seconds flash was generated and within 15 seconds

specimens was welded. The generation of flash (Figure 4.14) and weld time depends more on the force applied and RPM of the machine.

A thermocouple and a digital thermometer (Figure 4.13) were used to note down the temperature around the interface during friction welding. One end of the thermocouple was inserted in the hole while the other end was inserted in digital thermometer. After welding machine was stopped and the samples were ready for testing (Figure 4.15).

Figure 4.12 Complete setup for friction welding

Figure 4.13 Complete Setup while running the machine & doing temperature measurement

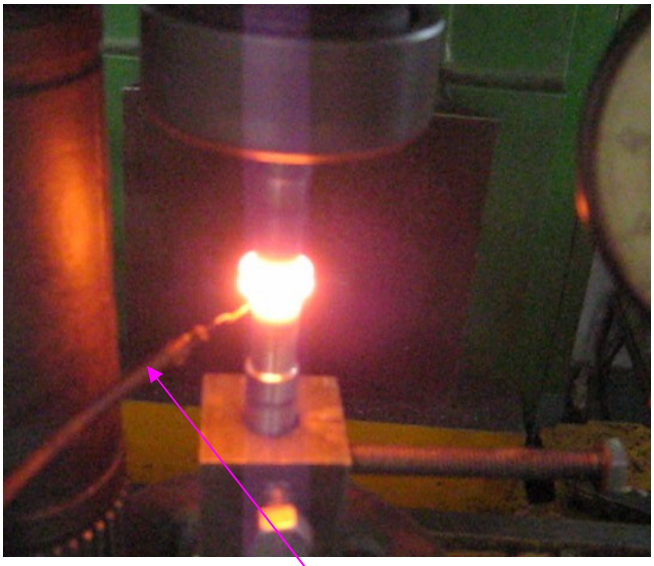

Figure 4.14 Close view of friction welding process and position of thermocouple

Figure 4.15 Close view of set up after welding

Figure 4.16 Specimen after friction welding

4.8 TESTING OF FRICTION WELDED SPECIMENS

4.8.1 Tensile testing: The tensile testing of friction welded specimens was performed on the Universal Testing Machine (Figure 4.17)

Figure 4.17 Universal Testing Machine

No. of Experiments (Specimen no.)	Parameters			
	Friction Force (F) in Newton (N)	Forge Force (f) in Newton (N)	Burn off Length (L) in mm	RPM (R)
1 (1)	5650	11300	1.5	1400
2 (5)	7910	11300	1.5	1400
3 (9)	5650	11300	2.5	1400
4 (13)	5650	11300	1.5	1800
5 (17)	7910	11300	2.5	1400
6 (21)	5650	11300	2.5	1800
7 (25)	7910	11300	1.5	1800
8 (29)	7910	11300	2.5	1800
9 (33)	7910	13560	2.5	1800
10 (37)	5650	13560	2.5	1800
11 (41)	7910	13560	1.5	1800
12 (45)	7910	13560	2.5	1400
13 (49)	5650	13560	1.5	1800
14 (53)	7910	13560	1.5	1400
15 (57)	5650	13560	2.5	1400
16 (61)	5650	13560	1.5	1400

Table 4.2 Test matrix for Tensile Strength

The Table 4.2 shows the specimen number for all experiments at different parameters for which tensile testing has been done.

4.8.2 Measurement of Temperature Profiles: Temperature was noted down experimentally with the help of a digital thermometer. On sixteen samples a hole of 2mm depth was drilled at a height of 10 mm from the interface on SS side where welding was to be done. While on another sixteen samples a hole of 2mm depth was drilled at a height of 15 mm from the interface on SS side where welding was to be done. One end of thermocouple was inserted in the hole while other end was attached with a digital thermometer. The temperature reading was noted down with the help of a camera on the screen of the digital thermometer. The Table 4.5 shows the specimens used for temperature measurement for all experiments at different parameters.

4.8.3 Chemical Composition: Chemical composition of the specimens at interface, on mild steel & stainless steel and on base samples of Mild Steel & Stainless Steel (Figure 4.18) was checked with the help of a Spectrometer (AAS – Atomic Absorption Spectrometer) shown in Figure 4.19.
The following tables 4.3 & 4.4 shows the composition of base materials.

Elements	Fe	C	Si	Mn	P	S	Cr	Mo	Ni	Al	Co
Percentage	98.7	.165	.216	.501	.0479	.0406	.0536	.006	.035	.0010	.007

Table 4.3 Percentage of different elements for Mild Steel

Elements	Fe	C	Si	Mn	P	S	Cr	Mo
Percentage	68.2	.0541	.855	1.89	.0097	.0050	19.6	.276

Elements	Ni	Al	Co	Cu	Nb	Ti	V	W
Percentage	8.31	.0010	.0901	.495	.0052	.0202	.0368	.0553

Table 4.4 Percentage of different elements for Stainless Steel - 304

No. of Experiments (Specimen no.)	**Parameters**			
	Friction Force (F) in Newton (N)	Forge Force (f) in Newton (N)	Burn off Length (L) in mm	RPM (R)
1 (3, 4)	5650	11300	1.5	1400
2 (7, 8)	7910	11300	1.5	1400
3 (11, 12)	5650	11300	2.5	1400
4 (15, 16)	5650	11300	1.5	1800
5 (19, 20)	7910	11300	2.5	1400
6 (23, 24)	5650	11300	2.5	1800
7 (27, 28)	7910	11300	1.5	1800
8 (31, 32)	7910	11300	2.5	1800
9 (35, 36)	7910	13560	2.5	1800
10 (39, 40)	5650	13560	2.5	1800
11 (43, 44)	7910	13560	1.5	1800
12 (47, 48)	7910	13560	2.5	1400
13 (51, 52)	5650	13560	1.5	1800
14 (55, 56)	7910	13560	1.5	1400
15 (59, 60)	5650	13560	2.5	1400
16 (63, 64)	5650	13560	1.5	1400

Table 4.5 Test matrix for Temperature measurement

The following Table 4.6 shows the test matrix used for chemical composition, Microstructure, Micro hardness, SEM and XRD.

No. of Experiments (Specimen no.)	**Parameters**			
	Friction Force (F) in Newton (N)	Forge Force (f) in Newton (N)	Burn off Length (L) in mm	RPM (R)
1 (3)	5650	11300	1.5	1400
2 (7)	7910	11300	1.5	1400
3 (11)	5650	11300	2.5	1400
4 (15)	5650	11300	1.5	1800
5 (19)	7910	11300	2.5	1400
6 (23)	5650	11300	2.5	1800
7 (27)	7910	11300	1.5	1800
8 (31)	7910	11300	2.5	1800
9 (35)	7910	13560	2.5	1800
10 (39)	5650	13560	2.5	1800
11 (43)	7910	13560	1.5	1800
12 (47)	7910	13560	2.5	1400
13 (51)	5650	13560	1.5	1800
14 (55)	7910	13560	1.5	1400
15 (59)	5650	13560	2.5	1400
16 (63)	5650	13560	1.5	1400

Table 4.6 Test Matrix for Chemical composition, Microstructure, Micro hardness, SEM, XRD

Figure 4.18 Specimens after composition

Figure 4.19 Spectrometer (AAS)

4.8.4 Microstructure Examination: For Microstructure examination round specimens were made flat from two opposite sides on lathe machine. After that flat sides were grinded on a disc which was attached to a belt grinder (Figure 4.20). After grinding on a rough emery paper polishing of the specimens were started. For this purpose different grades of emery papers were used. Specimens were polished on different grades of emery papers viz. 100, 220, 320, 400, 600, 800, and 1000. After polishing etching of the specimens were done with the help of etching liquid. Etching contains 98% of water plus 2% of HNO_3. After etching microstructure of the specimens was captured on an Optical Microscope (Figure 4.21) at 400X magnification with the help of a camera along the weld. Images were captured at different places along the weld, on interface, very near to the interface on Mild Steel side, very near to the interface on Stainless Steel side, on Mild Steel and on Stainless Steel.

Figure 4.20 Belt Grinder used for polishing

Figure 4.21 Optical Microscope used for Microstructure examination

The test matrix used for Microstructure examination is shown in table 4.6.

4.8.5 Micro hardness Measurements: Micro hardness measurement of the specimens was done along the weld and at the cross section on Micro hardness Machine (Figure 4.25). Along the weld hardness was taken on three different zones, at interface (Figure 4.22), on mild steel (Figure 4.23) and on stainless steel (Figure 4.24). On mild steel and on stainless steel hardness was taken at a constant distance of 0.5mm from the interface in 6 steps. Total of 13 readings were taken, one on intersection, 6 on Mild Steel side and 6 on Stainless Steel side. Load was constant for all the specimens i. e. 1000g. The test matrix used for Micro hardness measurements is shown in Table 4.6.

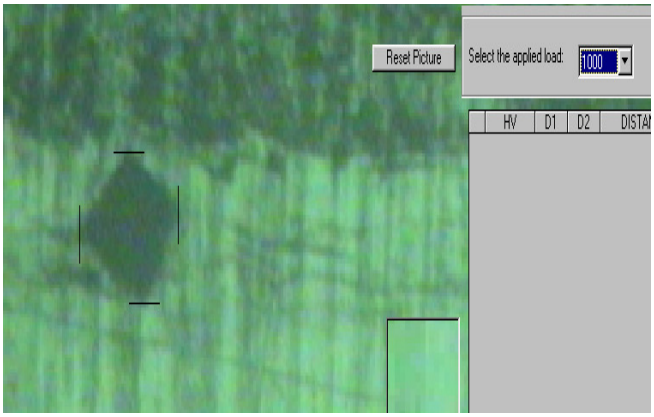

Figure 4.22 Indent on Interface

Figure 4.23 Indent on Mild Steel side

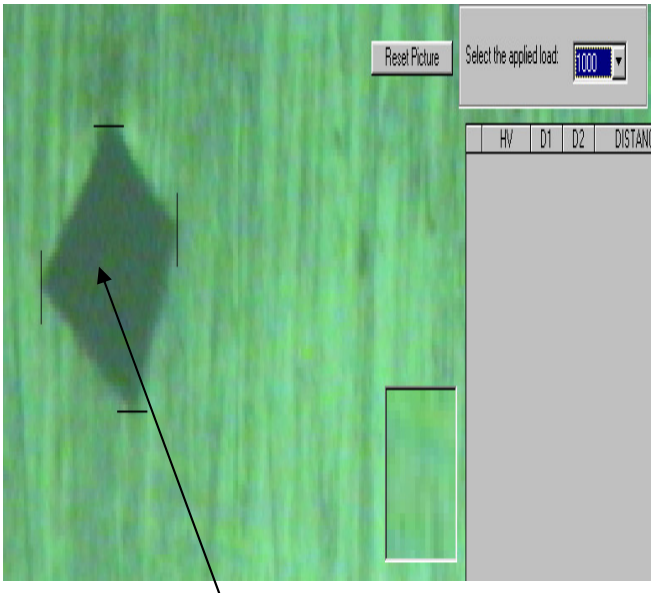

Figure 4.24 Indent on Stainless Steel side

Figure 4.25 Optical microscope

4.8.6 Scanning Electron Microscope examination: SEM results were carries out on Scanning Electron Microscope (Figure 4.26) at 2000X magnification. The test matrix used for SEM is shown in Table 4.6.

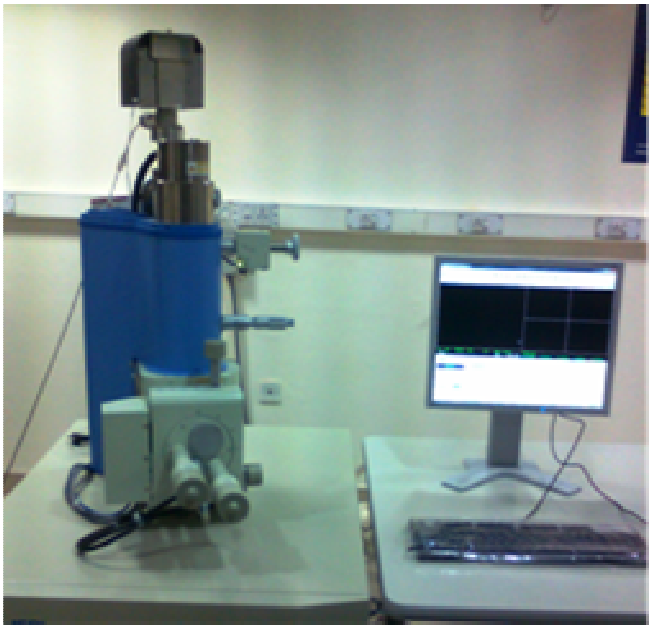

Figure 4.26 Scanning Electron Microscope

4.8.7 X-Ray Diffraction: XRD was carried out on X-Ray Diffractometer (Figure 4.27). XRD pattern show different phases and compounds present in the welded specimen. The test matrix used for XRD is shown in Table 4.6.

Figure 4.27 X-Ray Diffractometer

CHAPTER 5 RESULTS & DISCUSSION

5.1 MACROSCOPIC BEHAVIOUR

5.1.1 Tensile Strength: Following table shows the UTM, UTS and Percentage elongation.

No. of Experiments (Sample no.)	Parameters				UTM Results		
	Friction Force (F) in N	Forge Force (f) in N	Burn off Length (L) mm	RPM (R)	UTS (N/mm^2)	UTL (KN)	Percentage Elongation
1 (1)	5650	11300	1.5	1400	494.27	57.75	1.46
2 (5)	7910	11300	1.5	1400	488.49	55.68	2.14
3 (9)	5650	11300	2.5	1400	682.37	81.7	1.5
4 (13)	5650	11300	1.5	1800	502.91	57.8	1.6
5 (17)	7910	11300	2.5	1400	547.59	62	2.7
6 (21)	5650	11300	2.5	1800	536.12	58.6	5.4
7 (25)	7910	11300	1.5	1800	511.56	58.6	2.1
8 (29)	7910	11300	2.5	1800	667.38	76.45	5.5
9 (33)	7910	13560	2.5	1800	486.24	55.7	2.4
10 (37)	5650	13560	2.5	1800	488.54	56.8	2.8
11 (41)	7910	13560	1.5	1800	580.75	67.3	1.7
12 (45)	7910	13560	2.5	1400	493.93	56.3	2.9
13 (49)	5650	13560	1.5	1800	537.24	63.7	2.5
14 (53)	7910	13560	1.5	1400	532.24	58.67	1.8
15 (57)	5650	13560	2.5	1400	494.34	58.9	2.07
16 (61)	5650	13560	1.5	1400	480.77	54.8	1.3
Base MS					479.48	54.2	10
Base SS - 304					776.63	87.79	23.33

Table 5. 1 Test matrix for UTM results

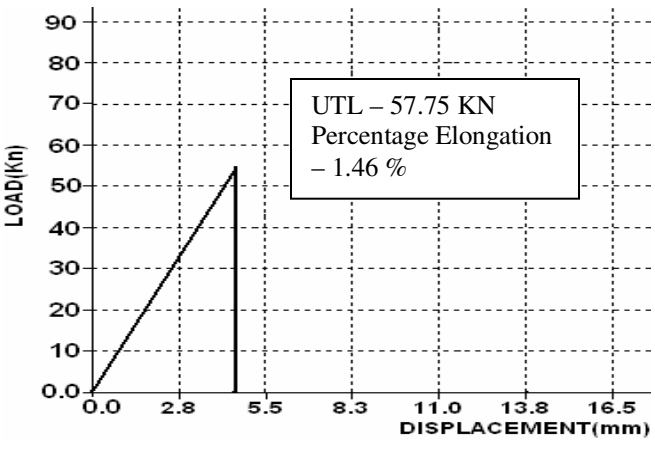

Figure 5.1 Graph of Load Vs Displacement for specimen no. 1

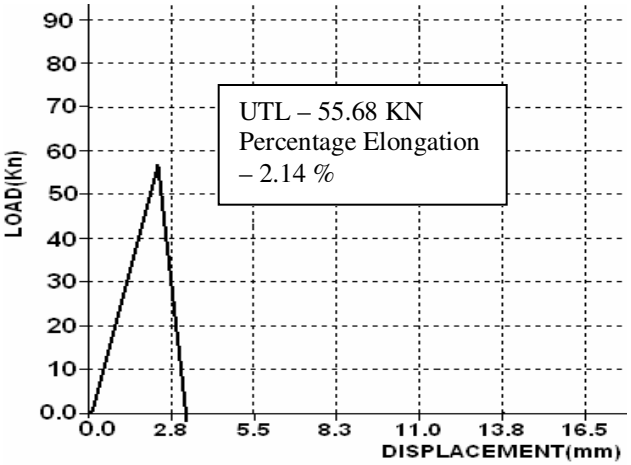

Figure 5.2 Graph of Load Vs Displacement for specimen no. 5

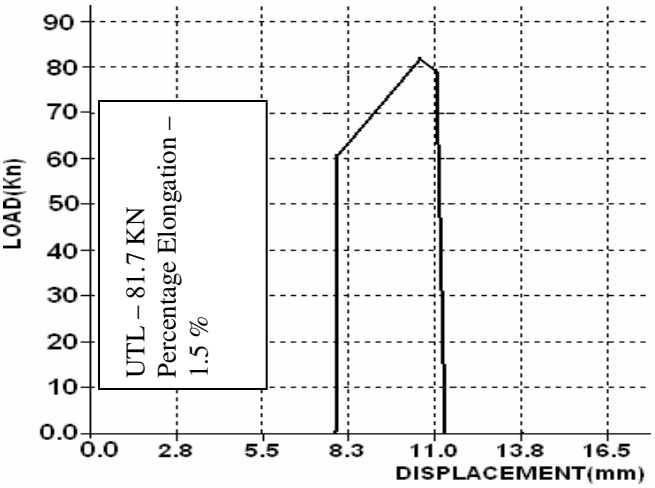

Figure 5.3 Graph of Load Vs Displacement for specimen no. 9

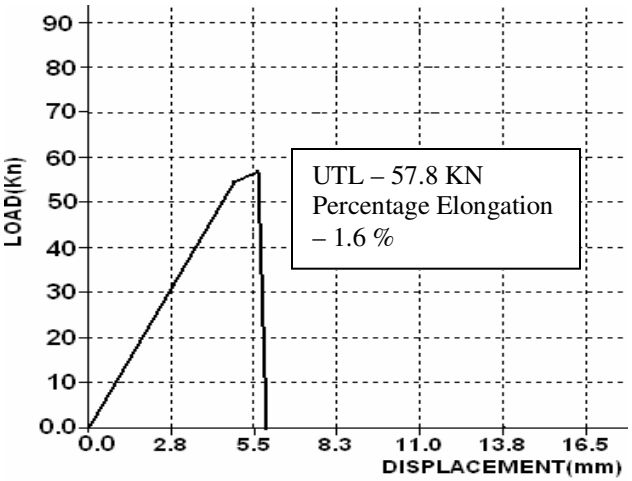

Figure 5.4 Graph of Load Vs Displacement for specimen no. 13

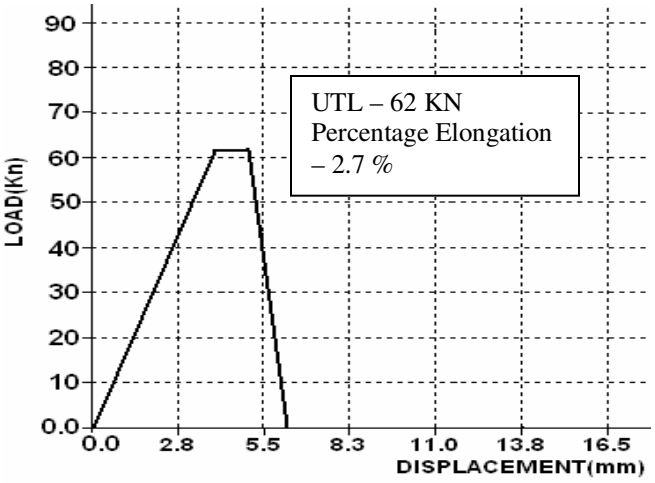

Figure 5.5 Graph of Load Vs Displacement for specimen no. 17

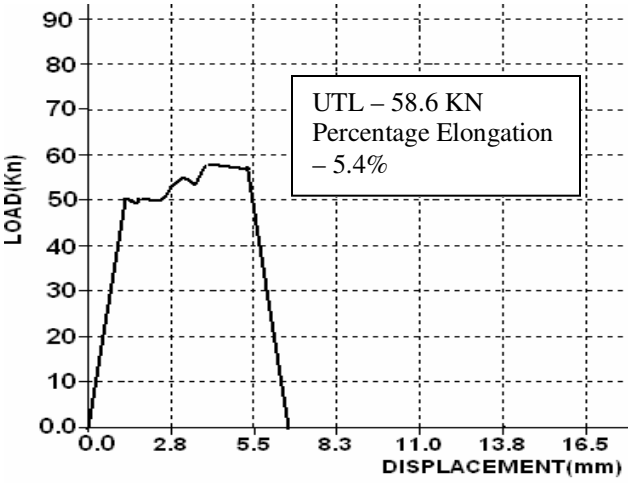

Figure 5.6 Graph of Load Vs Displacement for specimen no. 21

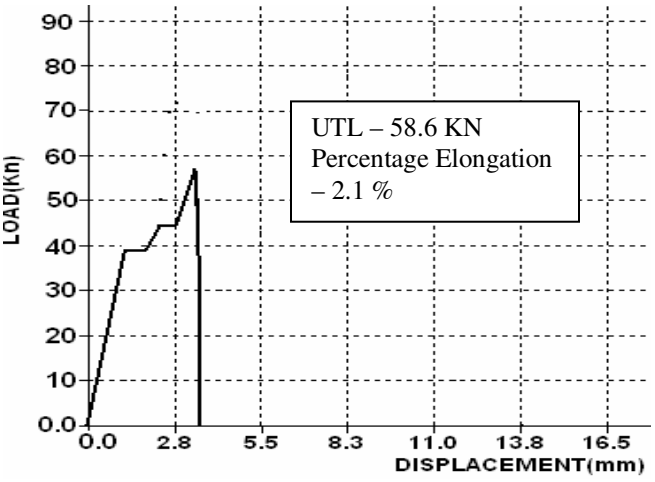

Figure 5.7 Graph of Load Vs Displacement for specimen no. 25

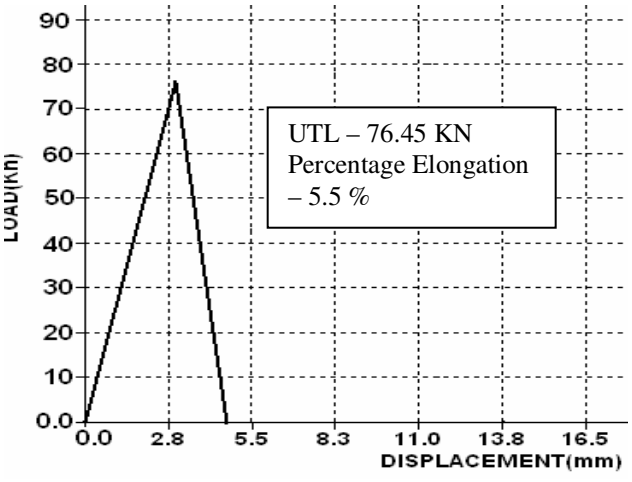

Figure 5.8 Graph of Load Vs Displacement for specimen no. 29

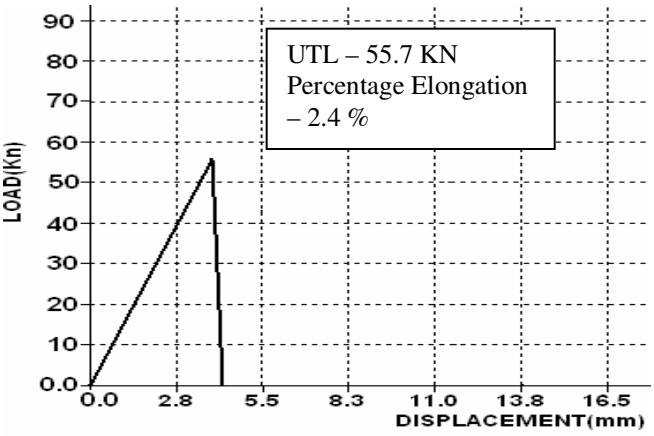

Figure 5.9 Graph of Load Vs Displacement for specimen no. 33

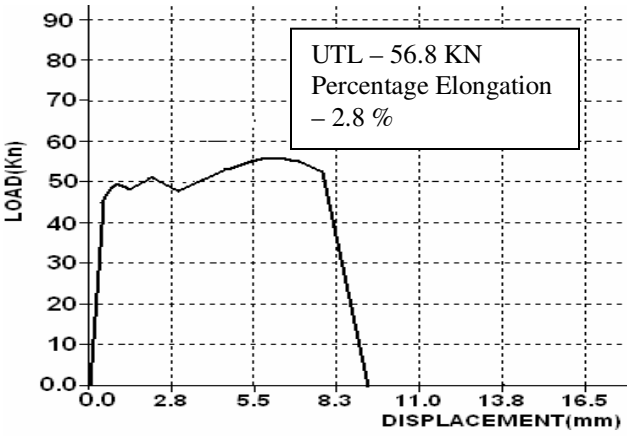

Figure 5.10 Graph of Load Vs Displacement for specimen no. 37

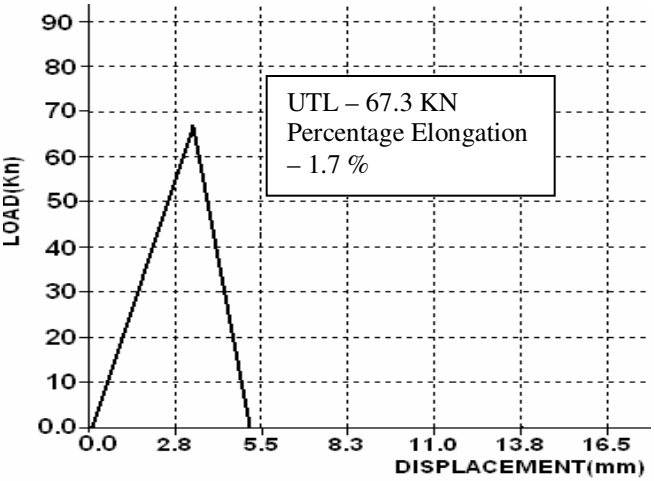

Figure 5.11 Graph of Load Vs Displacement for specimen no. 41

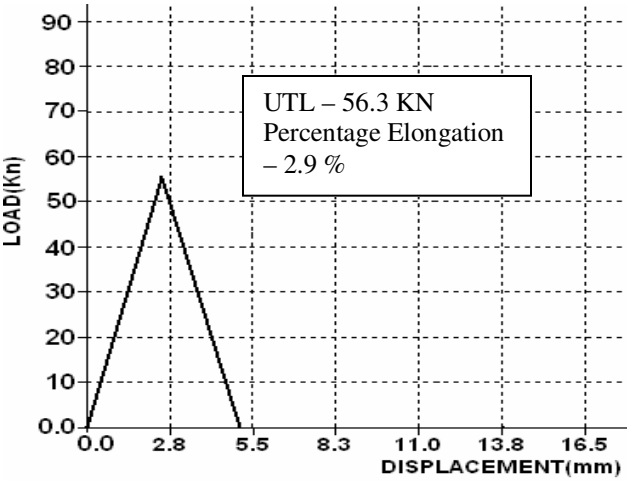

Figure 5.12 Graph of Load Vs Displacement for specimen no. 45

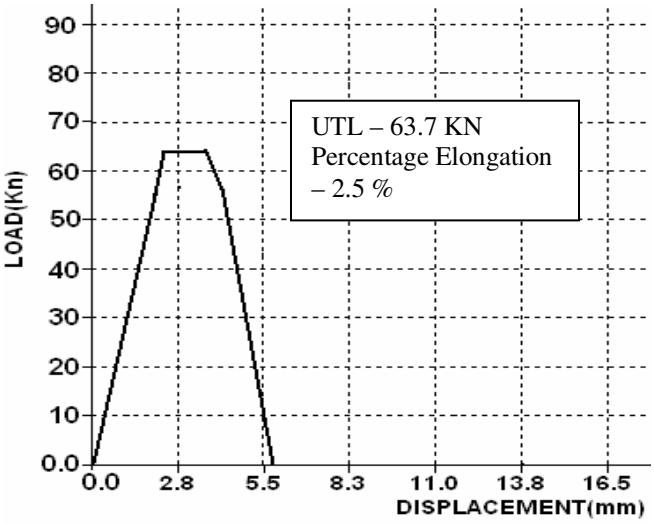

Figure 5.13 Graph of Load Vs Displacement for specimen no. 49

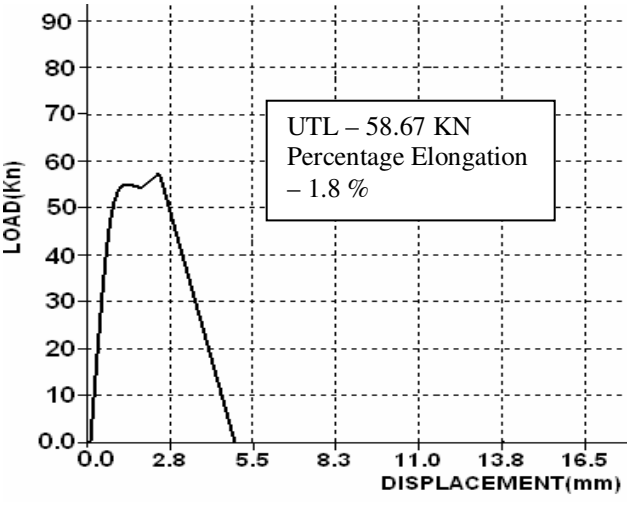

Figure 5.14 Graph of Load Vs Displacement for specimen no. 53

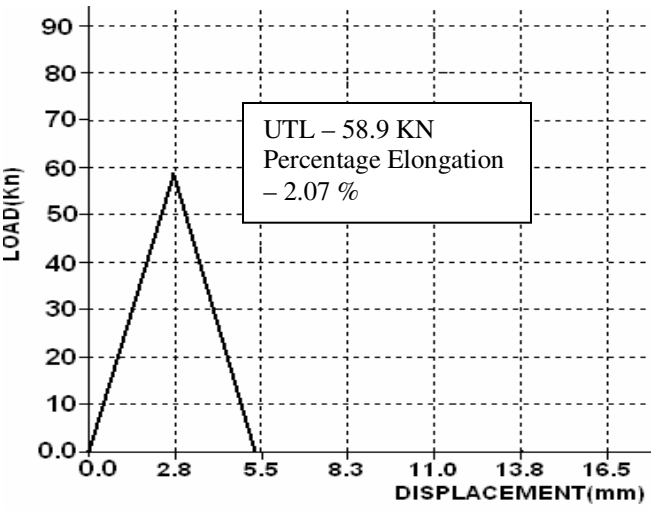

Figure 5.15 Graph of Load Vs Displacement for specimen no. 57

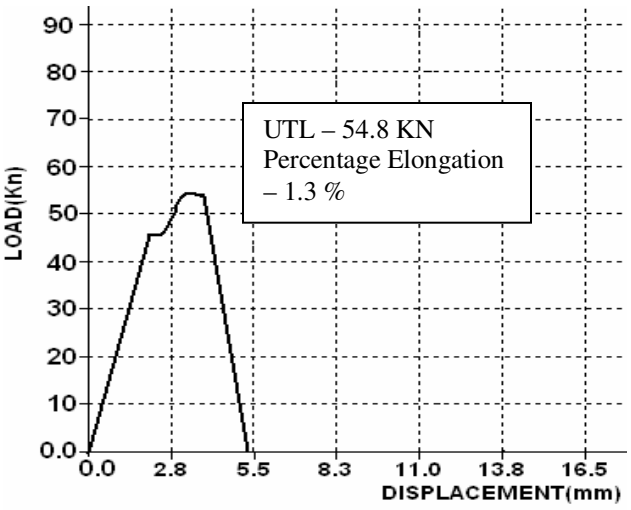

Figure 5.16 Graph of Load Vs Displacement for specimen no. 61

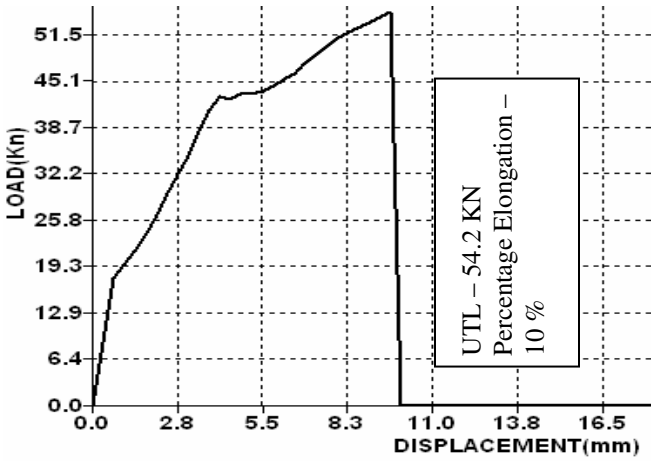

Figure 5.17 Graph of Load Vs Displacement for base sample of Mild Steel

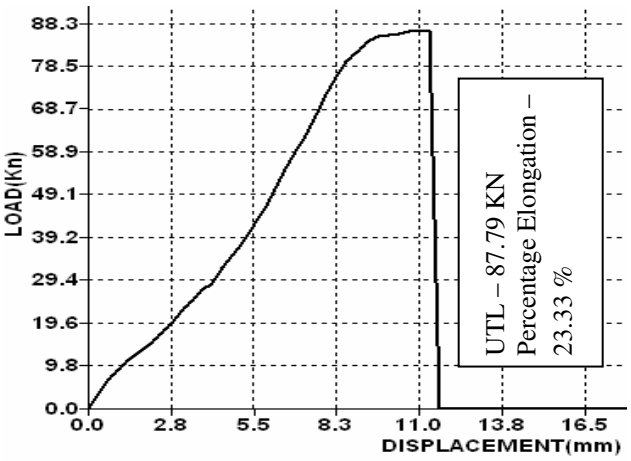

Figure 5.18 Graph of Load Vs Displacement for base sample of Stainless Steel - 304

Discussion on Tensile Strength: Since the friction welding process is characterized by a fast applied thermal and stress/strain cycle causing micro structural changes, it would be expected that the mechanical properties of welded joints would be quite different from those of the base materials. The effects of various parameters on the strength of the joints were examined in welding of equal diameter parts. From Table 5.1 and Figure 5.1-5.18, It appears that maximum Ultimate Tensile Strength was observed for welded specimen no. 9 i.e. 682.37 N/mm^2 and Ultimate Tensile Load 31.9 KN with percentage elongation 1.5 %. Lowest Ultimate Tensile Strength for specimen no. 61 i.e. 480.77 N/mm^2 and UTL 4.8 KN at which percentage elongation 1.3 %. The values of Ultimate Tensile Strength for welded specimens were greater than that of mild steel bars in all cases. It is further observed from the Table 5.1 that the Ultimate Tensile Strength values are better for lower level of forge force as compared to higher level of forge force.

5.1.2 Temperature Profiles: The following graphs show the variation of temperature with respect to friction time. Odd no. specimens were taken at 10 mm distance and Even no. specimens were taken at 15 mm distance from the interface which was being welded.

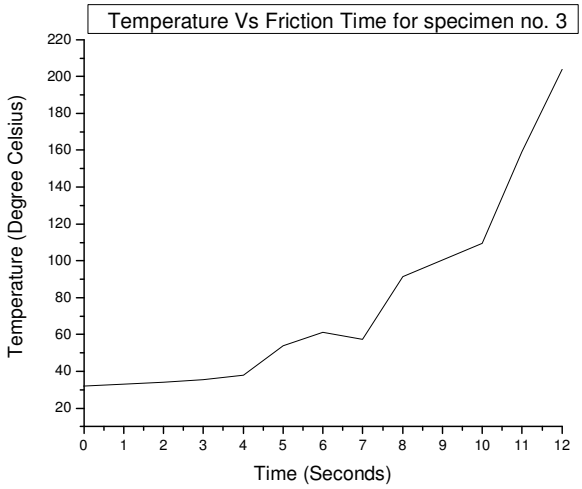

Figure 5.19 Temp. variation w.r.t friction time for specimen no. 3

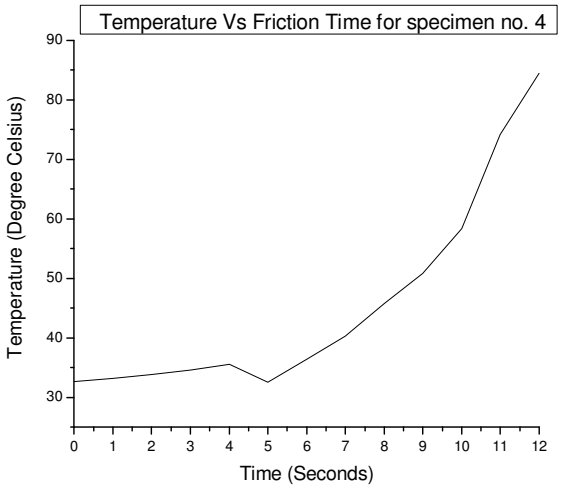

Figure 5.20 Temp. variation w.r.t friction time for specimen no. 4

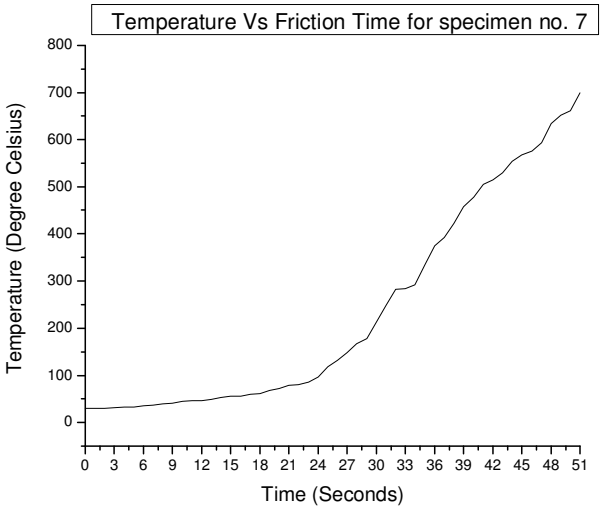

Figure 5.21 Temp. variation w.r.t friction time for specimen no. 7

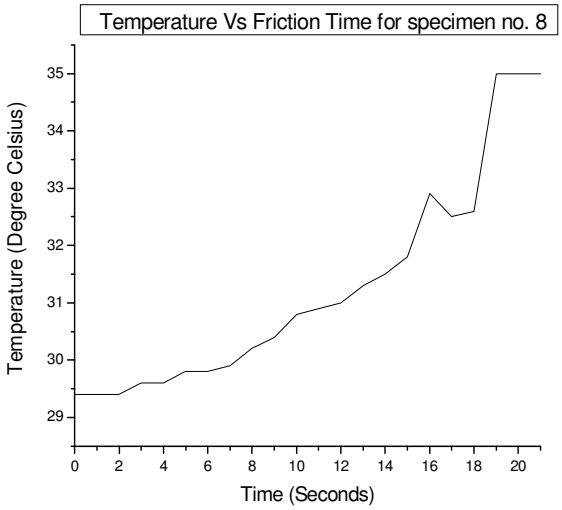

Figure 5.22 Temp. variation w.r.t friction time for specimen no. 8

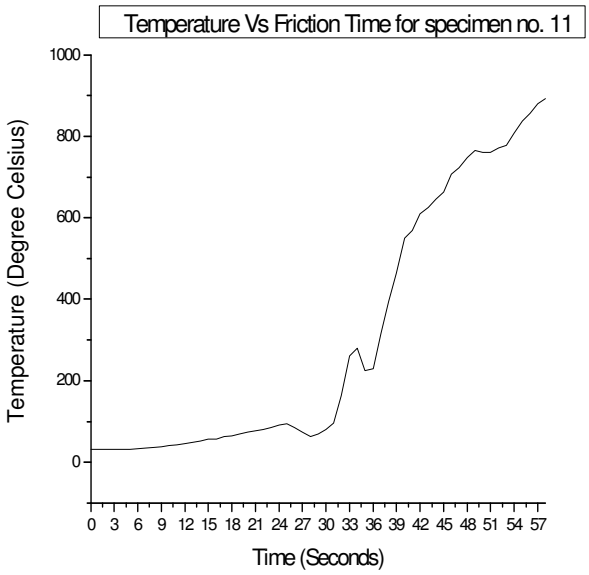

Figure 5.23 Temp. variation w.r.t friction time for specimen no. 11

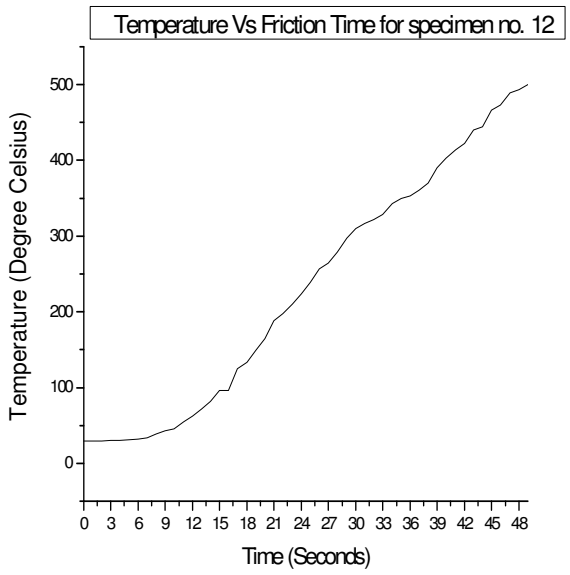

Figure 5.24 Temp. variation w.r.t friction time for specimen no. 12

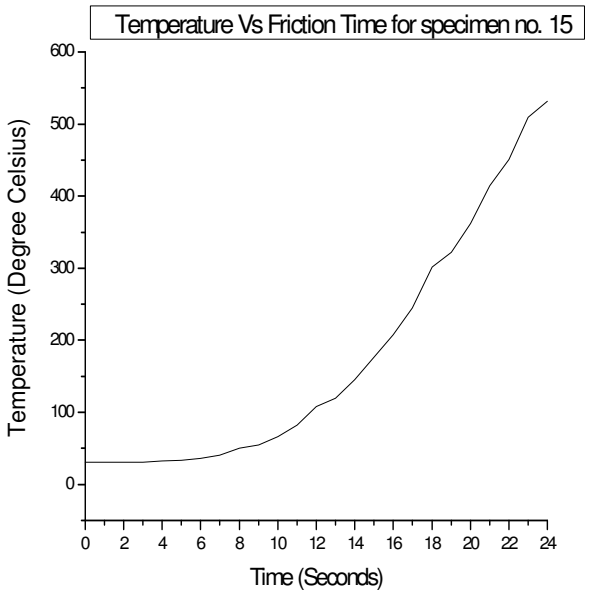

Figure 5.25 Temp. variation w.r.t friction time for specimen no. 15

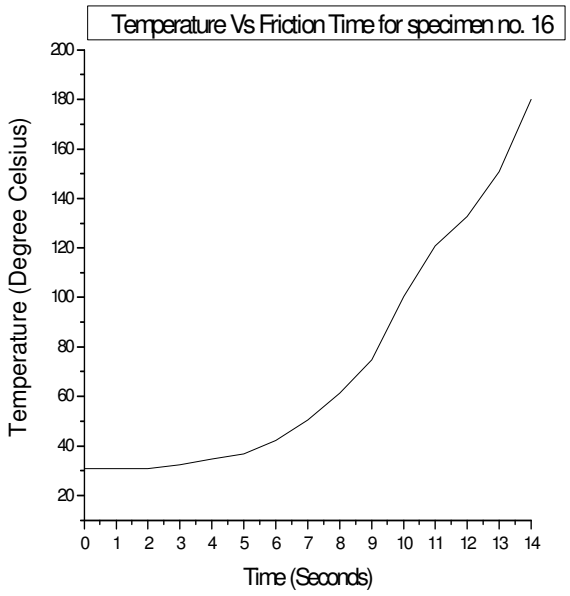

Figure 5.26 Temp. variation w.r.t friction time for specimen no. 16

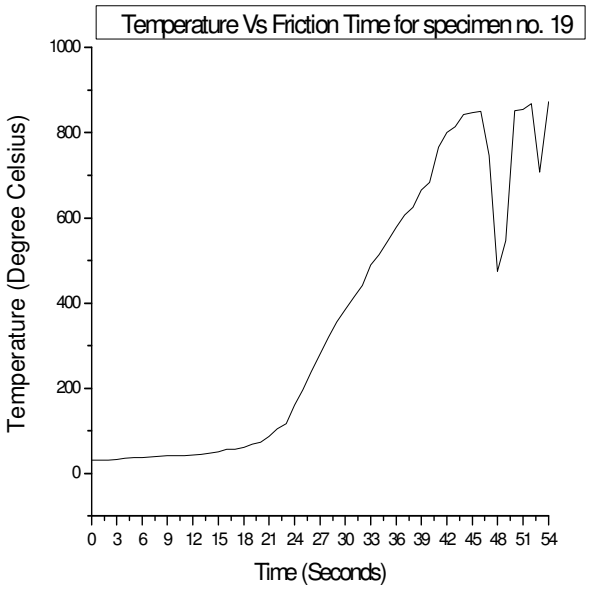

Figure 5.27 Temp. variation w.r.t friction time for specimen no. 19

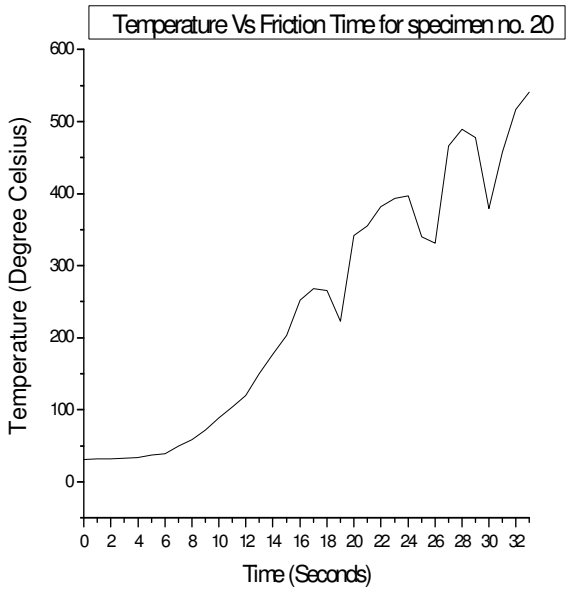

Figure 5.28 Temp. variation w.r.t friction time for specimen no. 20

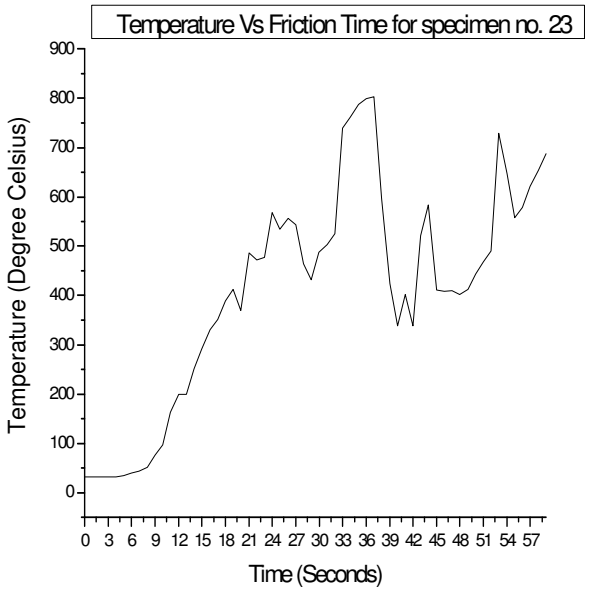

Figure 5.29 Temp. variation w.r.t friction time for specimen no. 23

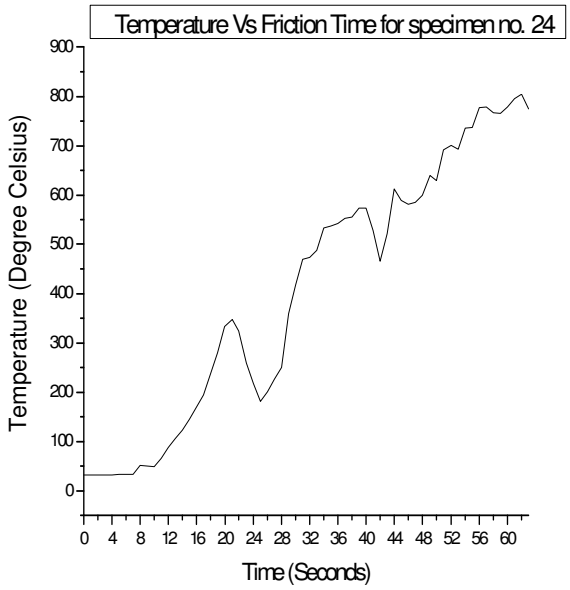

Figure 5.30 Temp. variation w.r.t friction time for specimen no. 24

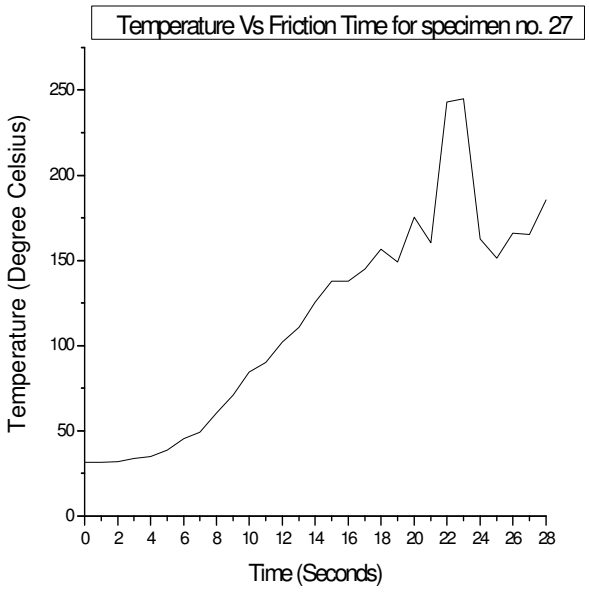

Figure 5.31 Temp. variation w.r.t friction time for specimen no. 27

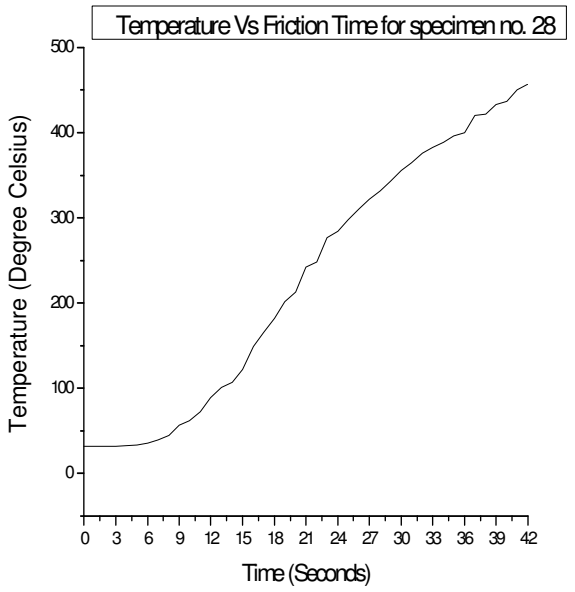

Figure 5.32 Temp. variation w.r.t friction time for specimen no. 28

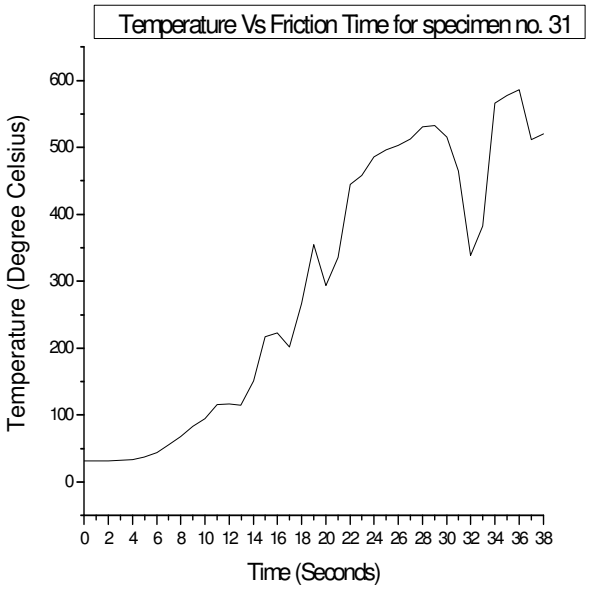

Figure 5.33 Temp. variation w.r.t friction time for specimen no. 31

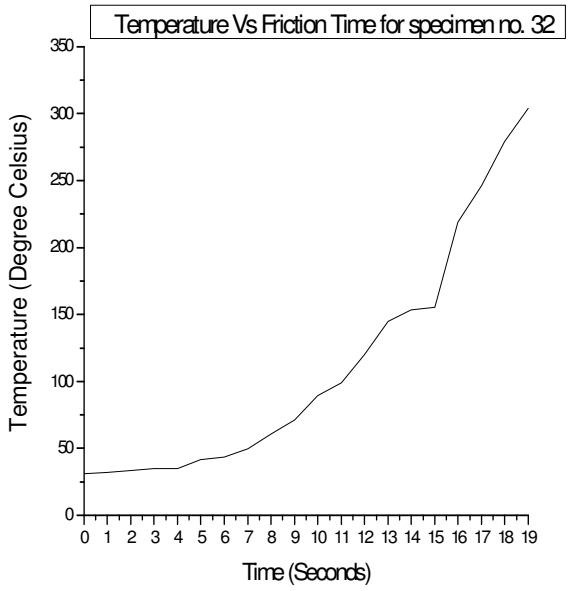

Figure 5.34 Temp. variation w.r.t friction time for specimen no. 32

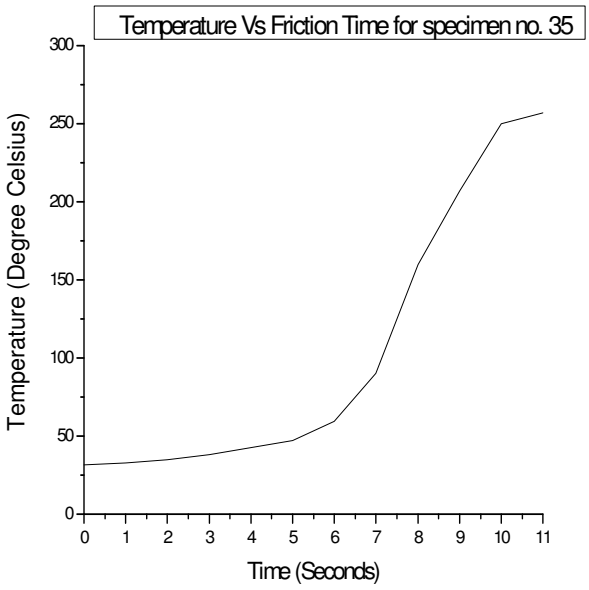

Figure 5.35 Temp. variation w.r.t friction time for specimen no. 35

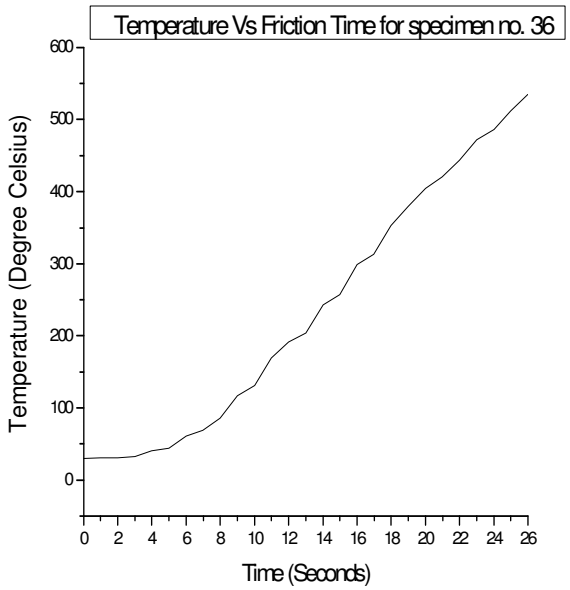

Figure 5.36 Temp. variation w.r.t friction time for specimen no. 36

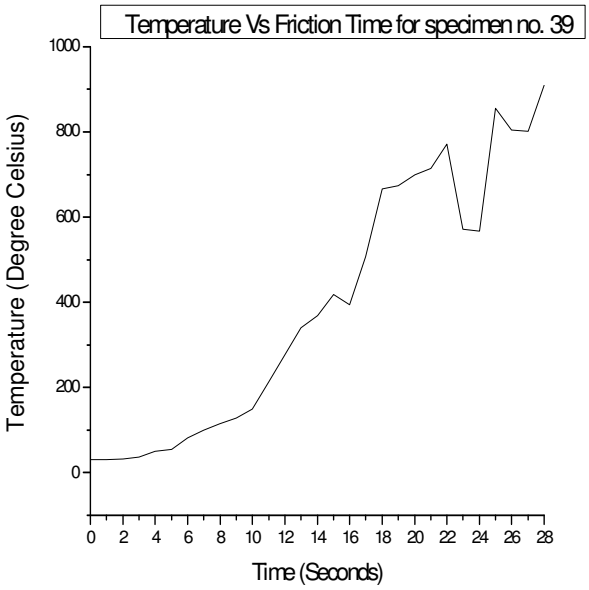

Figure 5.37 Temp. variation w.r.t friction time for specimen no. 39

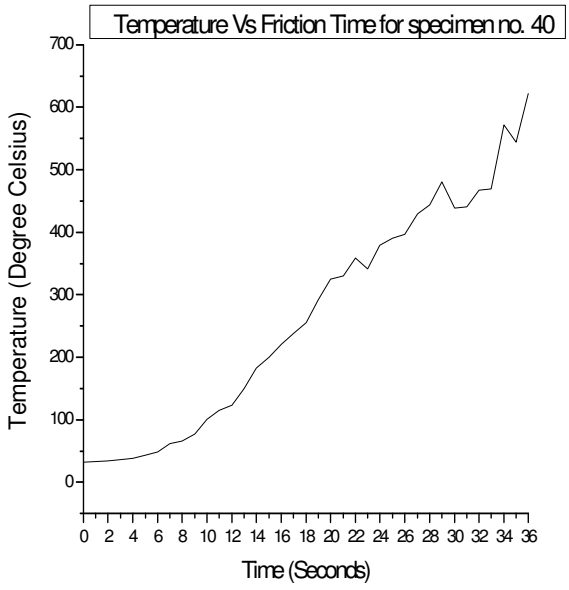

Figure 5.38 Temp. variation w.r.t friction time for specimen no. 40

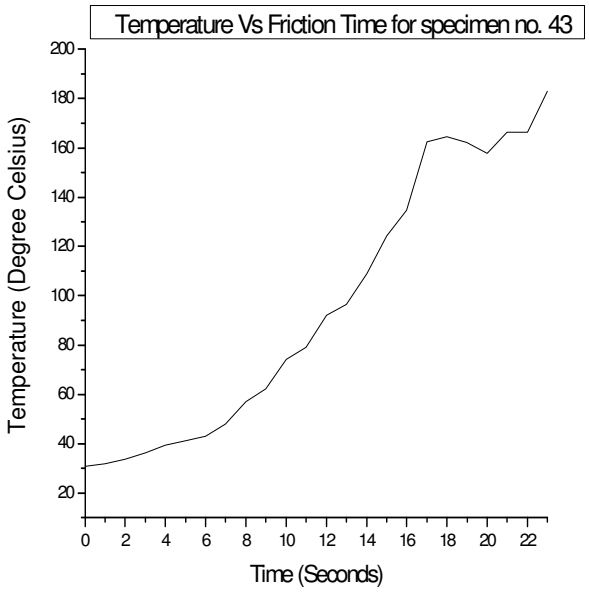

Figure 5.39 Temp. variation w.r.t friction time for specimen no. 43

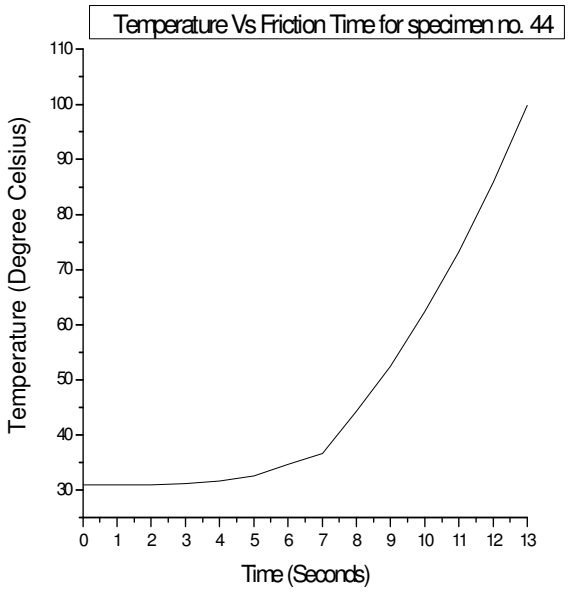

Figure 5.40 Temp. variation w.r.t friction time for specimen no. 44

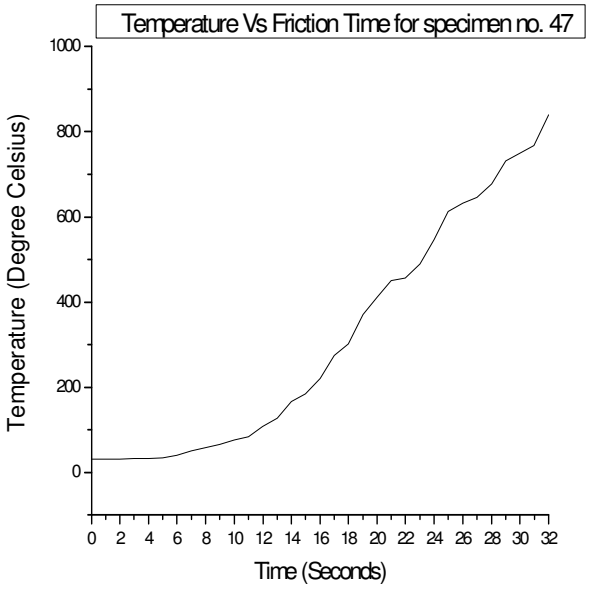

Figure 5.41 Temp. variation w.r.t friction time for specimen no. 47

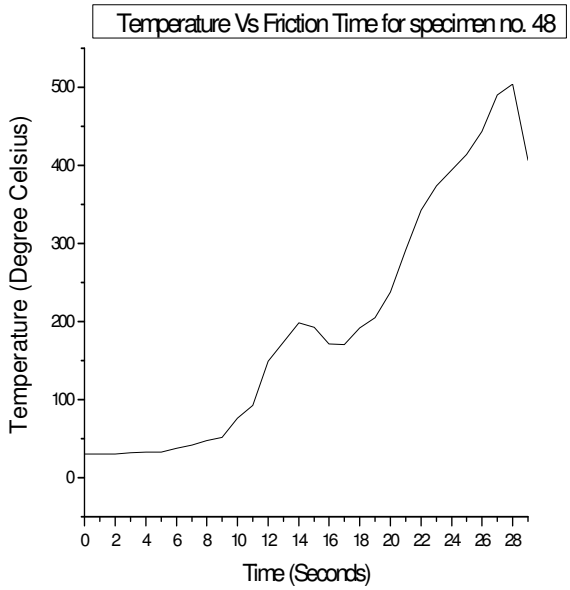

Figure 5.42 Temp. variation w.r.t friction time for specimen no. 48

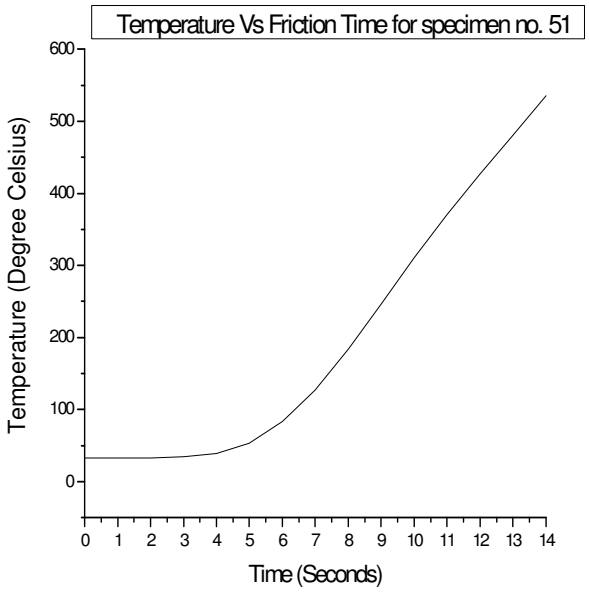

Figure 5.43 Temp. variation w.r.t friction time for specimen no. 51

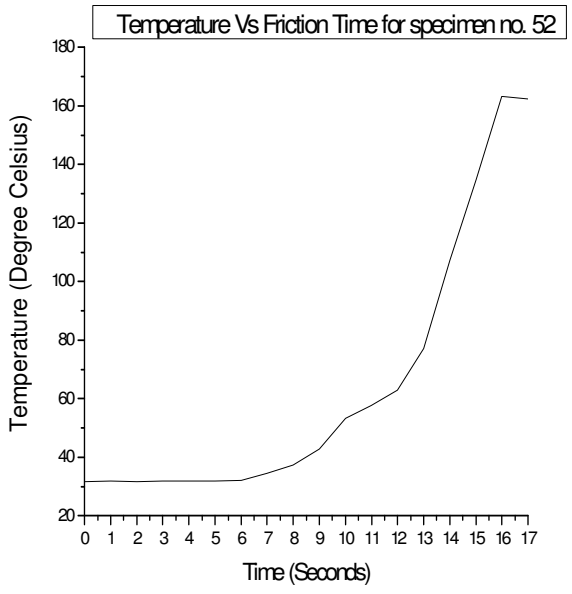

Figure 5.44 Temp. variation w.r.t friction time for specimen no. 52

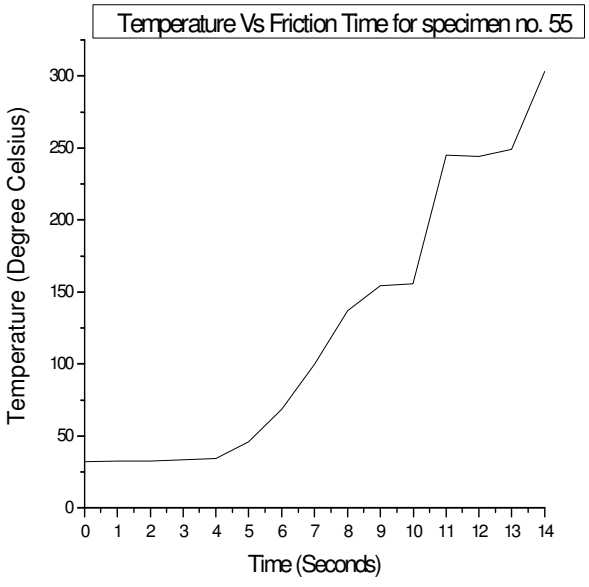

Figure 5.45 Temp. variation w.r.t friction time for specimen no. 55

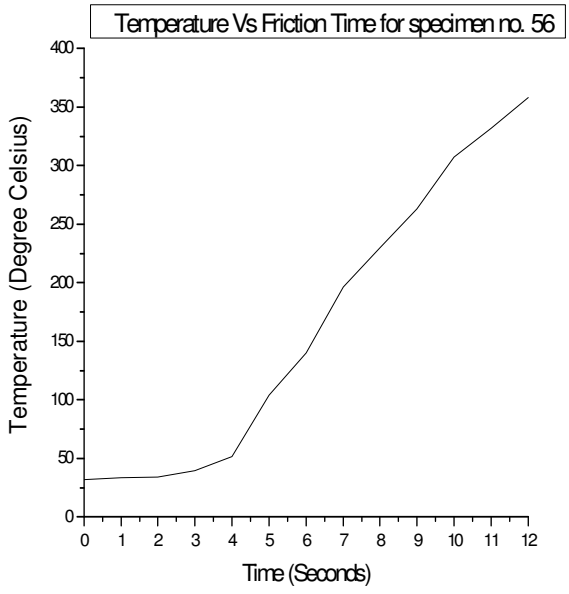

Figure 5.46 Temp. variation w.r.t friction time for specimen no. 56

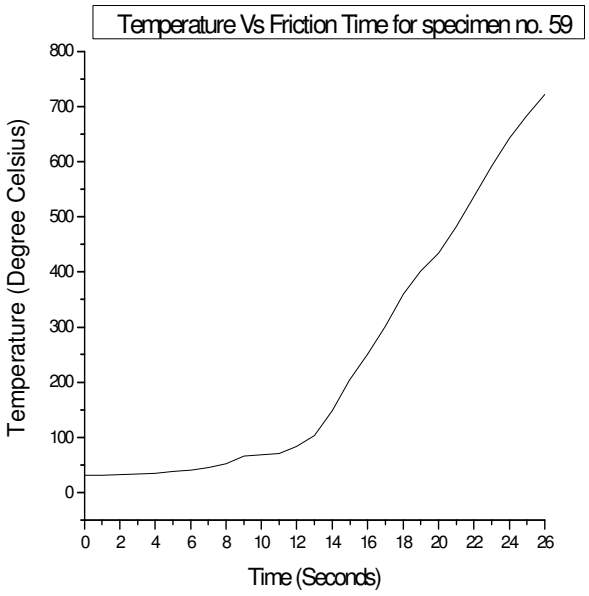

Figure 5.47 Temp. variation w.r.t friction time for specimen no. 59

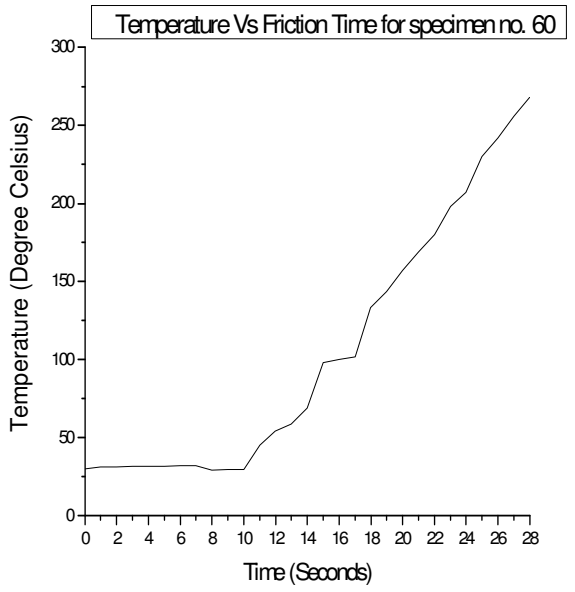

Figure 5.48 Temp. variation w.r.t friction time for specimen no. 60

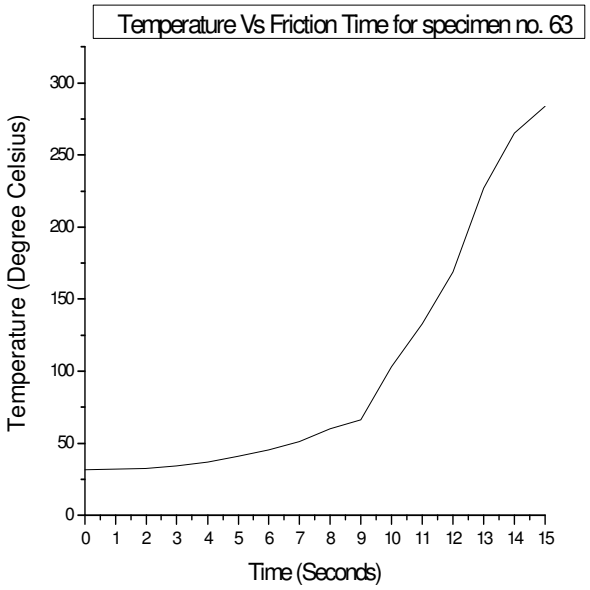

Figure 5.49 Temp. variation w.r.t friction time for specimen no. 63

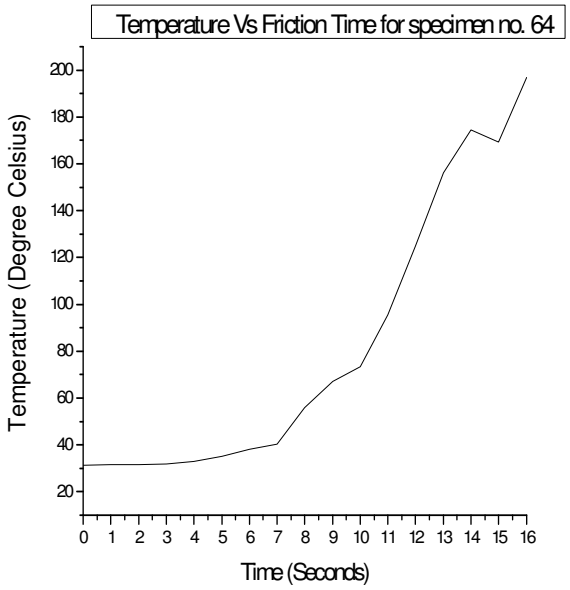

Figure 5.50 Temp. variation w.r.t friction time for specimen no. 64

The following table shows the peak temperature with respect to friction time for different parameters at different levels.

No. of Experiments [(Specimen no.)]	**Parameters**				
	Friction Force (F) in N	Forge Force (f) in N	Burn off Length (L) mm	RPM (R)	Peak Temperature (Degree Celsius)
1 (3) [4]	5650	11300	1.5	1400	(204) [84.5]
2 (7) [8]	7910	11300	1.5	1400	(700) [35]
3 (11) [12]	5650	11300	2.5	1400	(892) [500]
4 (15) [16]	5650	11300	1.5	1800	(532) [180]
5 (19) [20]	7910	11300	2.5	1400	(873) [541]
6 (23) [24]	5650	11300	2.5	1800	(803) [805]
7 (27) [28]	7910	11300	1.5	1800	(245) [457]
8 (31) [32]	7910	11300	2.5	1800	(586) [304]
9 (35) [36]	7910	13560	2.5	1800	(257) [535]
10 (39) [40]	5650	13560	2.5	1800	(909) [622]
11 (43) [44]	7910	13560	1.5	1800	(182.9) [99.8]
12 (47) [48]	7910	13560	2.5	1400	(839) [504]
13 (51) [52]	5650	13560	1.5	1800	(535) [163.2]
14 (55) [56]	7910	13560	1.5	1400	(303) [358]
15 (59) [60]	5650	13560	2.5	1400	(722) [268]
16 (63) [64]	5650	13560	1.5	1400	(284) [196.7]

Table 5.2 Test matrix for Peak temperature

Discussion of Temperature profile results: It is clear from the above Table 5.2 and Figures 5.19-5.50 that the highest peak temperature of 909 degree Celsius and lowest is 182.9 degree Celsius is observed when temperature is measured at a distance of 10 mm for specimen no. 39. When temperature is measured at 15 mm distance, maximum temperature observed is 805 degree Celsius. Lowest temperature is 35 degree Celsius for specimen no. 8. It is observed that with increase in friction force while other parameters are constant, there is increase in peak temperatures. While for other parameters no singular trend is visible with regards to peak temperatures.

5.1.3 Chemical Composition

The following are the graphs of percentage of different elements for all the specimens & percentage change.

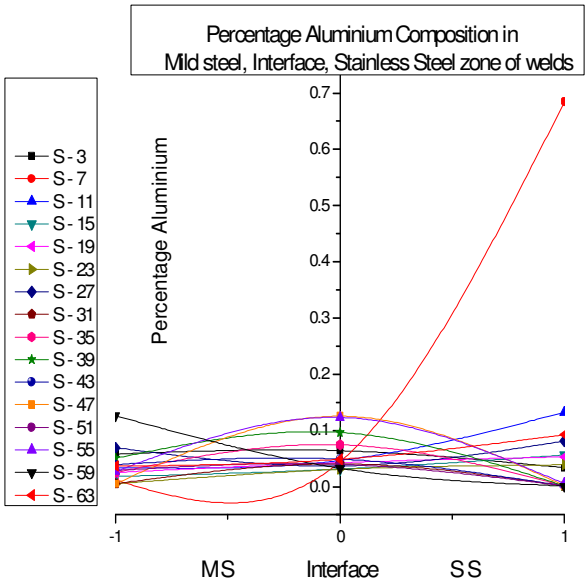

Figure 5.51 Percentage Aluminium composition in different zones

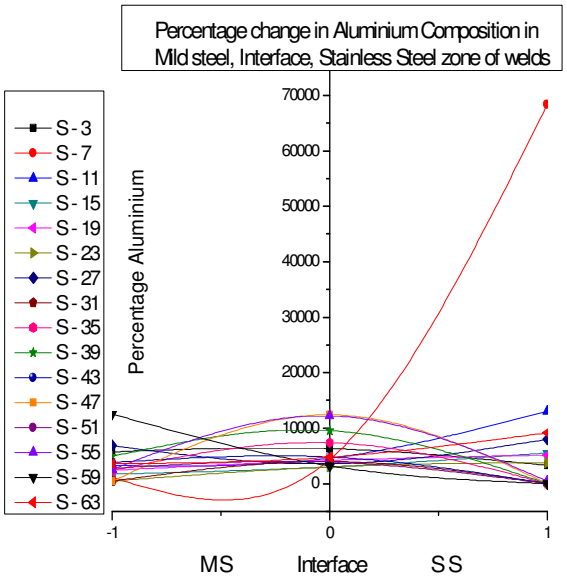

Figure 5.52 Percentage change in Aluminium composition in different zones

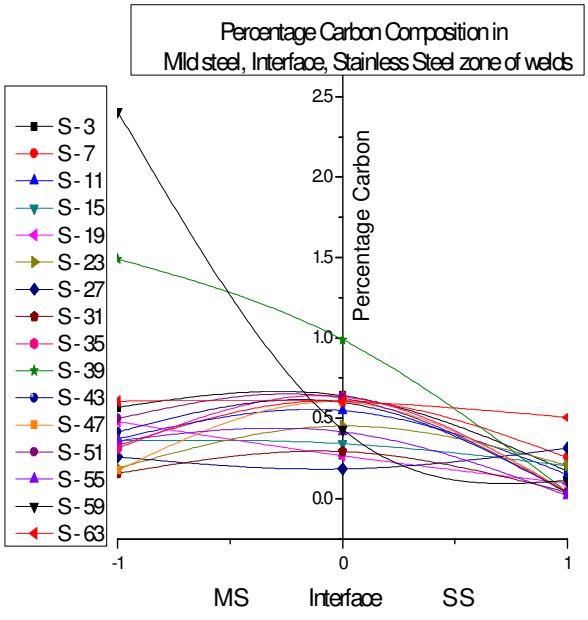

Figure 5.53 Percentage Carbon composition in different zones

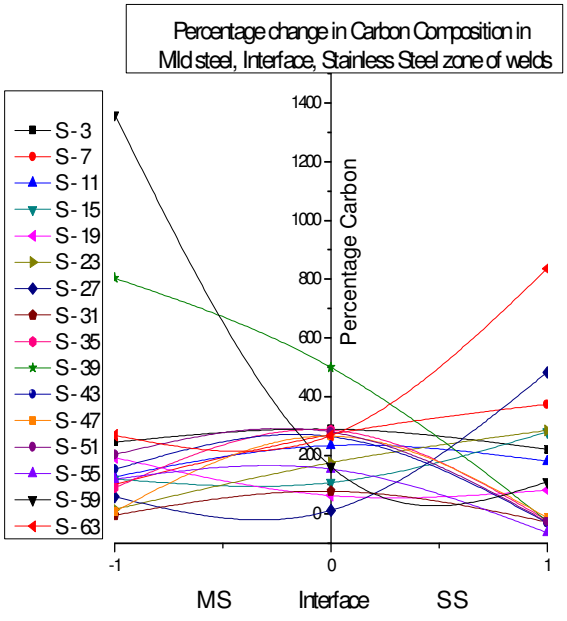

Figure 5.54 Percentage change in Carbon composition in different zones

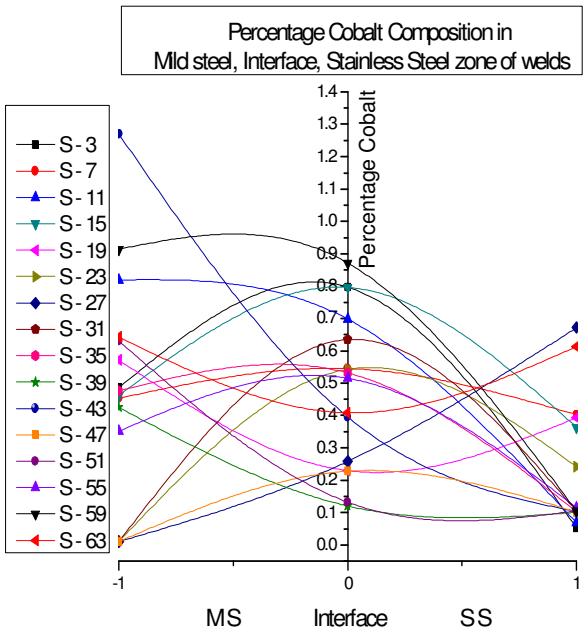

Figure 5.55 Percentage Cobalt composition in different zones

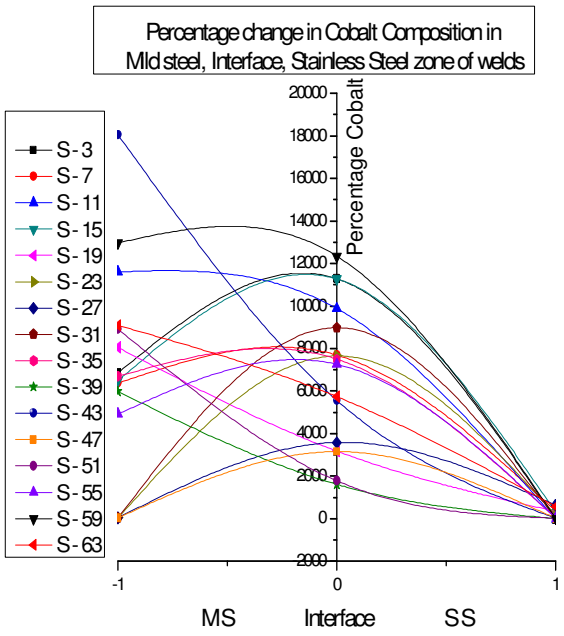

Figure 5.56 Percentage change in Cobalt composition in different zones

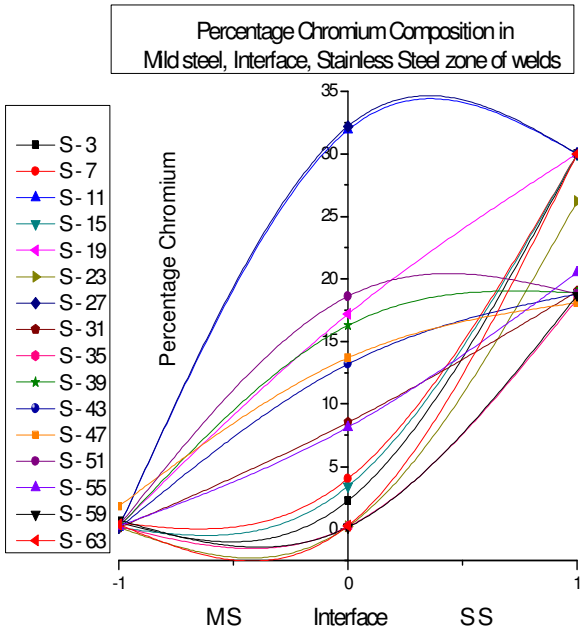

Figure 5.57 Percentage Chromium composition in different zones

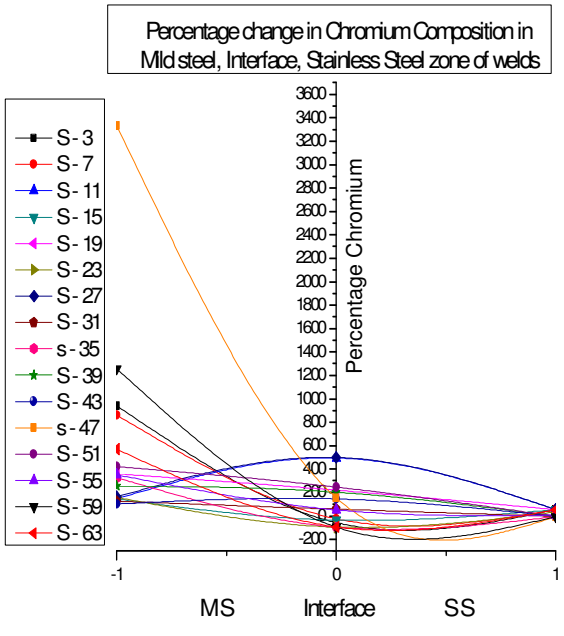

Figure 5.58 Percentage change in Chromium composition in different zones

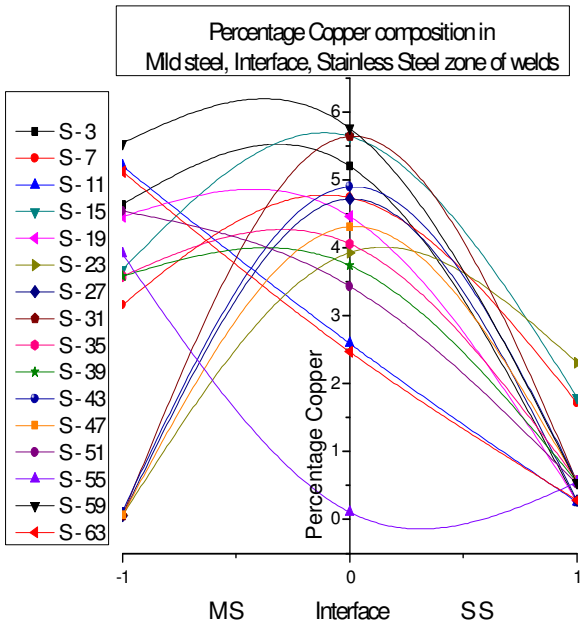

Figure 5.59 Percentage Copper composition in different zones

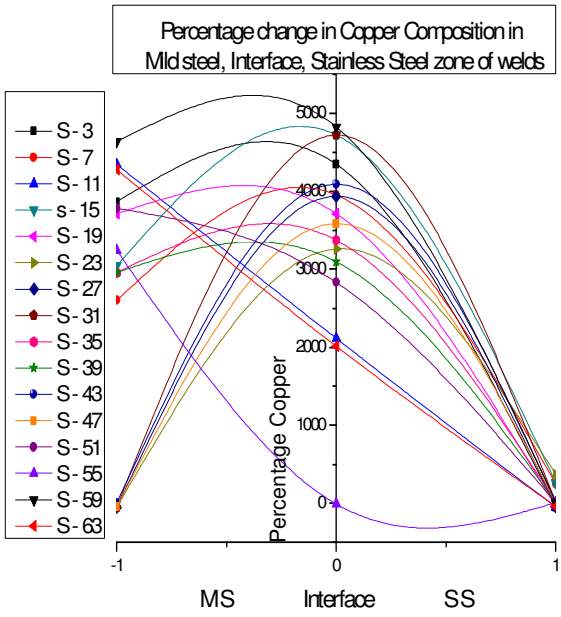

Figure 5.60 Percentage change in Copper composition in different zones

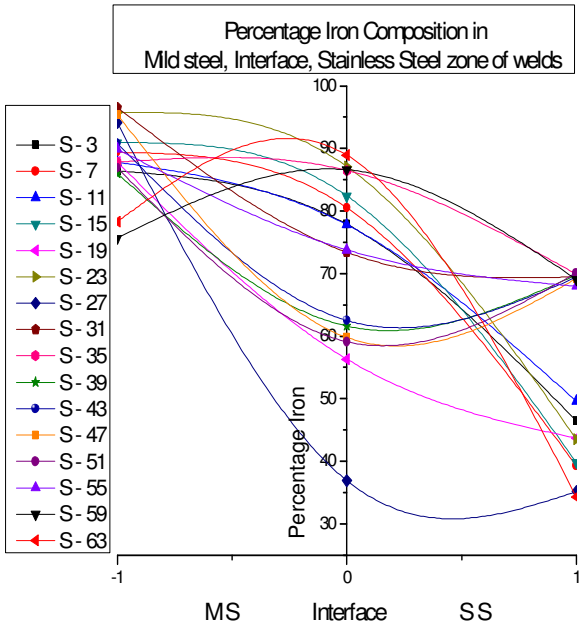

Figure 5.61 Percentage Iron composition in different zones

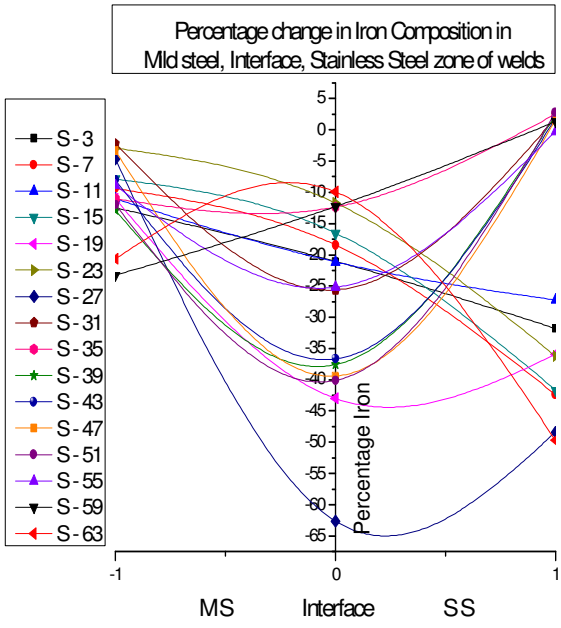

Figure 5.62 Percentage change in Iron composition in different zones

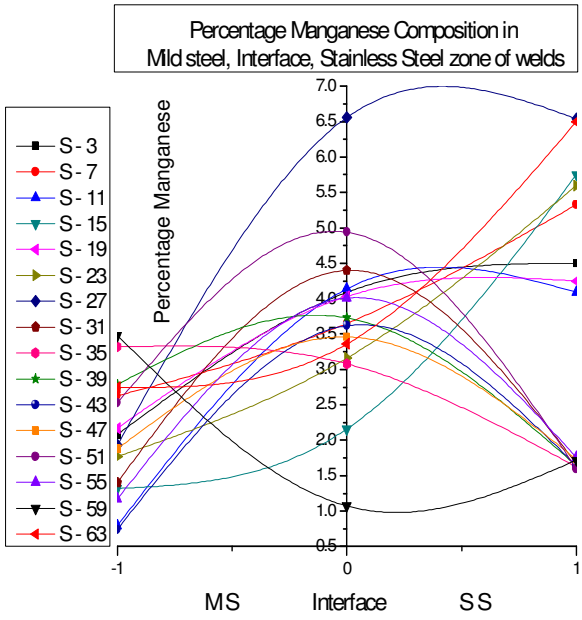

Figure 5.63 Percentage Manganese composition in different zones

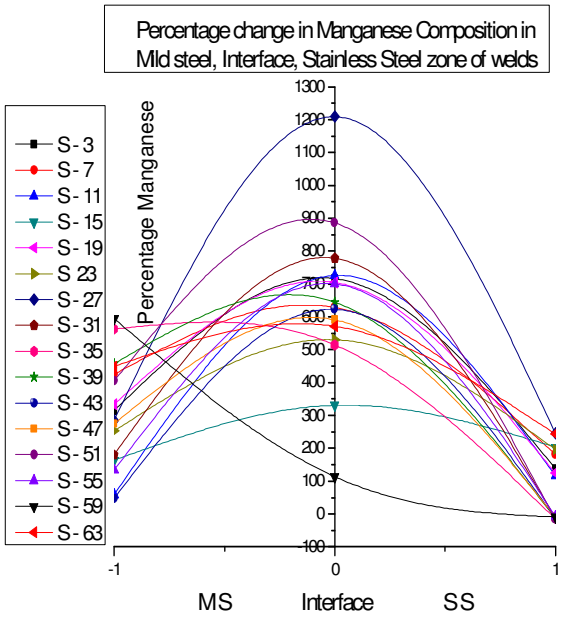

Figure 5.64 Percentage change in Manganese composition in different zones

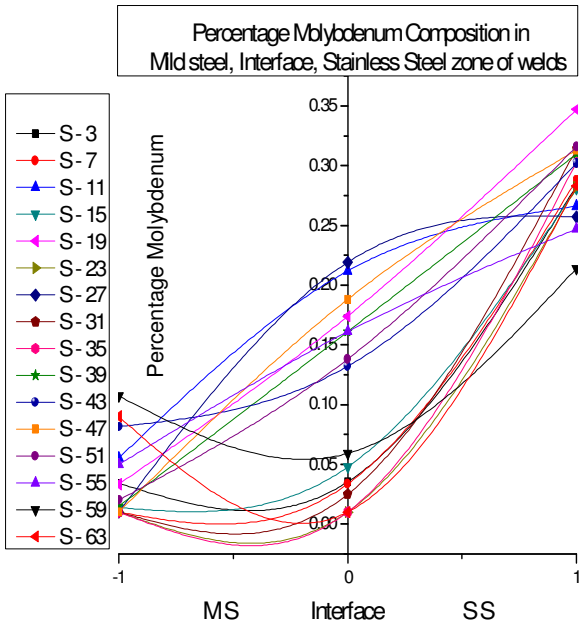

Figure 5.65 Percentage Molybdenum composition in different zones

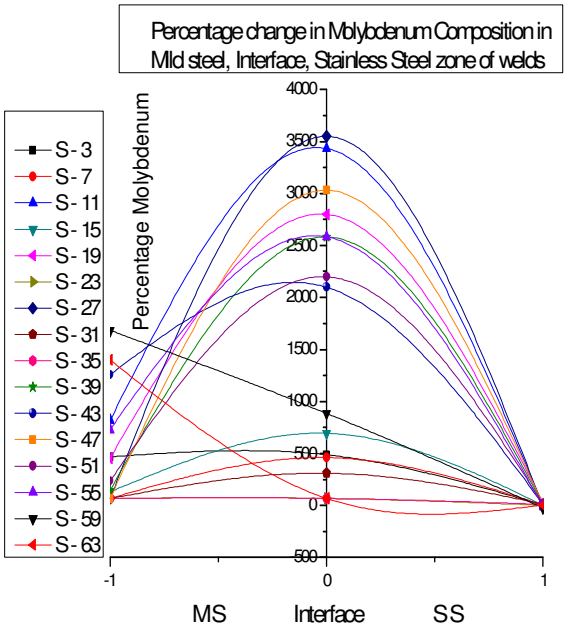

Figure 5.66 Percentage change in Molybdenum composition in different zones

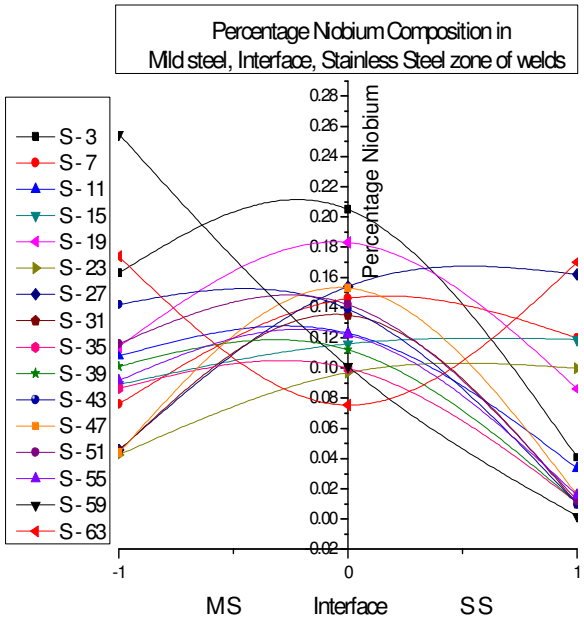

Figure 5.67 Percentage Niobium composition in different zones

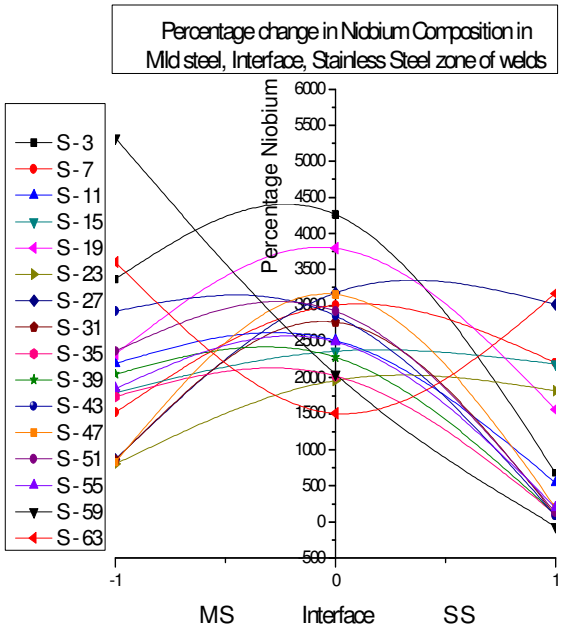

Figure 5.68 Percentage change in Niobium composition in different zones

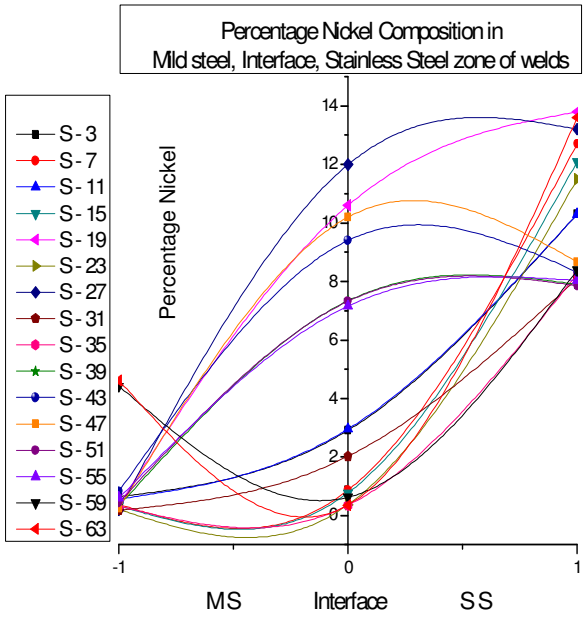

Figure 5.69 Percentage Nickel composition in different zones

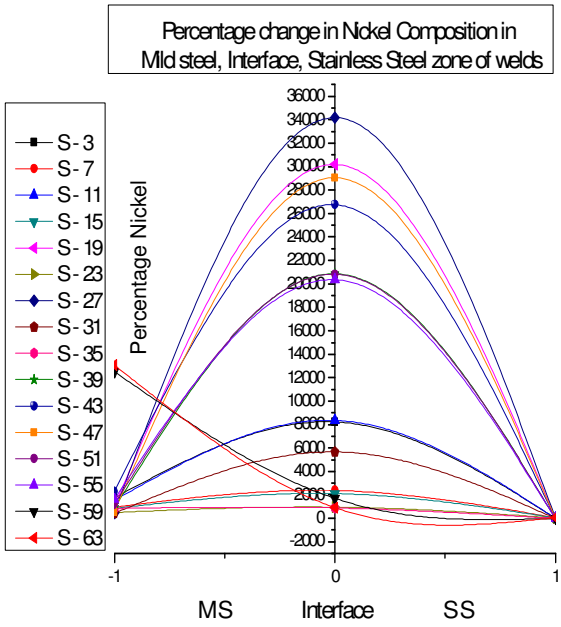

Figure 5.70 Percentage change in Nickel composition in different zones

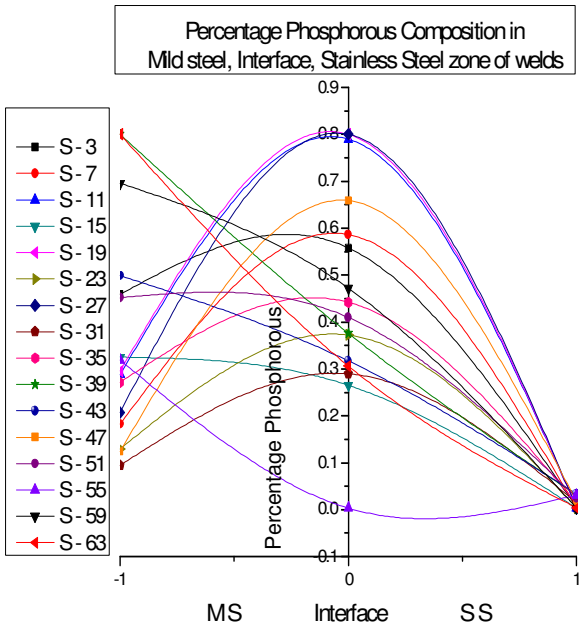

Figure 5.71 Percentage Phosphorous composition in different zones

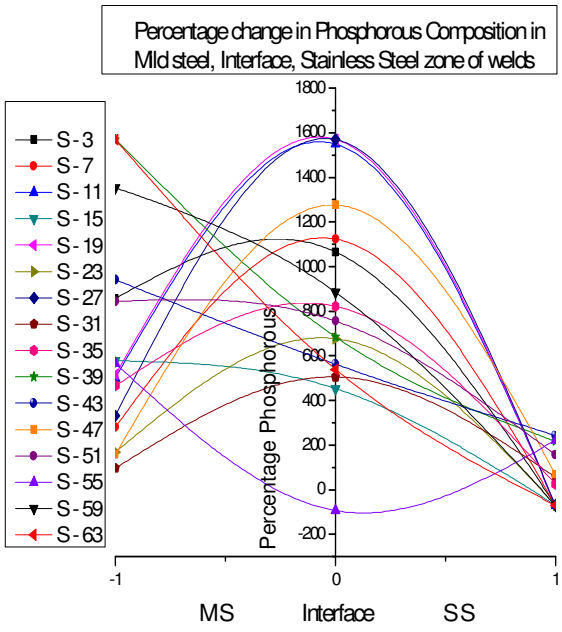

Figure 5.72 Percentage change in Phosphorous composition in different zones

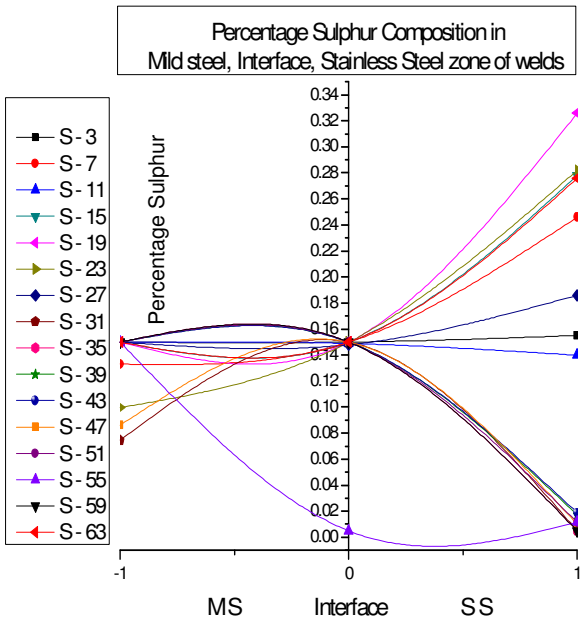

Figure 5.73 Percentage Sulphur composition in different zones

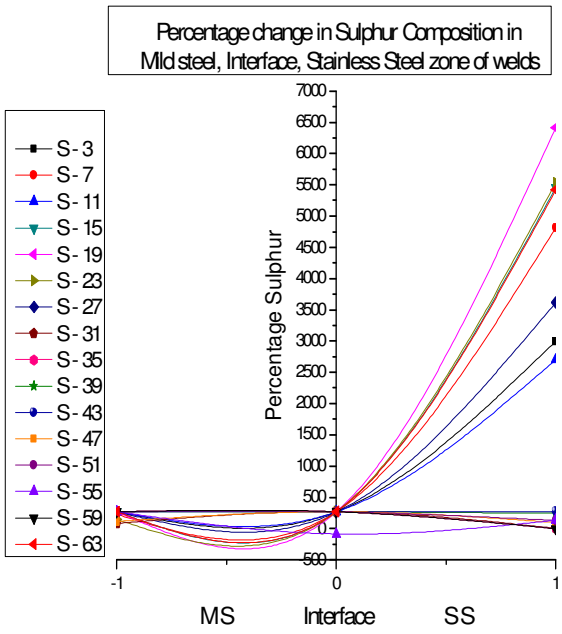

Figure 5.74 Percentage change in Sulphur composition in different zones

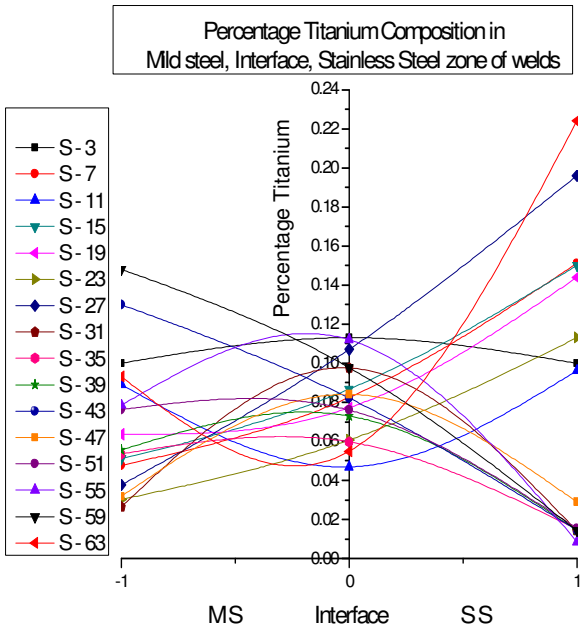

Figure 5.75 Percentage Titanium composition in different zones

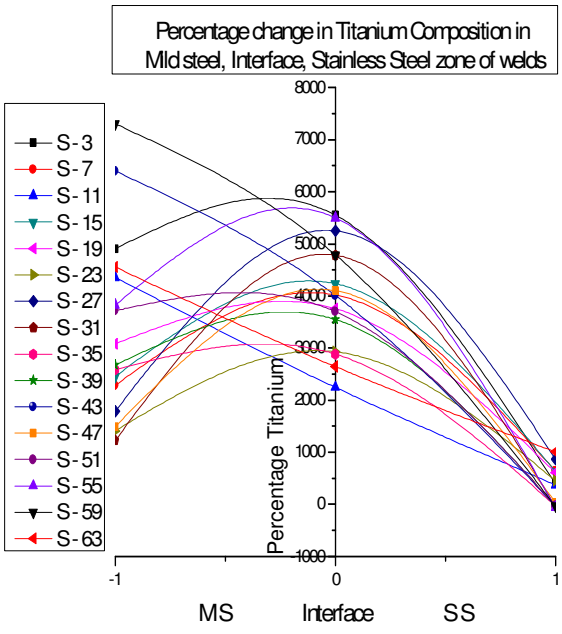

Figure 5.76 Percentage change in Titanium composition in different zones

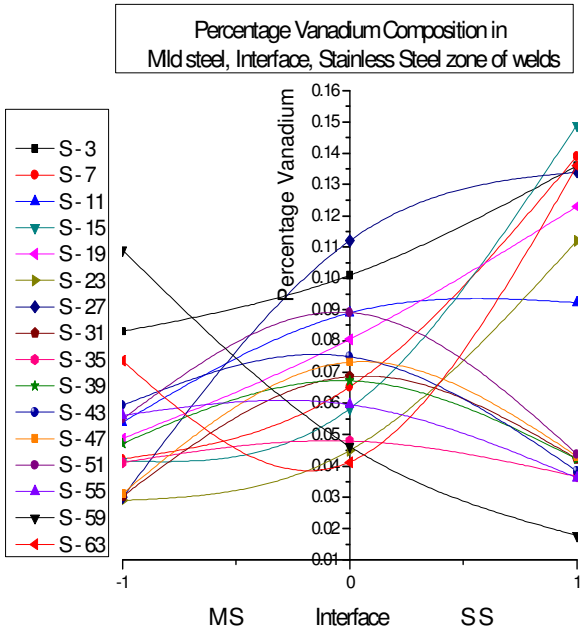

Figure 5.77 Percentage Vanadium composition in different zones

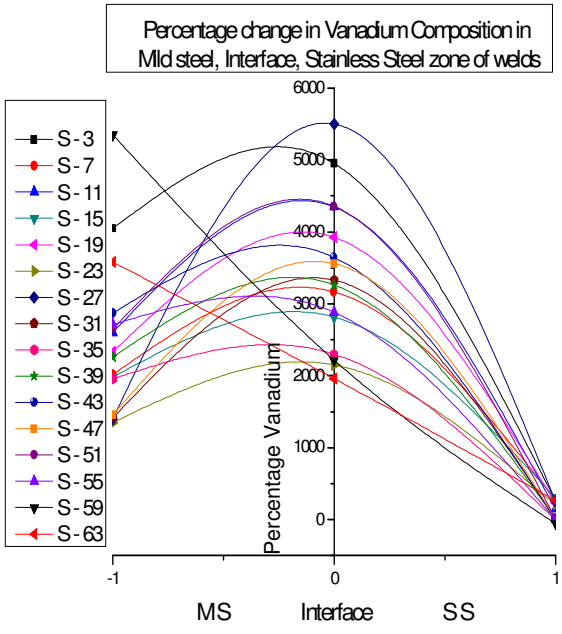

Figure 5.78 Percentage change in Vanadium composition in different zones

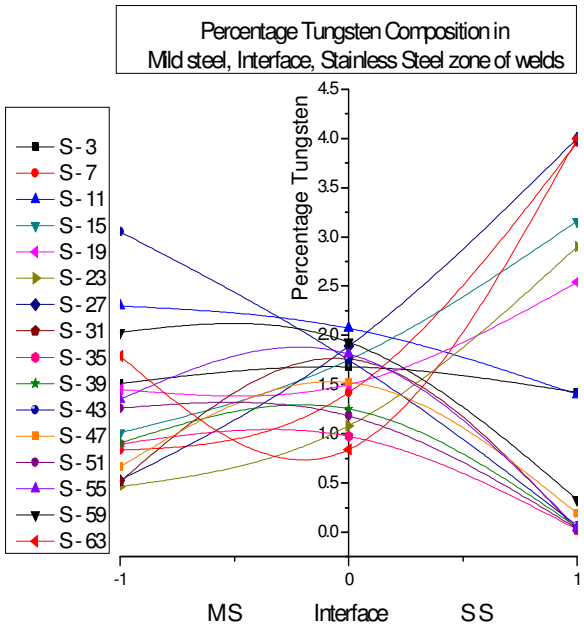

Figure 5.79 Percentage Tungsten composition in different zones

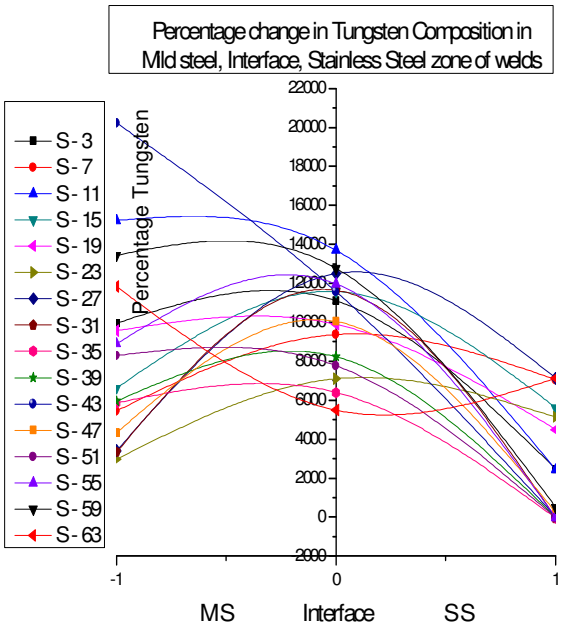

Figure 5.80 Percentage change in Tungsten composition in different zones

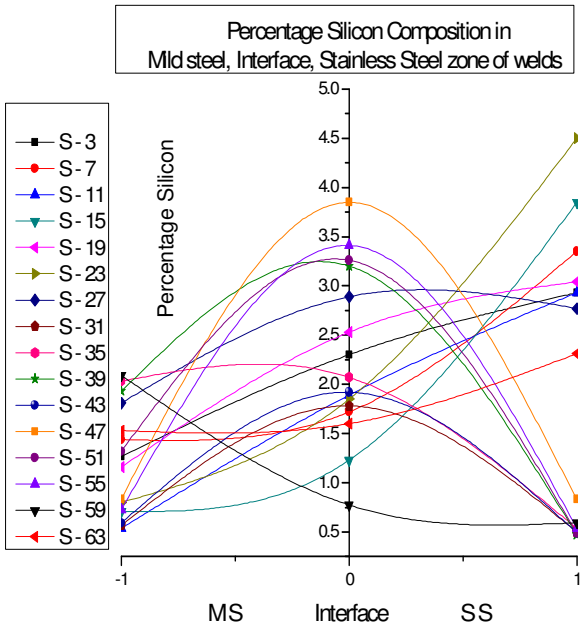

Figure 5.81 Percentage Silicon composition in different zones

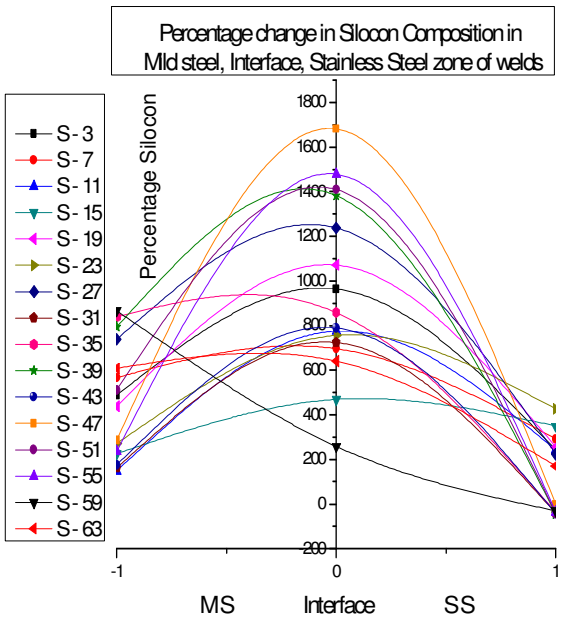

Figure 5.82 Percentage change in silicon composition in different zones

Specimen no.	Mild Steel			Interface						Stainless Steel			
	C	Mn	S	C	Cr	Mn	Ni	S	V	C	Cr	Ni	V
3	0.568	2.08	0.15	0.641	2.3	4.09	2.91	0.15	0.101	0.173	30	10.3	0.136
7	0.331	2.63	0.133	0.611	4.03	3.65	0.866	0.15	0.0653	0.256	30	12.7	0.139
11	0.373	0.794	0.15	0.549	31.9	4.14	2.96	0.149	0.0889	0.151	30	10.3	0.0922
15	0.362	1.32	0.15	0.342	3.44	2.16	0.773	0.15	0.0583	0.205	30	12.1	0.149
19	0.481	2.17	0.15	0.268	17.2	4.03	10.6	0.15	0.0805	0.0976	30	13.8	0.123
23	0.19	1.77	0.0997	0.452	0.219	3.16	0.37	0.15	0.045	0.208	26.2	11.5	0.112
27	0.267	1.93	0.15	0.185	32.2	6.56	12	0.148	0.112	0.315	30	13.2	0.134
31	0.157	1.4	0.0744	0.293	8.53	4.4	2.02	0.15	0.0686	0.0394	19	8.09	0.0423
35	0.313	3.32	0.15	0.635	0.211	3.08	0.343	0.15	0.048	0.0422	18.4	8.26	0.0366
39	1.49	2.79	0.15	0.989	16.3	3.73	7.34	0.15	0.0672	0.0409	18.9	7.9	0.0422
43	0.415	0.74	0.15	0.6	13.2	3.62	9.4	0.15	0.0749	0.0376	18.8	8.32	0.0383
47	0.178	1.88	0.0861	0.602	13.7	3.46	10.2	0.15	0.0732	0.0472	18.1	8.67	0.0431
51	0.499	2.53	0.15	0.262	18.6	4.94	7.32	0.15	0.0891	0.0395	18.8	7.86	0.0438
55	0.36	1.17	0.15	0.417	8.15	4.01	7.16	0.005	0.0596	0.0195	20.5	8.03	0.0362
59	2.41	3.48	0.15	0.431	0.166	1.07	0.627	0.15	0.0463	0.113	18.7	8.4	0.0178
63	0.607	2.75	0.15	0.605	0.293	3.36	0.352	0.15	0.0412	0.506	30	13.6	0.136

Table 5.3 Chemical composition at different zones of weld

Discussion of chemical composition results: The graphs in Figure 5.51-5.82 show the element percentage composition and element percentage change for MS, Interface and SS regions of friction welded joints. It is observed that at the interface there is a sudden increase in various elemental compositions such as Carbon, Aluminium, Chromium, Nickel, Cobalt and Manganese. This increase is because of elemental diffusion from stainless steel and mild steel regions towards interface. It is clearly evident that carbon diffusion takes place from MS, SS regions towards the MS HAZ, weld interface and SS HAZ regions. In case of Cobalt, diffusion takes place towards MS HAZ and weld interface. In case of Chromium, the diffusion occurs on MS HAZ region and weld interface. In case of manganese, the diffusion occurs towards weld interface from SS and MS regions. In case of Nickel, diffusion occurs from SS region towards interface.

5.2 MICROSCOPIC BEHAVIOUR

5.2.1 Microstructure Examination of Friction Welded Joints

On SS - Microstructure on SS side, NI SS – Microstructure near interface on SS side, On I- Microstructure on Interface, NI MS – Microstructure near interface on MS side, On MS – Microstructure on MS side.

Figure 5.83 on SS (3)

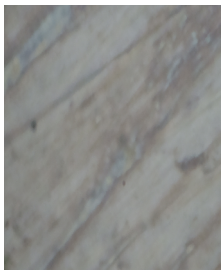

Figure 5.84 NI SS (3)

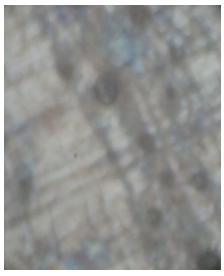

Figure 5.85 on I (3)

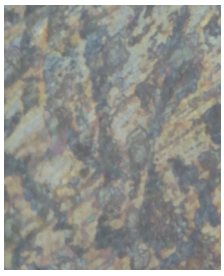

Figure 5.86 NI MS (3)

Figure 5.87 on MS (3)

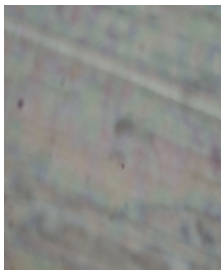

Figure 5.88 on SS (7)

Figure 5.89 NI SS (7)

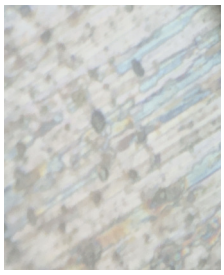

Figure 5.90 on I (7)

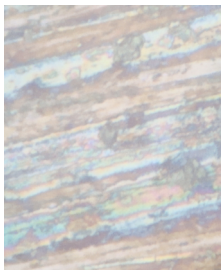

Figure 5.91 on MS (7)

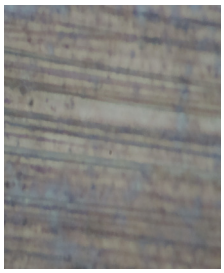

Figure 5.92 on SS (11)

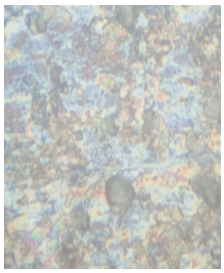

Figure 5.93 NI SS (11)

Figure 5.94 on I (11)

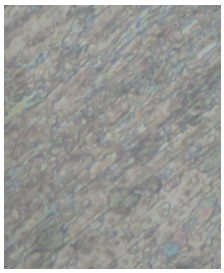

Figure 5.95 NI MS (11)

Figure 5.96 on MS (11)

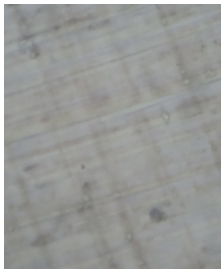

Figure 5.97 on SS (15)

Figure 5.98 NI SS (15)

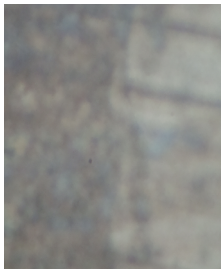

Figure 5.99 on I (15)

Figure 5.100 NI MS (15)

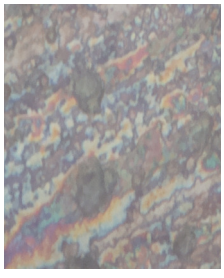

Figure 5.101 on MS (15)

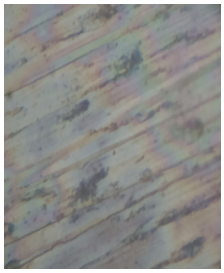
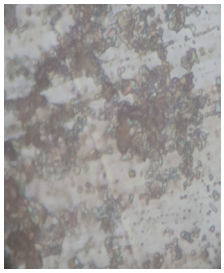
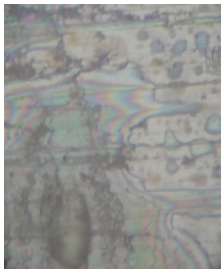
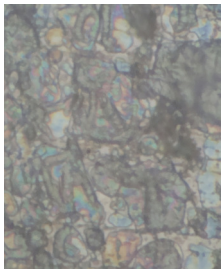


Figure 5.102 on SS (19) Figure 5.103 NI SS (19) Figure 5.104 on I (19) Figure 5.105 NI MS (19) Figure 5.106 on MS (19)


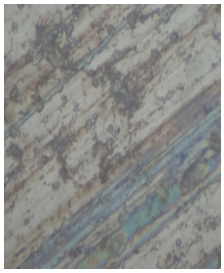
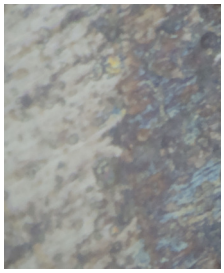

Figure 5.107 on SS (23) Figure 5.108 NI SS (23) Figure 5.109 on I (23) Figure 5.110 NI MS (23) Figure 5.111 on MS (23)



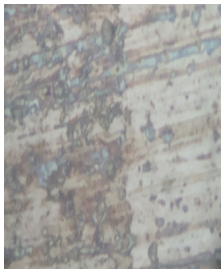
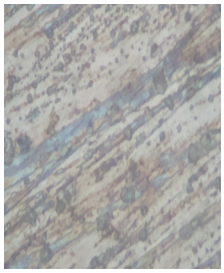


Figure 5.112 on SS (27) Figure 5.113 NI SS (27) Figure 5.114 on I (27) Figure 5.115 NI MS (27) Figure 5.116 on MS (27)

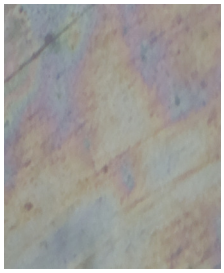


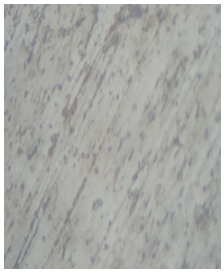

Figure 5.117 on SS (31) Figure 5.118 on I (31) Figure 5.119 NI MS (31) Figure 5.120 on MS (31)

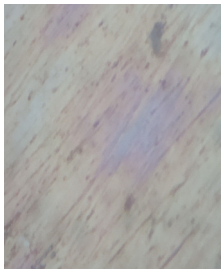


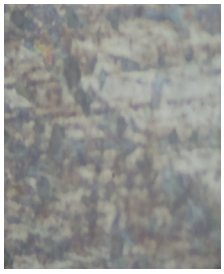


Figure 5.121 on SS (35) Figure 5.122 NI SS (35) Figure 5.123 on I (35) Figure 5.124 NI MS (35) Figure 5.125 on MS (35)




Figure 5.126 on SS (39) Figure 5.127 on I (39) Figure 5.128 NI MS (39) Figure 5.129 on MS (39)

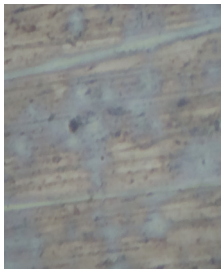
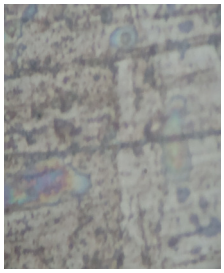
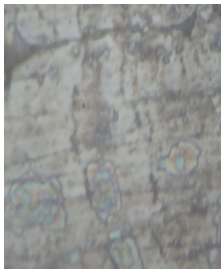
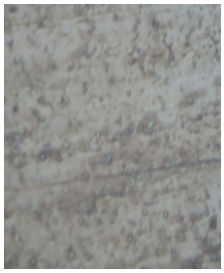

Figure 5.130 on SS (43) Figure 5.131 on I (43) Figure 5.132 NI MS (43) Figure 5.133 on MS (43)

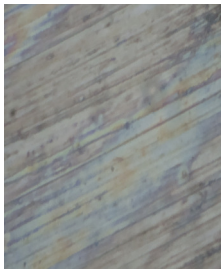


Figure 5.134 on SS (47) Figure 5.135 on I (47) Figure 5.136 NI MS (47) Figure 5.137 on MS (47)

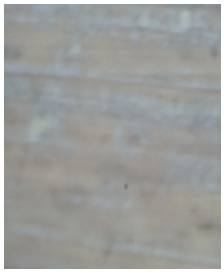
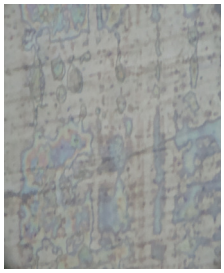
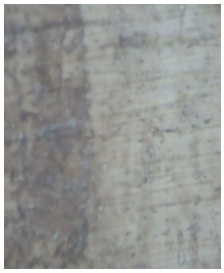
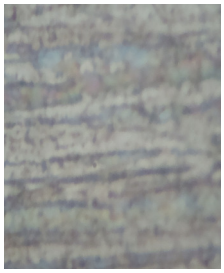

Figure 5.138 on SS (51) Figure 5.139 NI SS (51) Figure 5.140 on I (51) Figure 5.141 on MS (51)



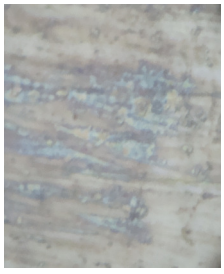
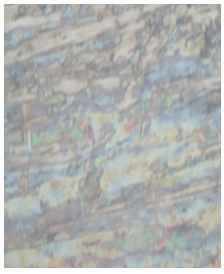
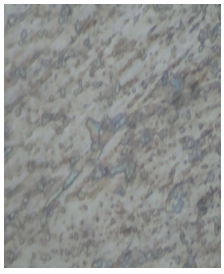

Figure 5.142 on SS (55) Figure 5.143 NI SS (55) Figure 5.144 on I (55) Figure 5.145 NI MS (55) Figure 5.146 on MS (55)

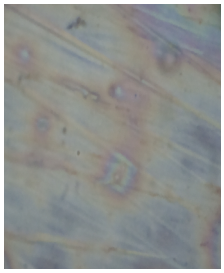


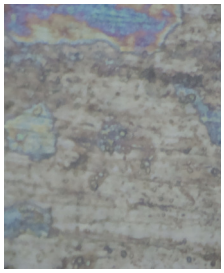


Figure 5.147 on SS (59) Figure 5.148 NI SS (59) Figure 5.149 in I (59) Figure 5.150 NI MS (59) Figure 5.151 on MS (59)

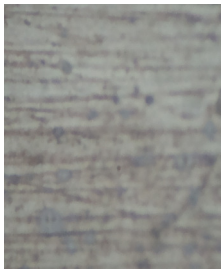

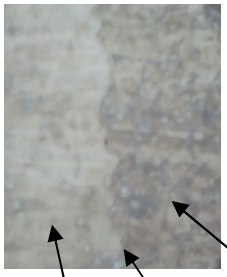

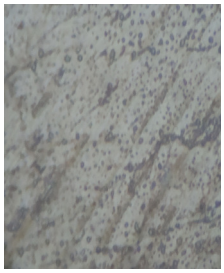

Figure 5.152 on SS (63) Figure 5.153 NI SS (63) Figure 5.154 on I (63) Figure 5.155 NI MS (63) Figure 5.156 on MS (63)


Figure 5.157 Base SS Figure 5.158 Base MS

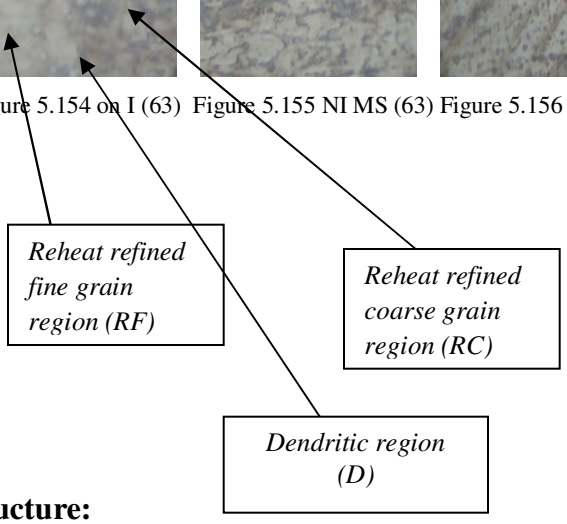

5.2.1.1 Discussion of Optical Microstructure:

5.2.1.1.1 Base Material

The microstructure of mild steel base at magnifications of 400X is shown in Figure 5.158. The micro-graph of the figure reveals the presence of typical ferrite (bright)-pearlite (dark) microstructure. The density of flow lines i.e. banding and the morphology of ferrite and pearlite has been found to vary in specimens. The microstructure of stainless steel base at magnifications of 400X is shown in Figure. The large austenitic grains (Figure 5.157) are clearly visible in the microstructure.

5.2.1.1.2 Weld Metal

Two microstructural regions featured by cast dendrite and reheat refined grains characterize the near interface regions of the weld as shown in in the interface (Figures 5.85, 5.90, 5.94, 5.99, 5.104, 5.109 etc.). The reheat refined region closed to the dendritic boundary develops comparatively coarser grain than the size observed in the reheat refined region away from the dendritic boundary of the interface. Therefore it can be said that the distribution of the microstructure in the weld consists of three distinctly different microstructural regions, such as the dendritic region at interface (D), reheat refined coarse grain region (RC) and reheat refined fine grain region (RF). The microstructures of the different interface regions of weld

metal as revealed in the friction weld are typically shown in the micrographs presented in Figures 5.83-5.158. The distribution of the three different microstructural regions has been found to be similar in all the welds.

The morphologies of the dendritic region at interface (D), coarse grain reheat refined region in MS HAZ (RC), and the grain reheat refined region (RF) in SS HAZ of all the welds have been comprehensively studied at different magnifications under optical microscope. The studies on these three regions of the welds have been typically shown in all Figures. The micrographs depict that the dendritic region (D) is possibly having lower bainite in combination of some amount of fine pearlite with pro-eutectoid ferrite at the grain boundary (Figures 5.85, 5.90, 5.94, 5.99, 5.104, 5.109 etc.). The coarse grain reheat refined region (RC) primarily contains austenite and a mixture of acicular and chunky ferrite (Figure 5.84, 5.89, 5.93, 5.98 etc.) whereas, the fine grain reheat refined region MS HAZ has been found to primarily consists of ferrite and pearlite (Figure 5.86, 5.96, 5.100, 5.105 etc.). The variation in coarseness of the morphology of different welds, as revealed in the weld joints, inherently occurs at different locations of different welds depending upon randomness and heterogeneity in distribution of weld temperature cycle. Thus, it may be concluded that the morphology of the weld prepared varies within a broad range of coarseness as typically marked in the micrographs.

5.2.2 Micro hardness Measurements

5.2.2.1 Micro hardness measurement along the weld: The following are the graphs showing micro hardness on different specimens along the weld:

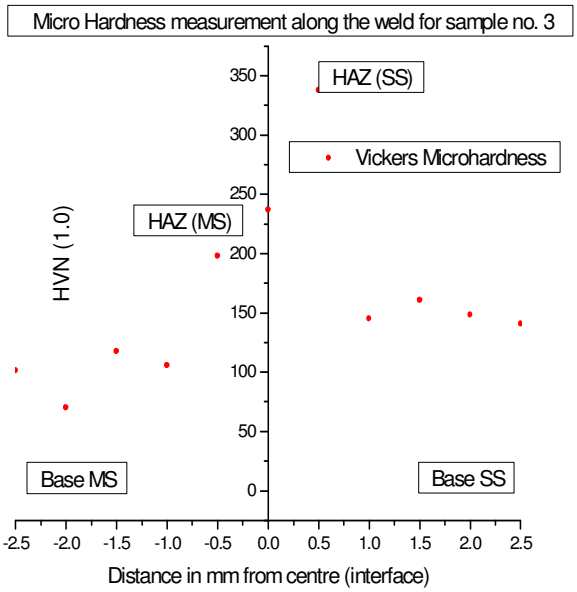

Figure 5.159 Micro hardness measurement along the weld for specimen no. 3

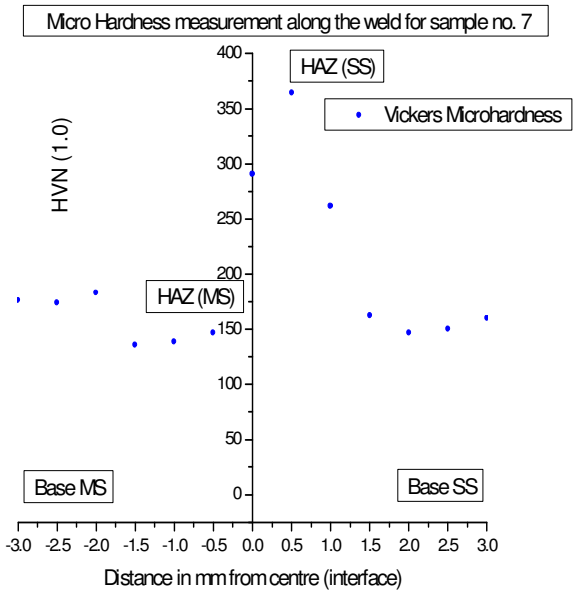

Figure 5.160 Micro hardness measurement along the weld for specimen no. 7

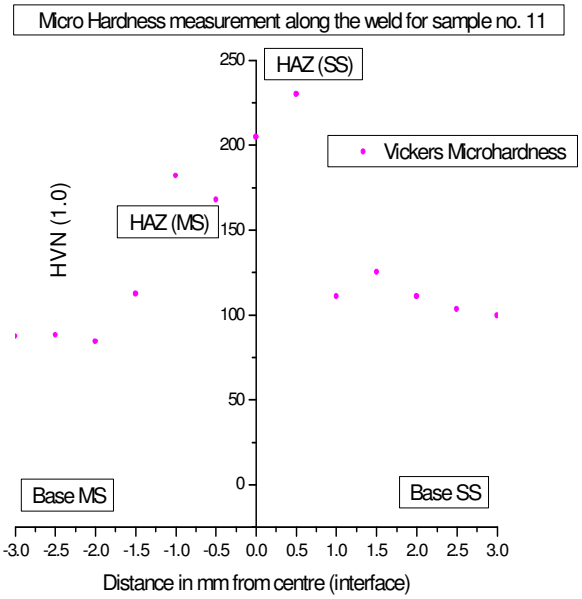

Figure 5.161 Micro hardness measurement along the weld for specimen no. 11

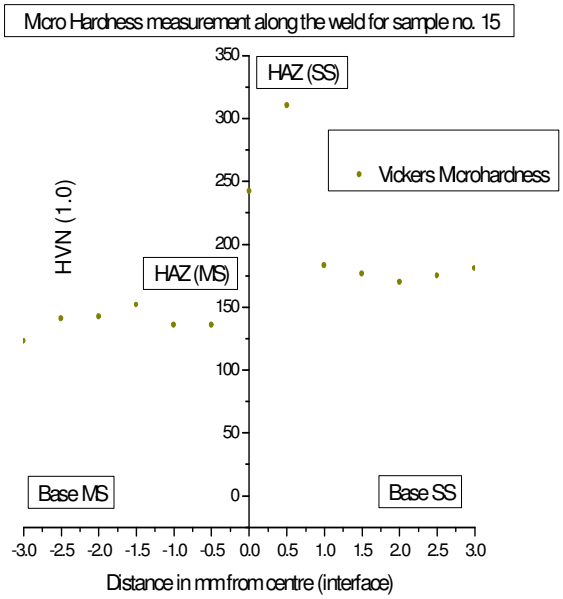

Figure 5.162 Micro hardness measurement along the weld for specimen no. 15

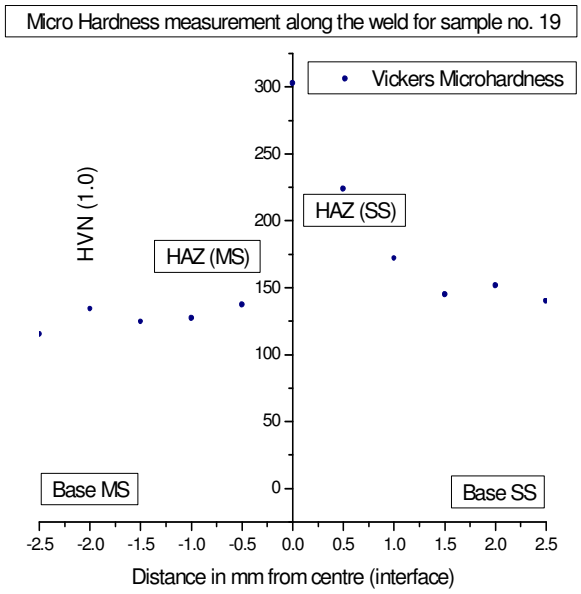

Figure 5.163 Micro hardness measurement along the weld for specimen no. 19

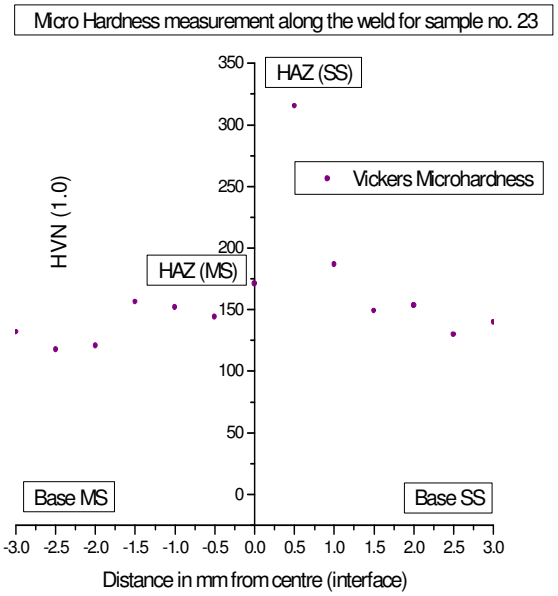

Figure 5.164 Micro hardness measurement along the weld for specimen no. 23

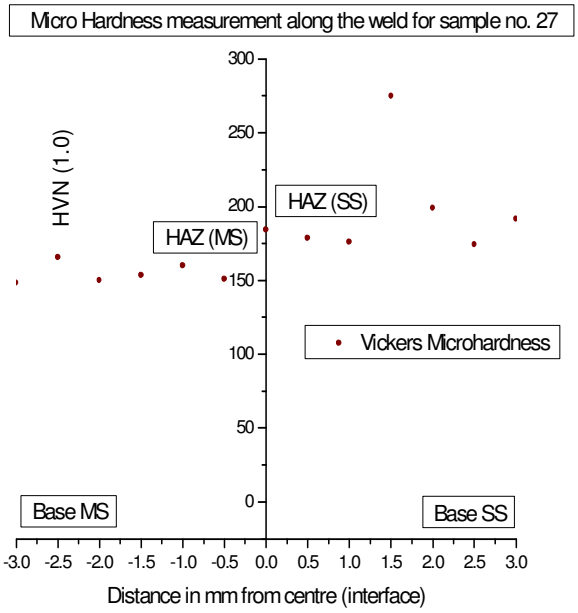

Figure 5.165 Micro hardness measurement along the weld for specimen no. 27

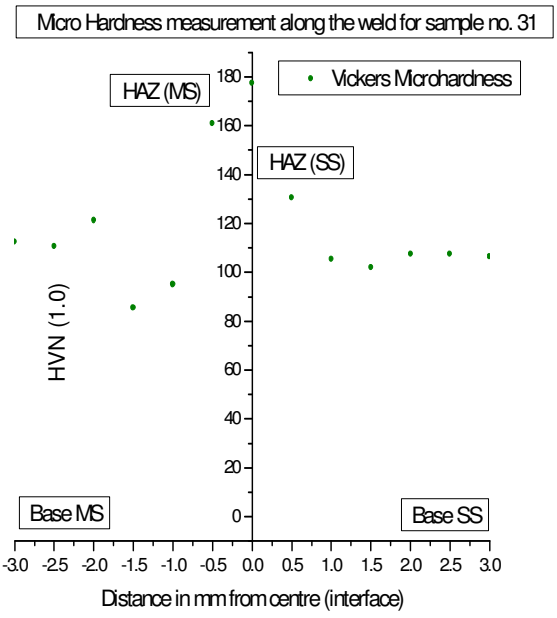

Figure 5.166 Micro hardness measurement along the weld for specimen no. 31

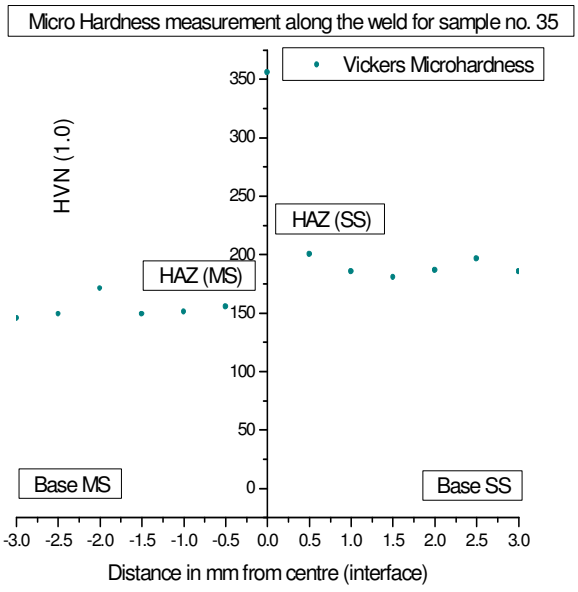

Figure 5.167 Micro hardness measurement along along the weld for specimen no. 35

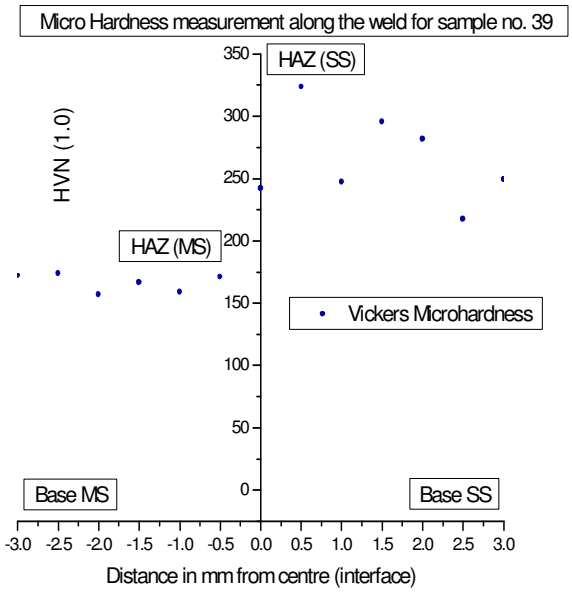

Figure 5.168 Micro hardness measurement the weld for specimen no. 39

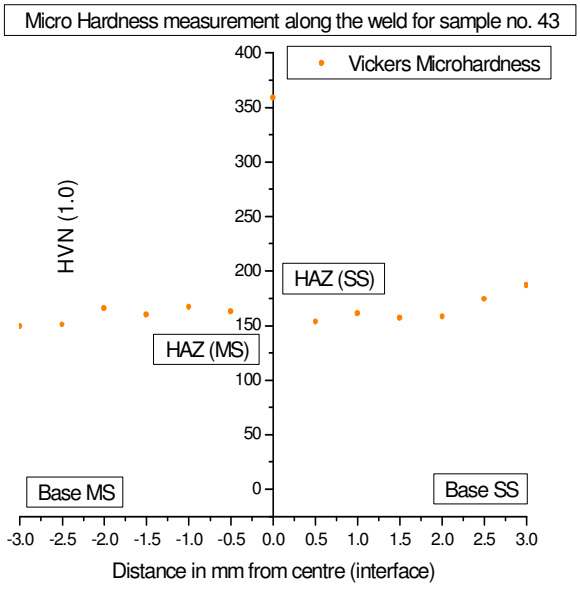

Figure 5.169 Micro hardness measurement along along the weld for specimen no. 43

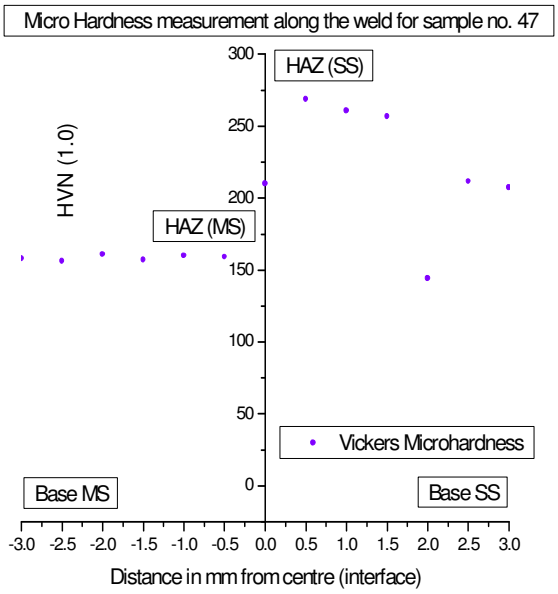

Figure 5.170 Micro hardness measurement the weld for specimen no. 47

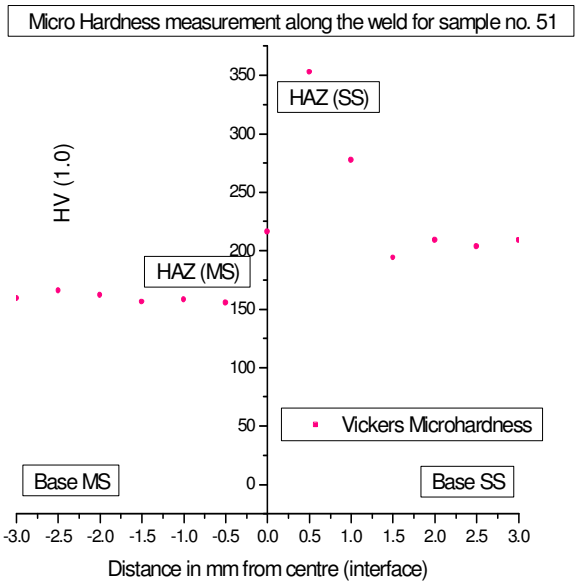

Figure 5.171 Micro hardness measurement along along the weld for specimen no. 51

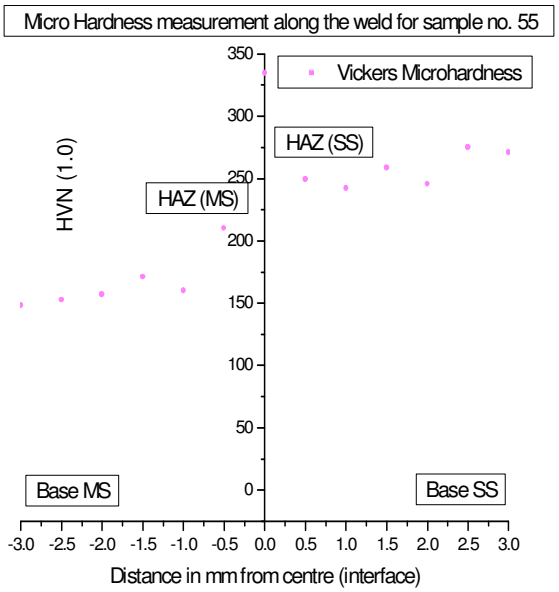

Figure 5.172 Micro hardness measurement the weld for specimen no. 55

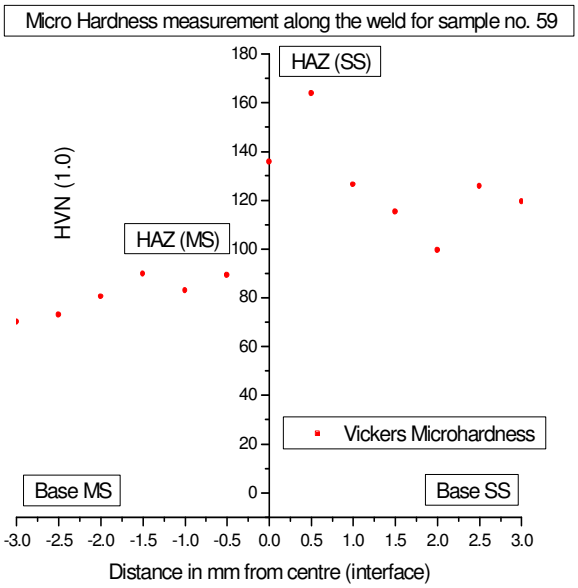

Figure 5.173 Micro hardness measurement along along the weld for specimen no. 59

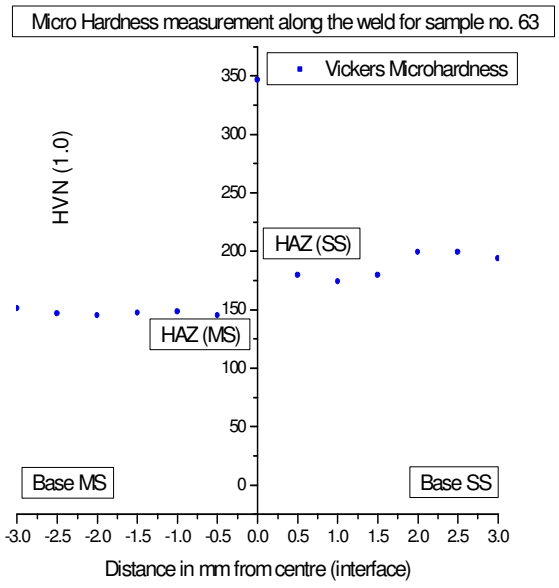

Figure 5.174 Micro hardness measurement the weld for specimen no. 63

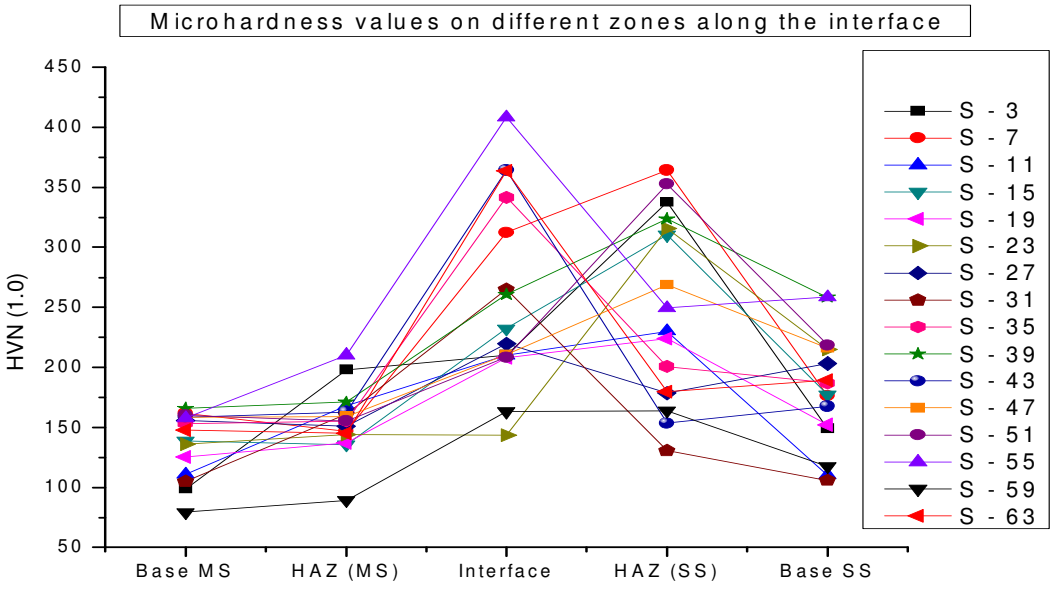

Figure 5.175 Micro hardness distribution along the weld on different zones

Discussion of Micro hardness measurement along the weld: Micro hardness measurements are taken at the base metal (Mild Steel side), HAZ (Mild Steel side), at interface, HAZ (Stainless Steel side), base metal (Stainless Steel side). Vickers micro hardness test was used and the micro harness measurements were done. Six readings at each location were taken & the average of the six readings was taken for analysis.

Micro hardness variations have been studied. A maximum micro hardness of 408.3392 H_v has been obtained near the weld interface.

Studies on austenitic stainless steel joints using friction welding have reported a decrease in micro hardness at the interface zone of the joint.

The increase in micro hardness at the welding interface is probably due to friction and oxidation processes which took place during welding processes. This explanation is also corroborated by microscopic studies which revealed a plastically deformed zone at the weld interface. The highest micro hardness values are found to be at the weld interface and at the HAZ (Stainless Steel side). This area seems to have borne the burnt of the work hardening effect due to the applied forging pressure. Higher upset pressure of about 13560 N in specimens 31, 35, 43, 47 & 55 have yielded higher micro hardness at the weld interface. In other cases, where upset pressure is lower, the micro hardness values at the interface are not so high.

5.2.2.2 Micro hardness measurement at cross section: The following graphs show the micro hardness on different specimens at the cross section:

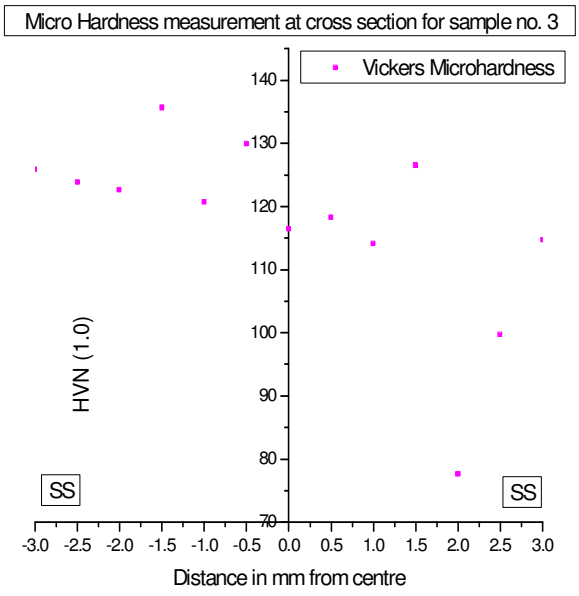

Figure 5.176 Micro hardness measurement at Cross section for specimen no. 3

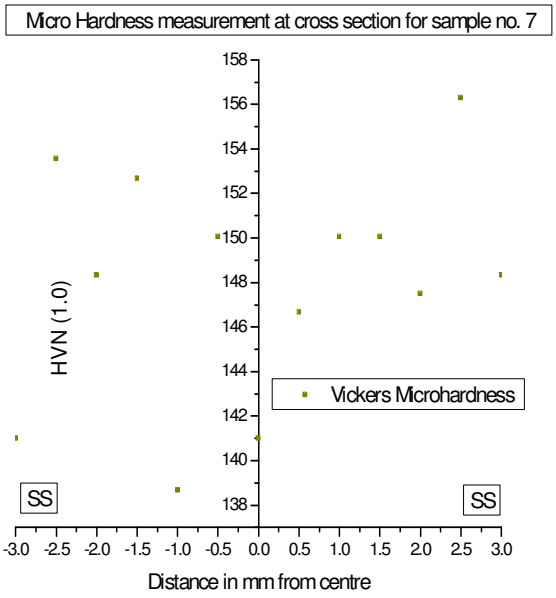

Figure 5.177 Micro hardness measurement at Cross section for specimen no. 7

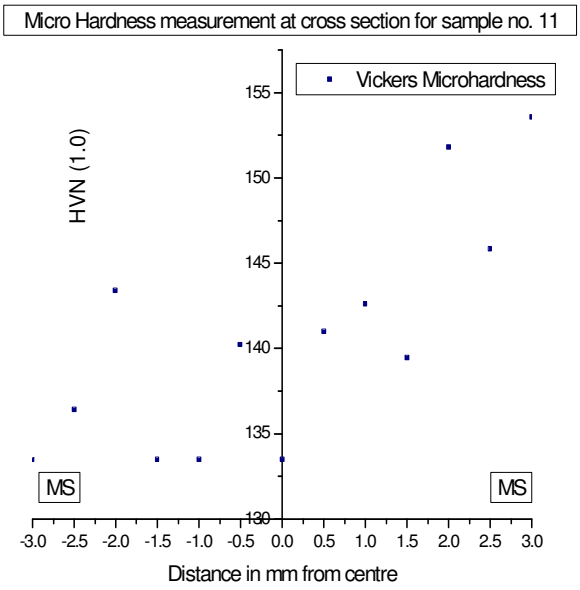

Figure 5.178 Micro hardness measurement at Cross section for specimen no. 11

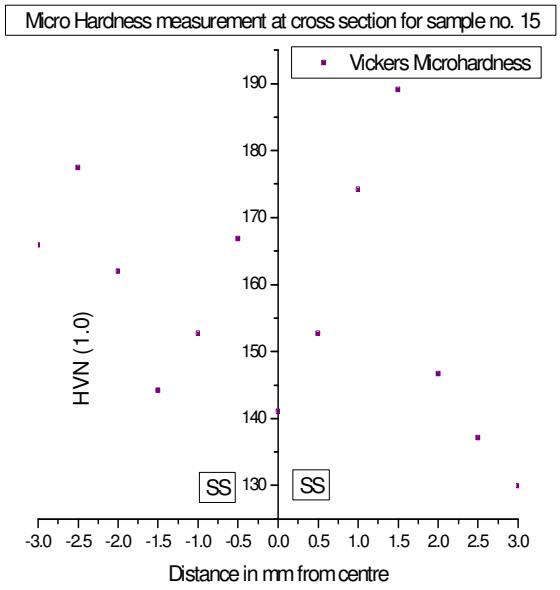

Figure 5.179 Micro hardness measurement at Cross section for specimen no. 15

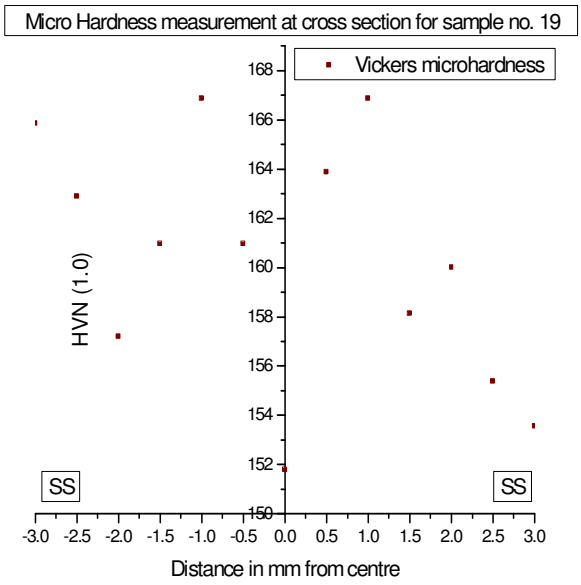

Figure 5.180 Micro hardness measurement at Cross section for specimen no. 19

Figure 5.181 Micro hardness measurement at Cross section for specimen no. 23

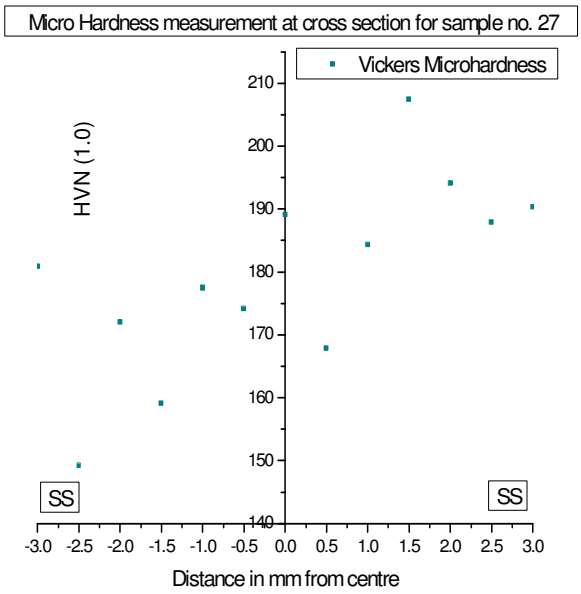

Figure 5.182 Micro hardness measurement at Cross section for specimen no. 27

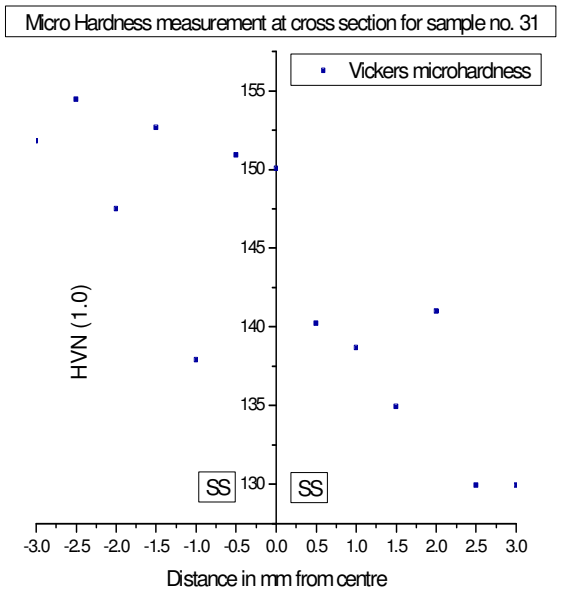

Figure 5.183 Micro hardness measurement at Cross section for specimen no. 31

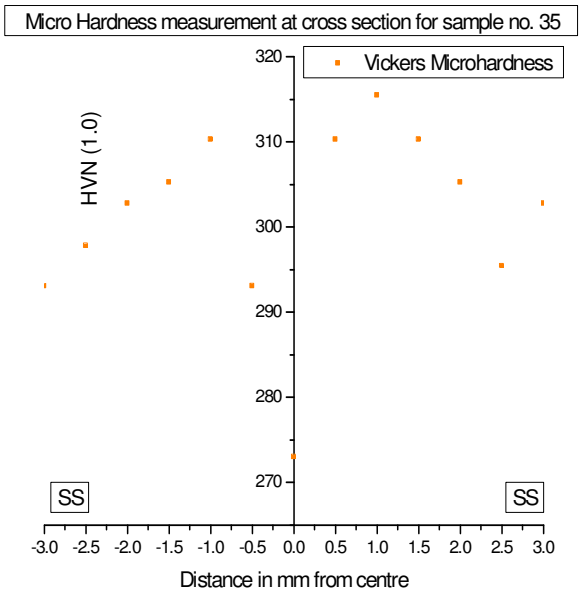

Figure 5.184 Micro hardness measurement at Cross section for specimen no. 35

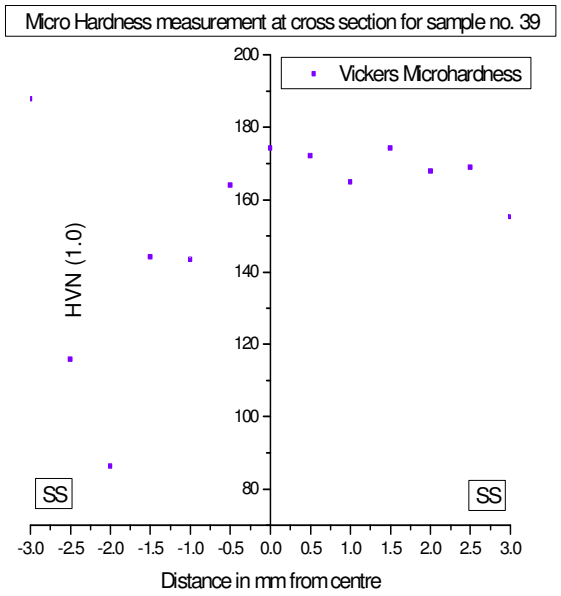

Figure 5.185 Micro hardness measurement at Cross section for specimen no. 39

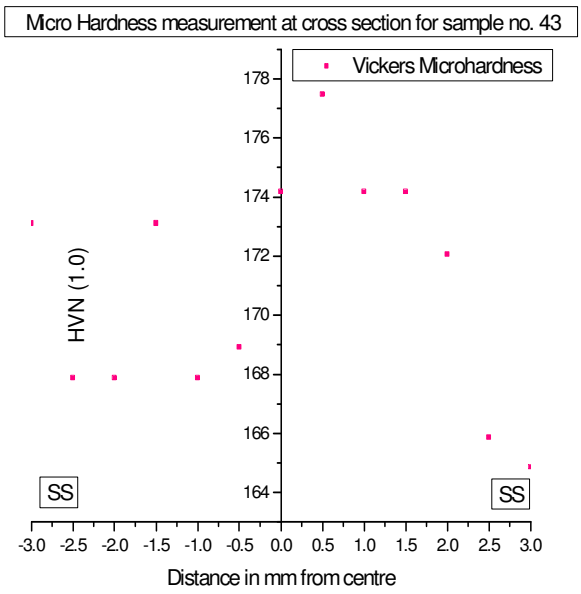

Figure 5.186 Micro hardness measurement at Cross section for specimen no. 43

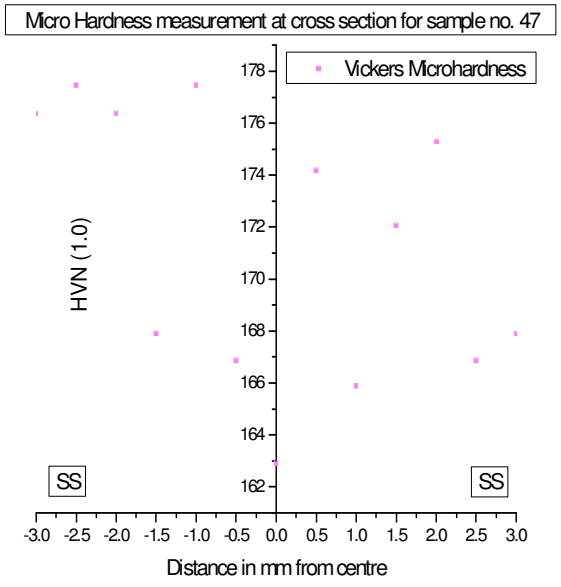

Figure 5.187 Micro hardness measurement at Cross section for specimen no. 47

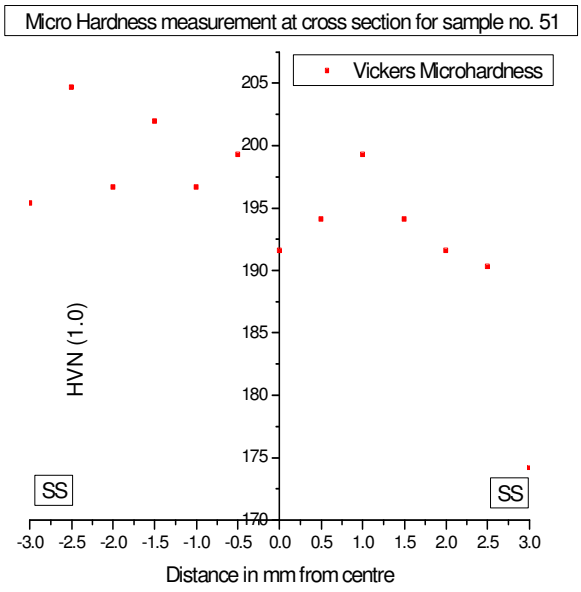

Figure 5.188 Micro hardness measurement at Cross section for specimen no. 51

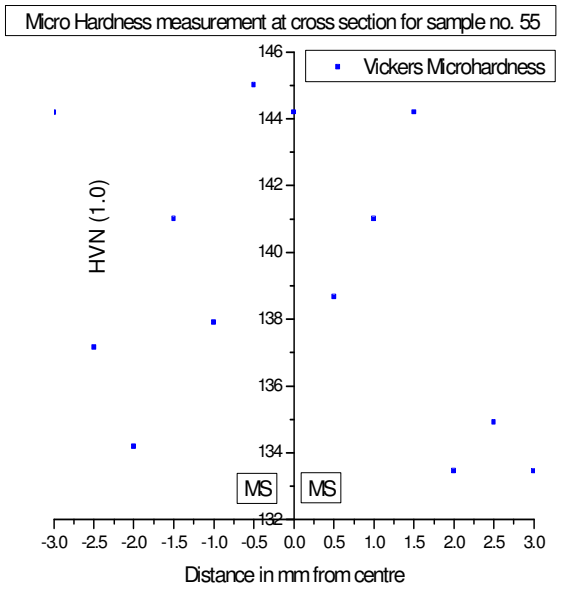

Figure 5.189 Micro hardness measurement at Cross section for specimen no. 55

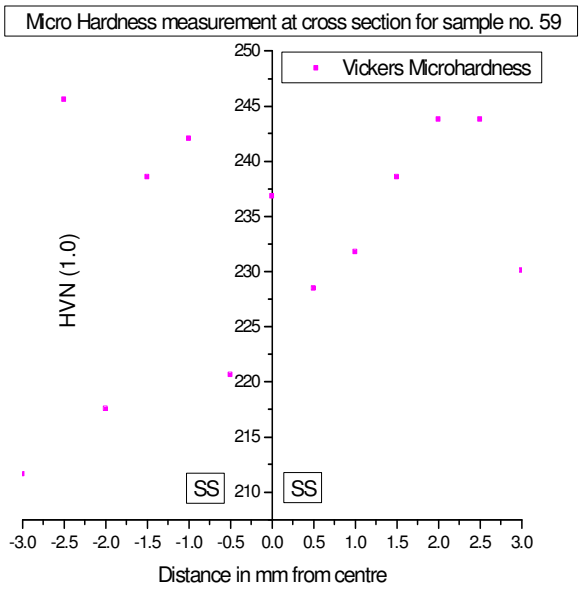

Figure 5.190 Micro hardness measurement at Cross section for specimen no. 59

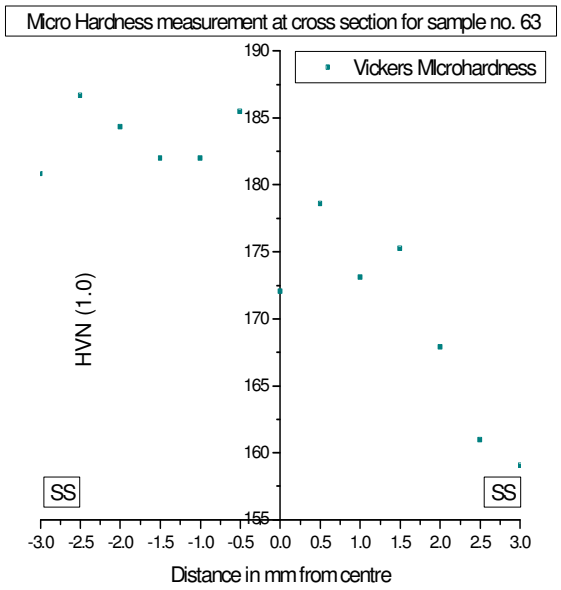

Figure 5.191 Micro hardness measurement at Cross section for specimen no. 63

No. of Experiments (Sample no.)	Parameters				Micro hardness values		
	Friction Force (F) in N	Forge Force (f) in N	Burn off Length (L)mm	RPM (R)	MS	Interface	SS
1 (3)	5650	11300	1.5	1400	98.723	210.28	148.83
2 (7)	7910	11300	1.5	1400	161.61	312.48	176.14
3 (11)	5650	11300	2.5	1400	110.88	210.34	109.99
4 (15)	5650	11300	1.5	1800	138.86	232.36	177.12
5 (19)	7910	11300	2.5	1400	125.30	207.97	152.27
6 (23)	5650	11300	2.5	1800	135.70	143.29	215.02
7 (27)	7910	11300	1.5	1800	155.57	219.75	203.30
8 (31)	7910	11300	2.5	1800	105.05	265.01	105.85
9 (35)	7910	13560	2.5	1800	153.23	341.65	187.03
10 (39)	5650	13560	2.5	1800	165.88	260.61	258.29
11 (43)	7910	13560	1.5	1800	158.58	364.11	167.43
12 (47)	7910	13560	2.5	1400	158.52	210.69	216.17
13 (51)	5650	13560	1.5	1800	160.26	208.30	218.46
14 (55)	7910	13560	1.5	1400	157.85	408.33	258.50
15 (59)	5650	13560	2.5	1400	79.278	163.02	117.36
16 (63)	5650	13560	1.5	1400	147.69	363.85	189.30

Table 5.4 Test matrix for values of micro hardness at interface, on MS & on SS

From the above Table 5.4 it is clear that for sample no. 55 the value of micro hardness is highest and lowest for sample no. 23 at the interface. It is also observed that with the increase in friction force the value of micro hardness increases at the interface. The value of micro hardness is lowest on Mild Steel side for sample no. 59 and highest for sample no. 39. The values on mild steel side are nearly equal for most of the specimens. For sample no. 31 the value of micro hardness is lower and higher for sample no. 55 on Stainless Steel side.

Discussion of Micro hardness measurement at cross section: It is observed that the micro hardness values are higher near the centre of the cross section and decreases as the distance from the centre of cross section increases. The micro hardness is lower for the cross section having more MS region as compared to those having more SS region.

5.2.3 SEM Examination of Friction Welded Bimetallic Joints

The following are the images taken on SEM machine (Figure 5.)

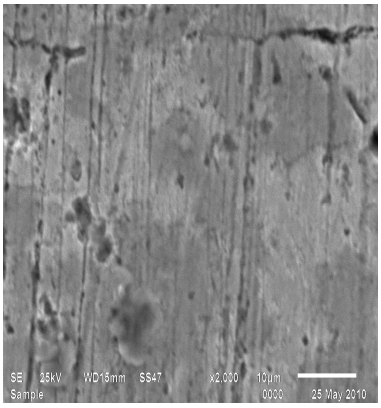

Figure 5.192 SEM measurement on MS side for specimen no. 3

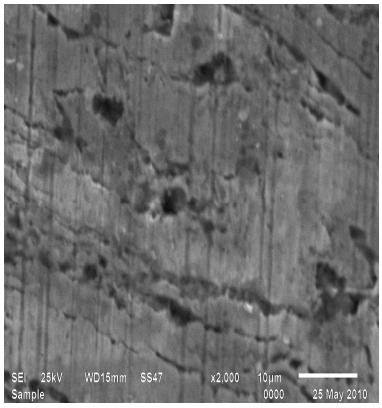

Figure 5.193 SEM measurement on interface for specimen no. 3

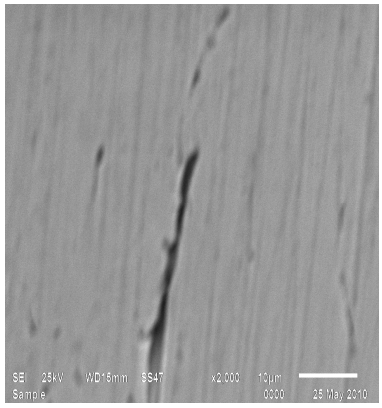

Figure 5.194 SEM measurement on SS side for specimen no. 3

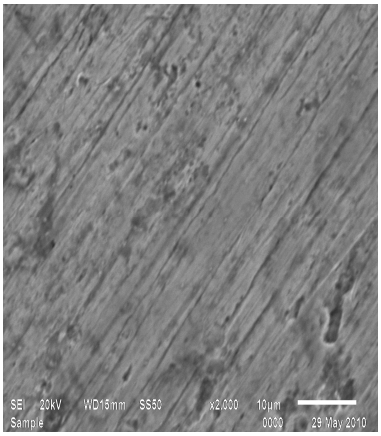

Figure 5.195 SEM measurement on MS side for specimen no. 7

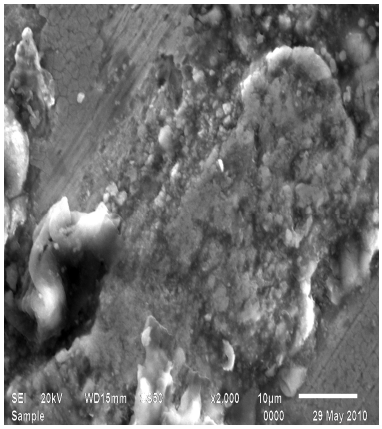

Figure 5.196 SEM measurement on interface for specimen no. 7

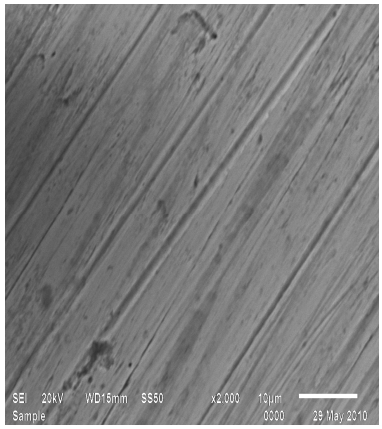

Figure 5.197 SEM measurement on SS side for specimen no. 7

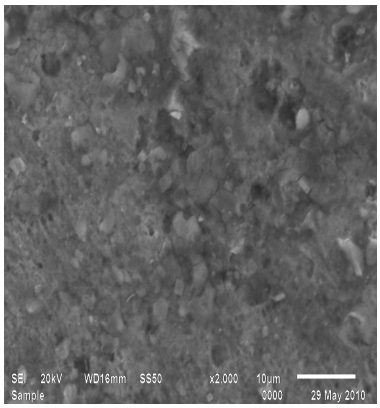

Figure 5.198 SEM measurement on MS side for specimen no. 11

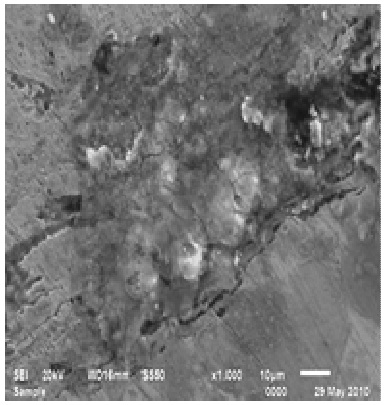

Figure 5.199 SEM measurement on interface for specimen no. 11

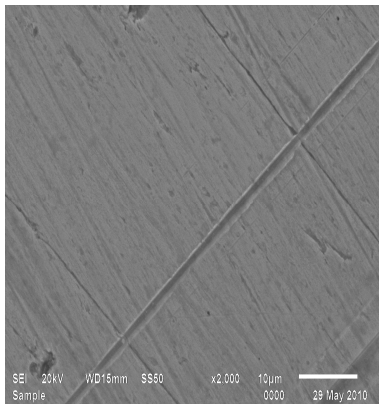

Figure 5.200 SEM measurement on SS side for specimen no. 11

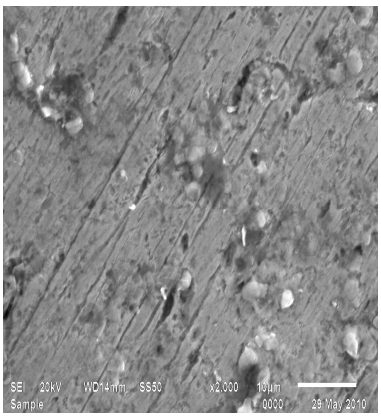

Figure 5.201 SEM measurement on MS side for specimen no. 15

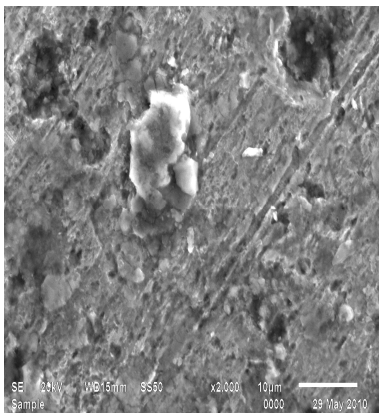

Figure 5.202 SEM measurement on interface for specimen no. 15

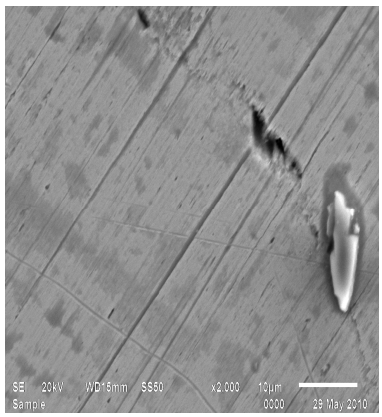

Figure 5.203 SEM measurement on SS side for specimen no. 15

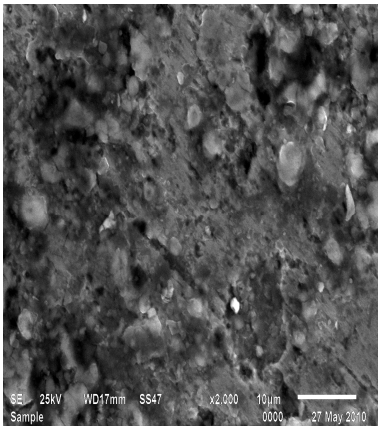

Figure 5.204 SEM measurement on MS side for specimen no. 23

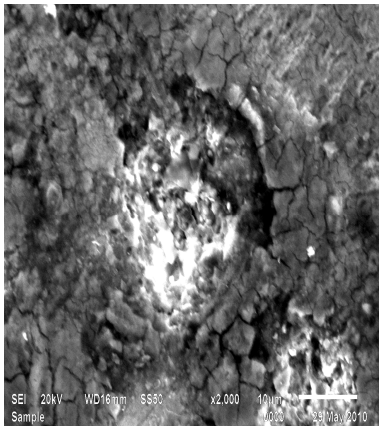

Figure 5.205 SEM measurement on interface for specimen no. 23

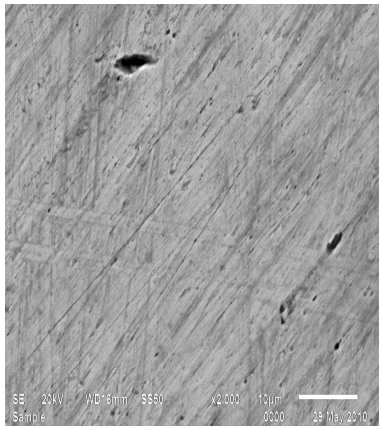

Figure 5.206 SEM measurement on SS side for specimen no. 23

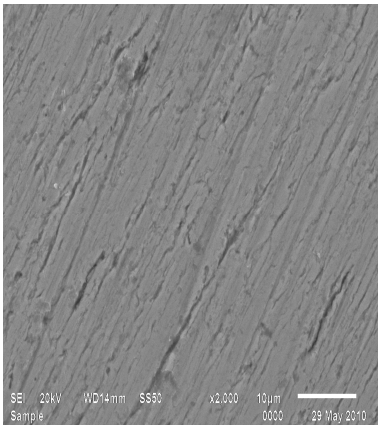

Figure 5.207 SEM measurement on MS side for specimen no. 27

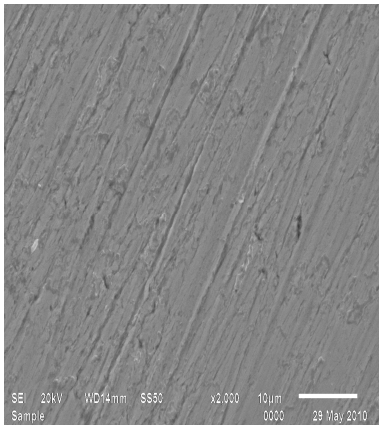

Figure 5.208 SEM measurement on interface for specimen no. 27

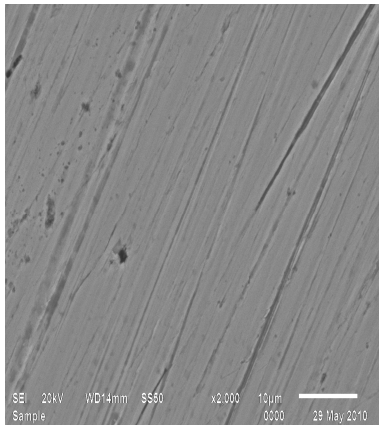

Figure 5.209 SEM measurement on SS side for specimen no. 27

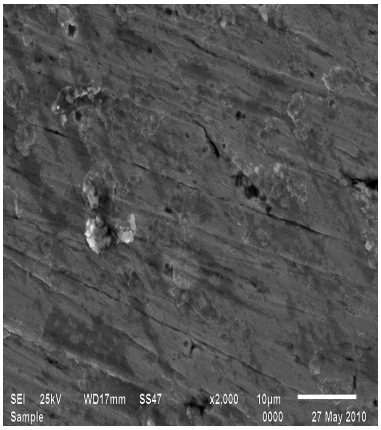

Figure 5.210 SEM measurement on MS side for specimen no. 31

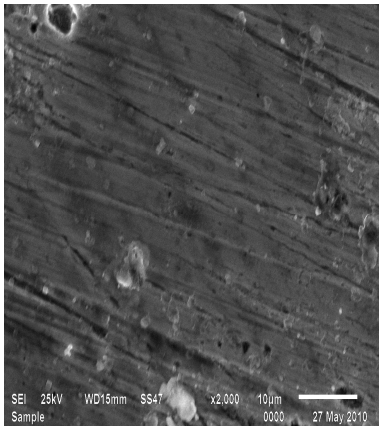

Figure 5.211 SEM measurement on interface for specimen no. 31

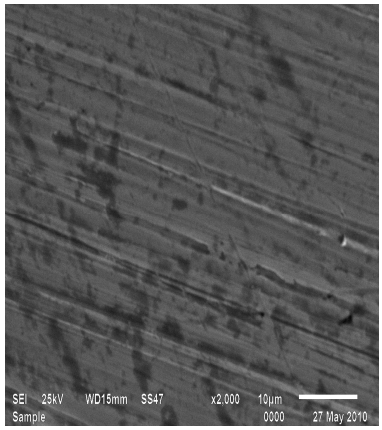

Figure 5.212 SEM measurement on SS side for specimen no. 31

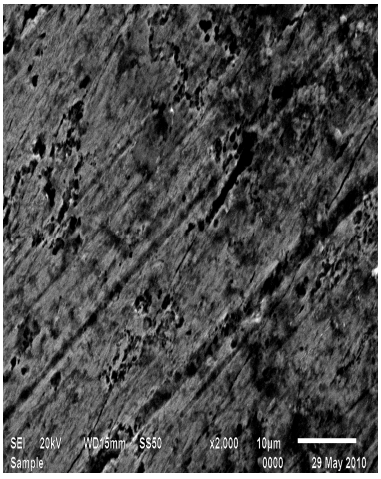

Figure 5.213 SEM measurement on MS side for specimen no. 35

Figure 5.214 SEM measurement on interface for specimen no. 35

Figure 5.215 SEM measurement on SS side for specimen no. 35

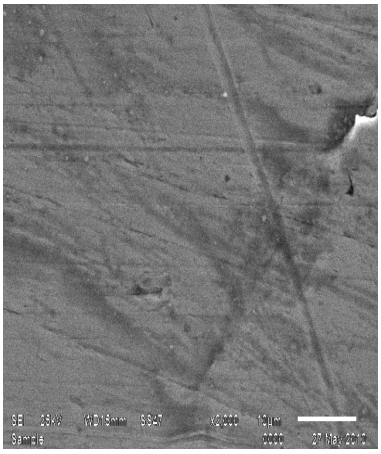

Figure 5.216 SEM measurement on MS side for specimen no. 39

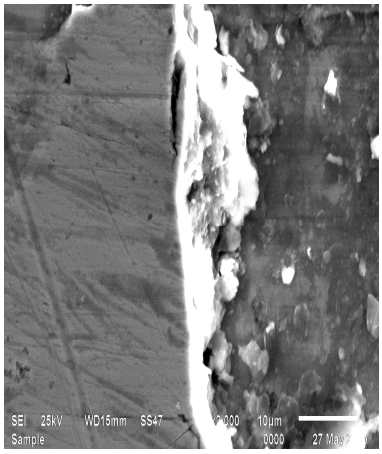

Figure 5.217 SEM measurement on interface for specimen no. 39

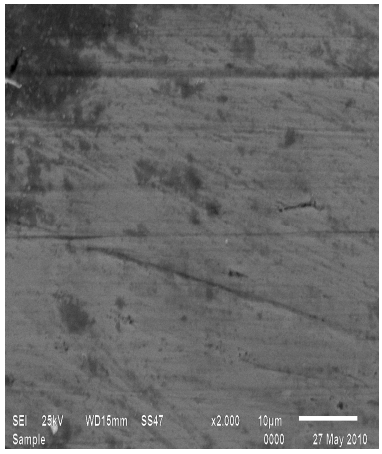

Figure 5.218 SEM measurement on SS side for specimen no. 39

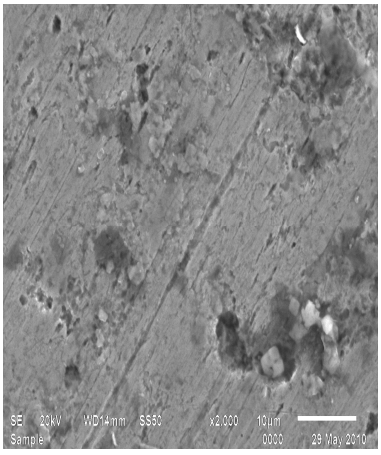

Figure 5.219 SEM measurement on MS side for specimen no. 43

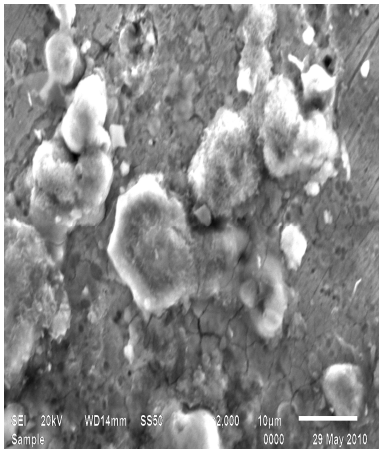

Figure 5.220 SEM measurement on interface for specimen no. 43

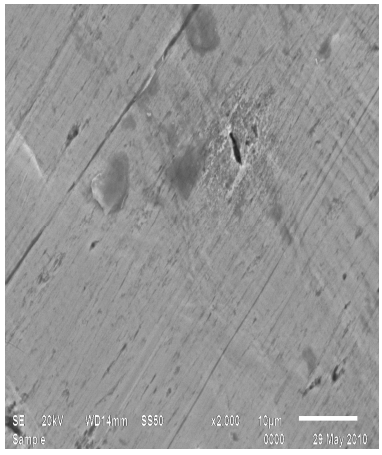

Figure 5.221 SEM measurement on SS side for specimen no. 43

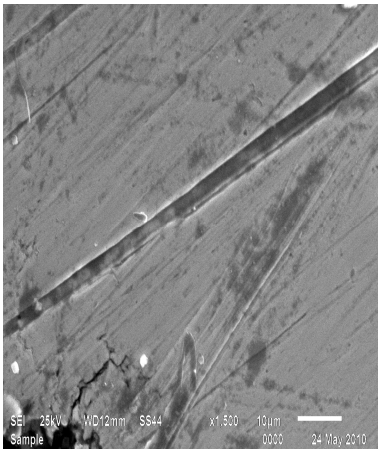

Figure 5.222 SEM measurement on MS side for specimen no. 47

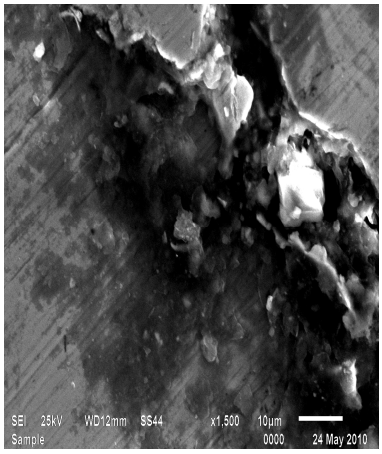

Figure 5.223 SEM measurement on interface for specimen no. 47

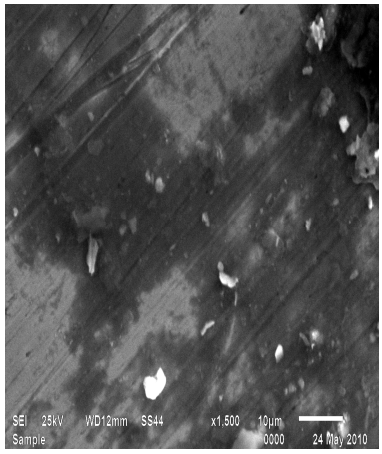

Figure 5.224 SEM measurement on SS side for specimen no. 47

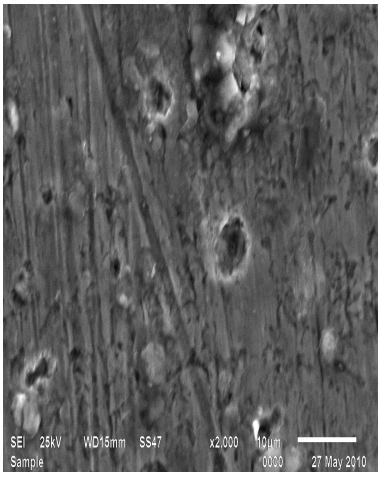

Figure 5.225 SEM measurement on MS side for specimen no. 51

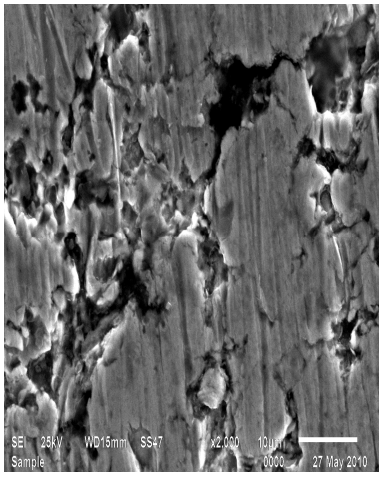

Figure 5.226 SEM measurement on interface for specimen no. 51

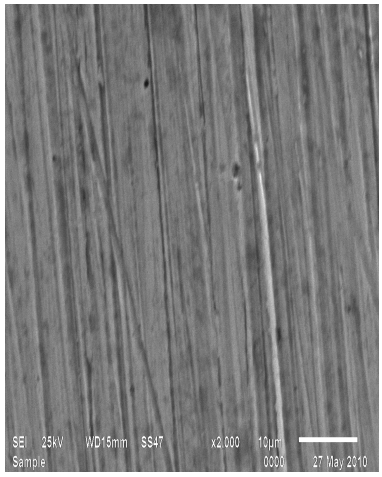

Figure 5.227 SEM measurement on SS side for specimen no. 51

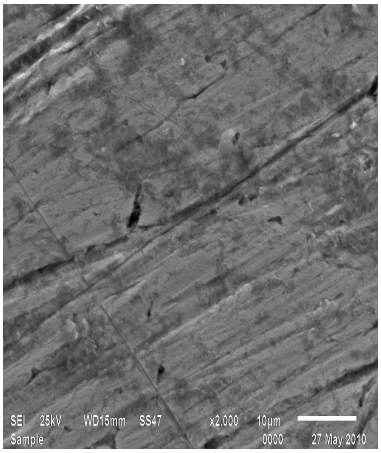

Figure 5.228 SEM measurement on MS side for specimen no. 55

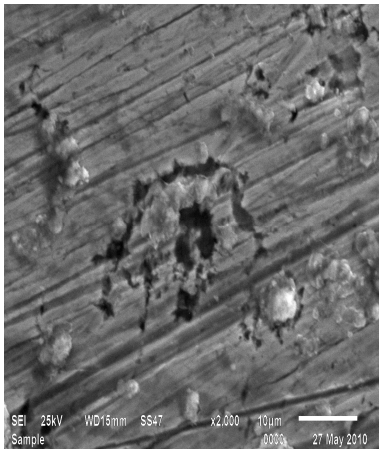

Figure 5.229 SEM measurement on interface for specimen no. 55

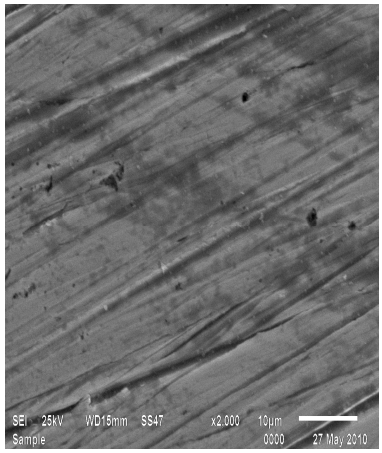

Figure 5.230 SEM measurement on SS side for specimen no. 55

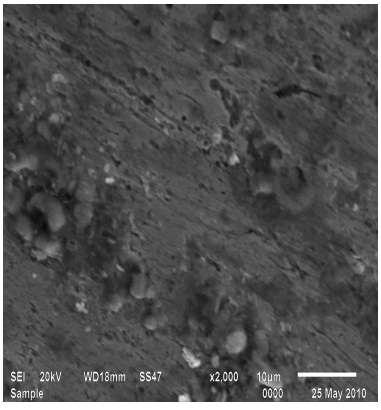

Figure 5.231 SEM measurement on MS side for specimen no. 59

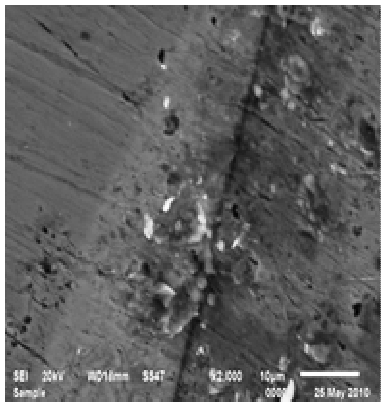

Figure 5.232 SEM measurement on interface for specimen no. 59

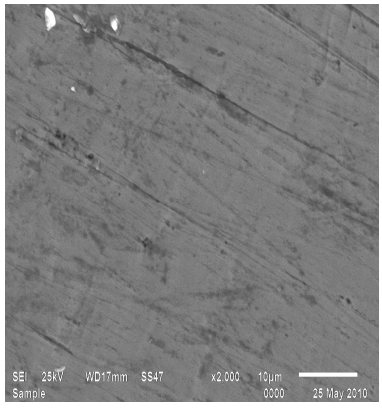

Figure 5.233 SEM measurement on SS side for specimen no. 59

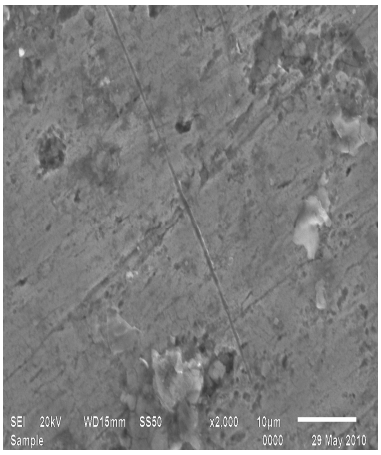

Figure 5.234 SEM measurement on MS side for specimen no. 63

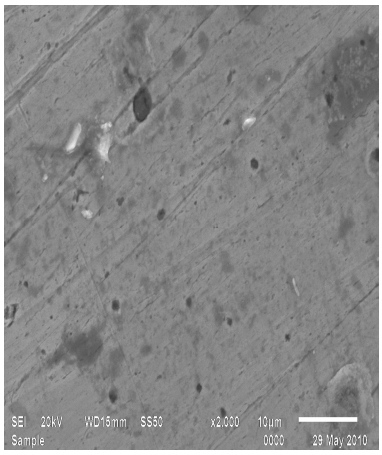

Figure 5.235 SEM measurement on interface for specimen no. 63

Figure 5.236 SEM measurement on SS side for specimen no. 63

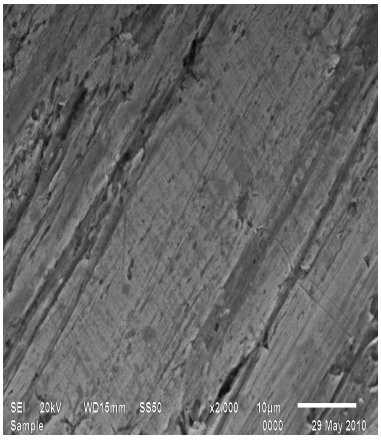

Figure 5.237 SEM measurement for base sample of MS

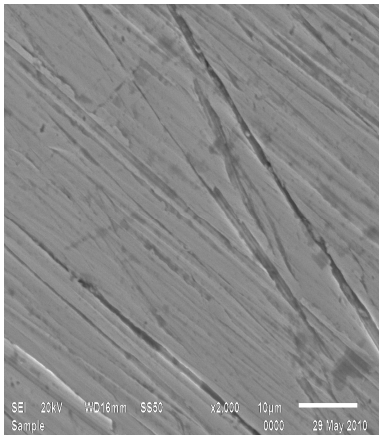

Figure 5.238 SEM measurement for base sample of MS

5.2.3.1 Image Analysis By "Image-J" Analyser Software: The analysis of all the SEM images was done in order to compare the area fraction. The commercially available software Image J was used for analysis of images. Image J is open source software developed by National Institute of Health and considered as powerful for image analysis. Few representative images after analysis by software are shown from Fig.5.239 to Fig.5.242.

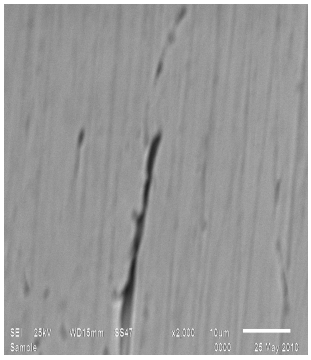

Figure 5.239 Before exposure on SS

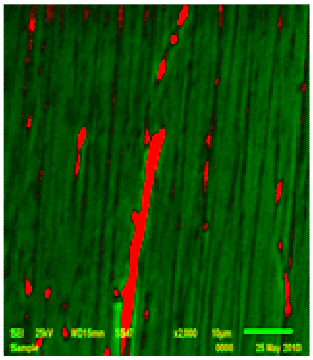

Figure 5.240 After using Image J

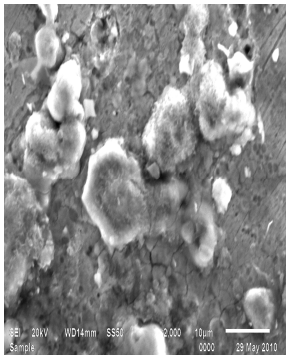

Figure 5.241 Before exposure on interface

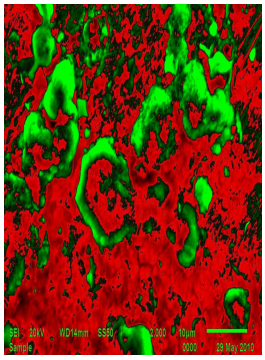

Figure 5.242 After using Image J

Specimen no.	Area fraction of undissolved regions		
	MS HAZ	Interface	SS HAZ
3	39.7	64.1	1.9
7	68.4	50.4	65.2
11	55.6	45.1	83.8
15	34.6	50.9	17.2
19	49.5	19	36
23	40.4	60	33.8
27	80.3	75.1	91.8
31	61	45.2	67.3
35	48.1	33.6	17.3
39	61.7	49.5	81.7
43	73.2	65.5	17.6
47	22.3	45.6	34.1
51	50.9	55.9	60.2
55	63	60.6	63.8
59	58.6	63.5	74.5
63	69	80.8	68.9
Base MS	59.1		
Base SS	81.2		

Table 5.5 Test matrix of area fraction for all specimens

Discussion on SEM results: Area fraction of undissolved regions in the matrix during is given in the above Table 5.5. For specimen no. 63, at the interface area fraction of undissolved regions is maximum and minimum for specimen no. 19. It is observed that by increasing the forge force area fraction of inclusions is also increasing at the interface. It is also observed that area fraction is increased by increasing the RPM and by decreasing the burn off length on mild steel side. By increasing RPM burn off length and friction force, keeping other parameters constant, area fraction is increasing on stainless steel side. Those undissolved regions result in increase in micro hardness values.

5.2.4 XRD

The following are the graphs showing XRD taken on XRD machine (Figure 5.) results at an angle from 0 to 100 degree.

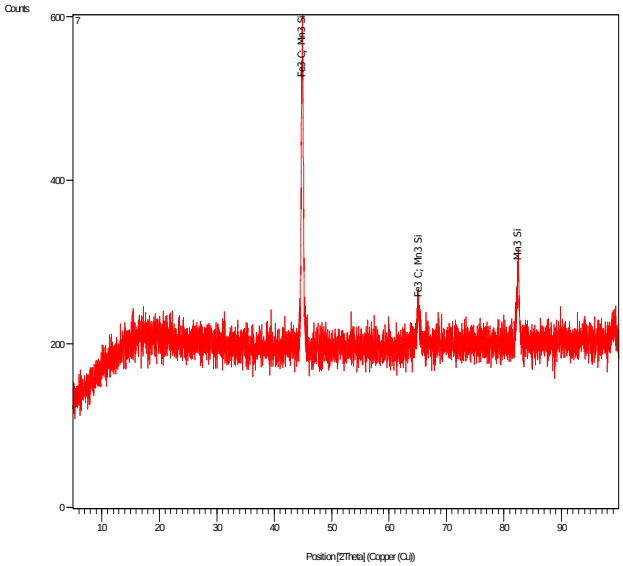

Figure 5.243 XRD examination for specimen no. 7

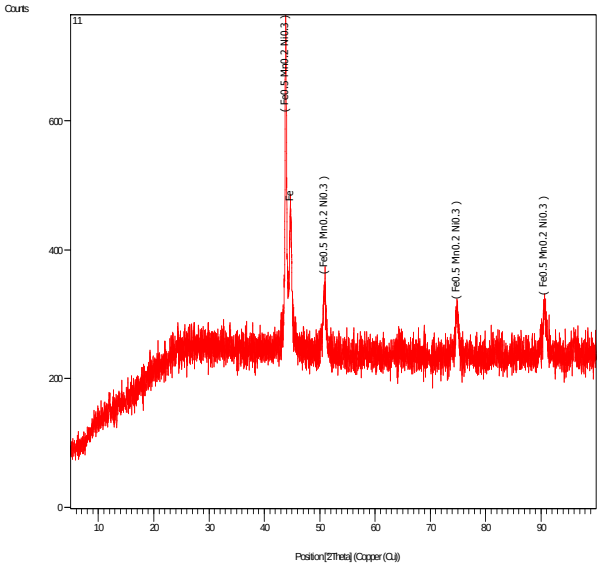

Figure 5.244 XRD examination for specimen no. 11

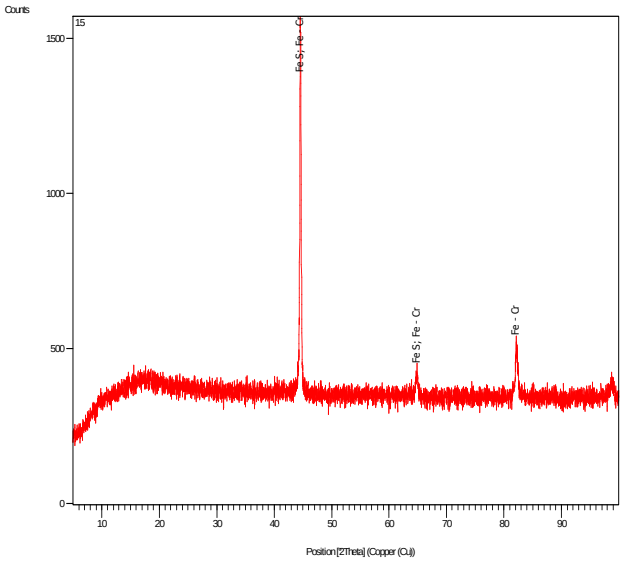

Figure 5.245 XRD examination for specimen no. 15

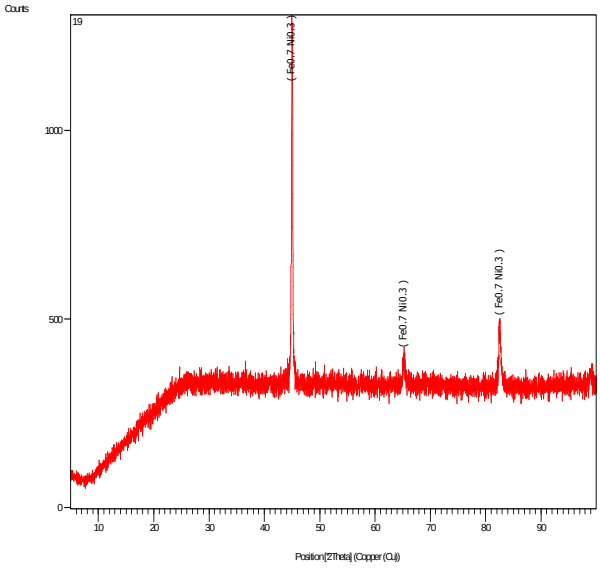

Figure 5.246 XRD examination for specimen no. 19

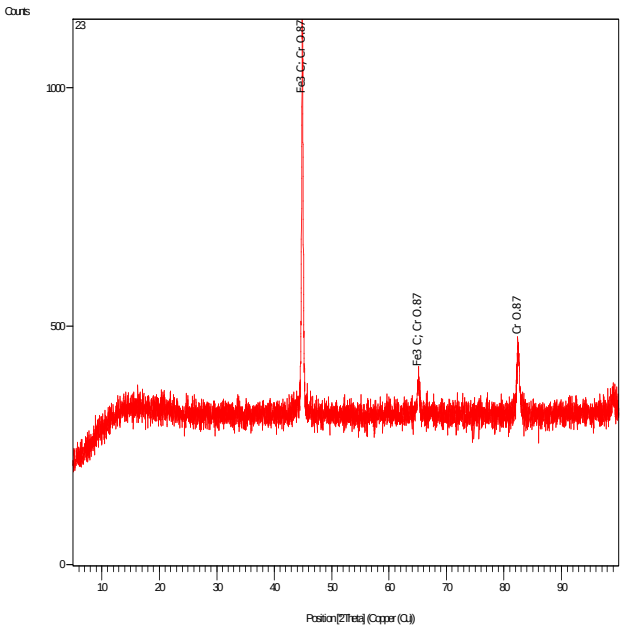

Figure 5.247 XRD examination for specimen no. 23

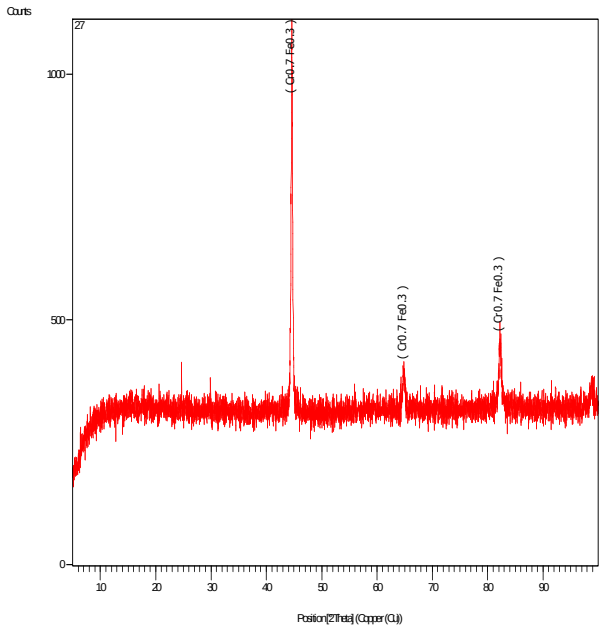

Figure 5.248 XRD examination for specimen no. 27

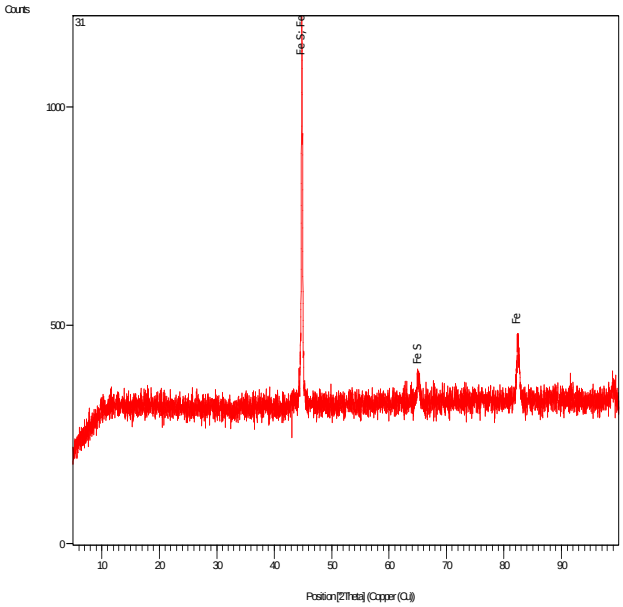

Figure 5.249 XRD examination for specimen no. 31

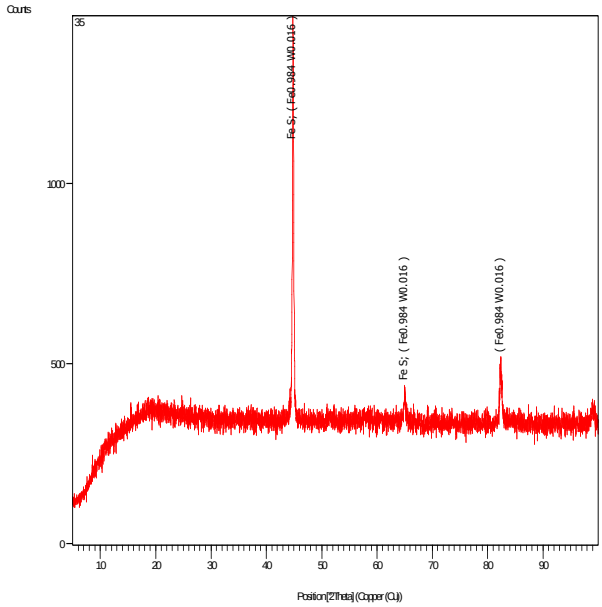

Figure 5.250 XRD examination for specimen no. 35

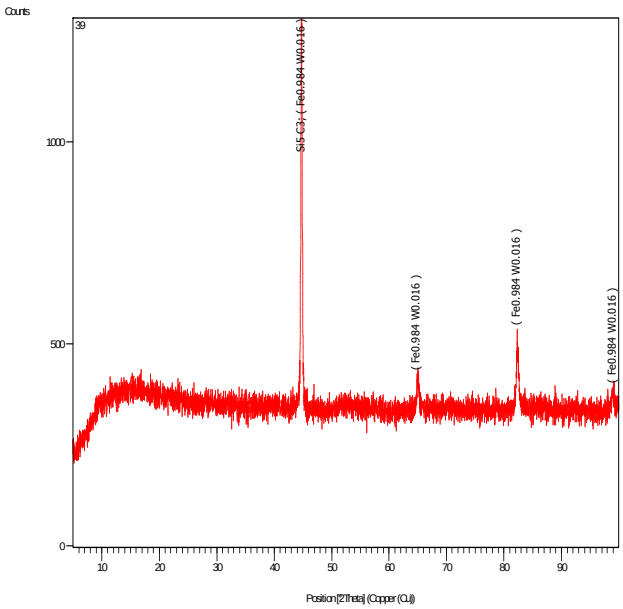

Figure 45.251 XRD examination for specimen no. 39

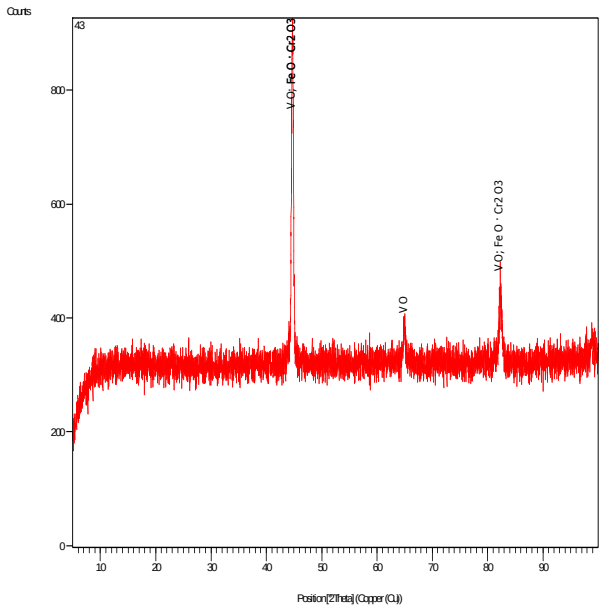

Figure 5.252 XRD examination for specimen no. 43

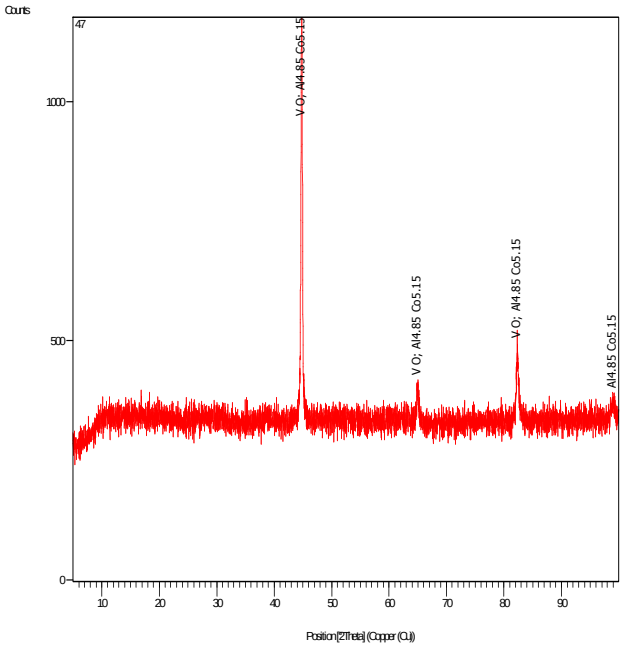

Figure 5.253 XRD examination for specimen no. 47

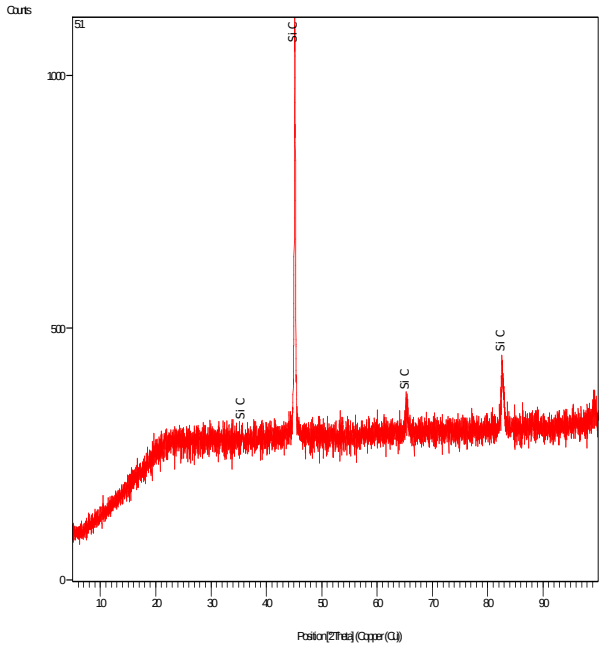

Figure 5.254 XRD examination for specimen no. 51

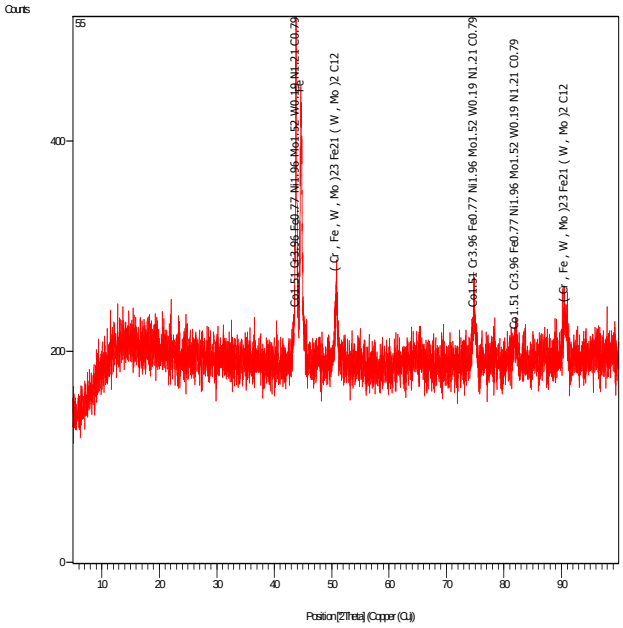

Figure 5.255 XRD examination for specimen no. 55

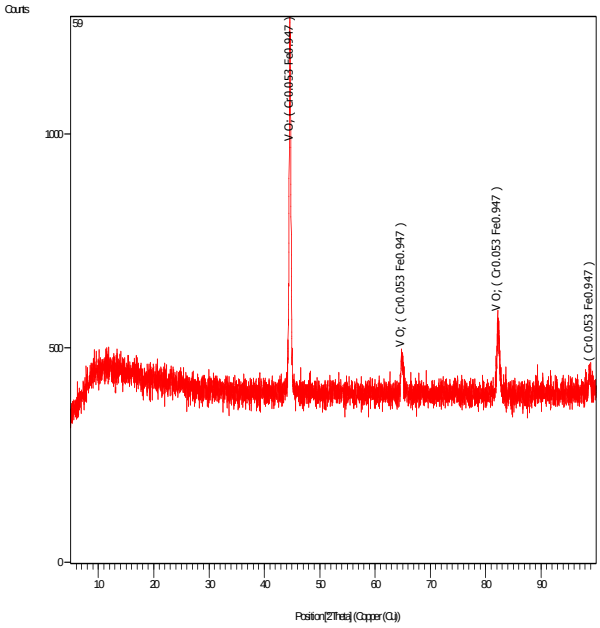

Figure 5.256 XRD examination for specimen no. 59

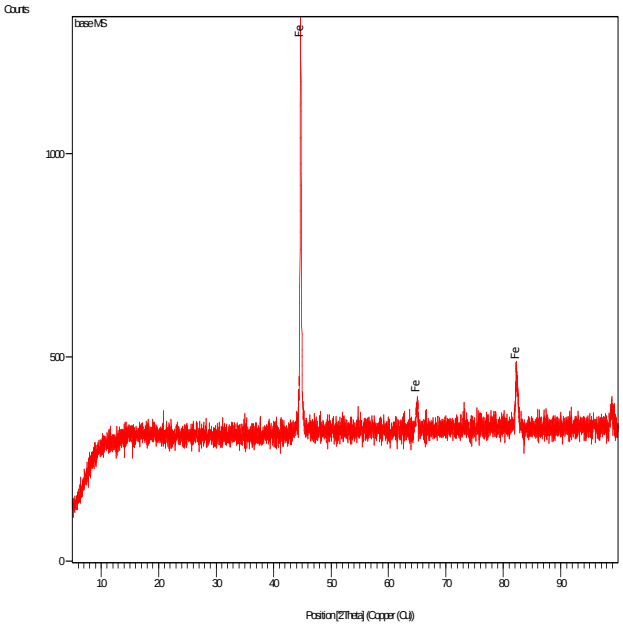

Figure 5.257 XRD examination on base sample of MS

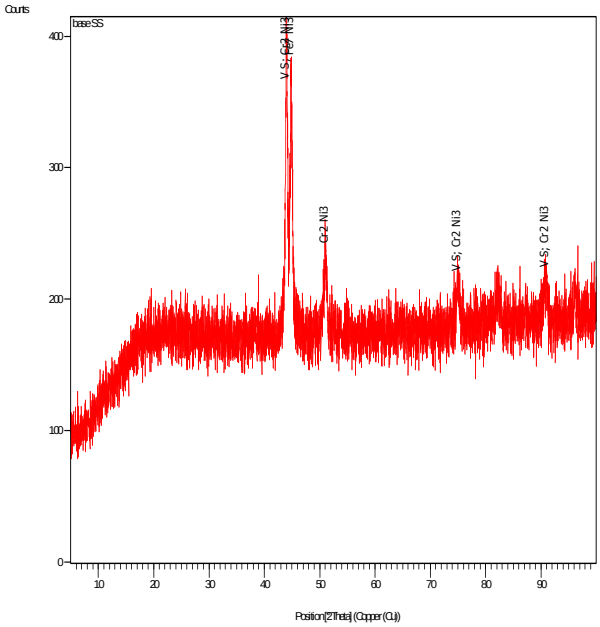

Figure 5.258 XRD examination on base sample of SS

Specimen no.	Compound Name	Chemical Formula	Semiquant [%]
3	Iron Carbide Iron Carbide	Fe_3 C Fe C	
7	Iron Carbide Manganese Silicide	Fe_3 C Mn_3 Si	84 16
11	Iron Manganese Nickel Iron	Fe(0.5) Mn(0.2) Ni(0.3) Fe	42 58
15	Iron Sulfide Iron-Chromium	Fe S Fe-Cr	21 79
19	Iron Nickel	Fe(0.7) Ni(0.3)	100
23	Iron Carbide Chromium Oxide	Fe_3 C Cr O(0.87)	72 28
27	Chromium Iron	Cr(0.7) Fe(0.3)	100
31	Iron Sulfide Iron	Fe S Fe	
35	Iron Sulfide Iron Tungsten	Fe S Fe(0.984) W(0.012)	85 15
39	Silicon Carbide Iron Tungsten	Si_5 C_3 Fe(0.984) W(0.016)	
43	Vanadium Oxide Iron Oxide-Chromium Oxide	VO FeO-Cr_2O_3	
47	Vanadium Oxide Aluminum Cobalt	VO Al(4.85) Co(5.15)	
51	Silicon carbide	Si C	100
55	Cobalt Chromium Iron Nickel Molybdenum Tungsten Nitride Carbide (Chromium Iron Tungsten Molybdenum)	Co(1.51) Cr(3.96) Fe(0.77) Ni(1.96) Mo(1.52) W(0.19) N(1.21) C(0.79) (Cr, Fe, W, Mo)23 Fe21(W, Mo,)2 C12	
59	Vanadium Oxide Chromium Iron	VO Cr(0.053) Fe(0.947)	66 34
63	Vanadium Oxide Iron	VO Fe	
Base MS	Iron	Fe	100
Base SS	Vanadium Sulfide Chromium Nickel Iron Nickel	VS Cr_2 Ni_3 Fe_7 Ni_3	70 13 16

Table 5.6 Percentage and compound formed on friction welded specimen

Discussion on XRD results: XRD analysis was performed in order to investigate the phases formed during friction welding and to confirm the occurrence of crystallization during friction welding. XRD traces are shown in Figures 5.243-5.258. Above Table 5.6 shows the percentage, compounds, phases formed on friction welded specimens. Oxides, sulfides and carbides are formed due to inclusions. Iron is present in most of the specimens. Iron carbide and Iron sulfide is formed for specimen no. 3, 7, 15, 23, 31 and 35. Vanadium oxide and Vanadium sulfide, chromium oxide is also presents in some of the specimens. This change is due to the different friction welding parameters (Friction force, Forge force, Burn off length and RPM).

5.3 RELATION BETWEEN MACROSCOPIC & MICROSCOPIC BEHAVIOUR

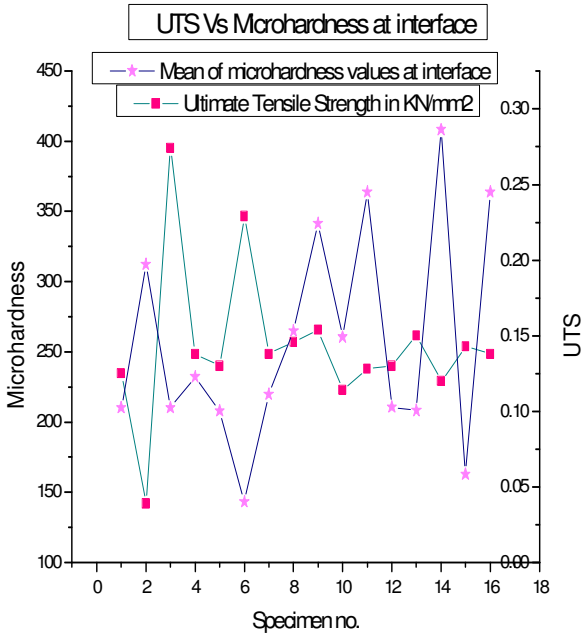

Figure 5.259 UTS Vs Micro hardness at interface

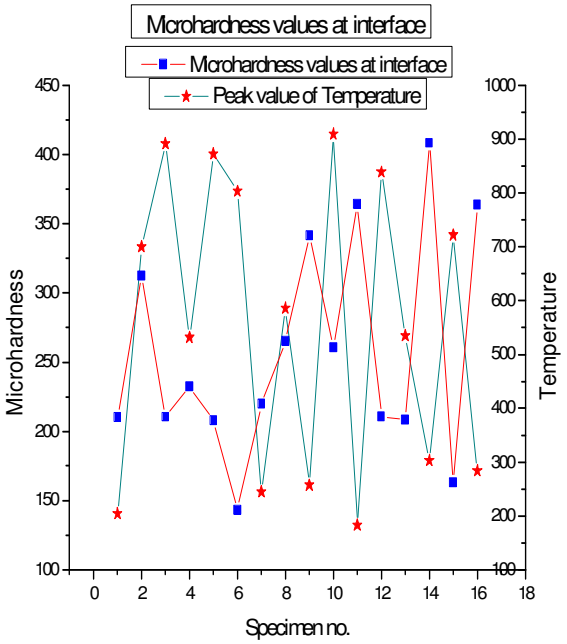

Figure 5.260 value of Micro hardness Vs Peak Temperature

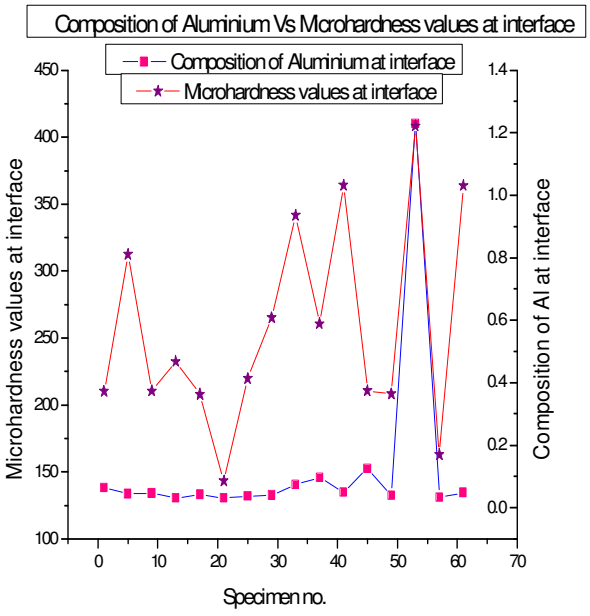

Figure 5.261 Composition of Aluminium Vs Micro hardness values at interface

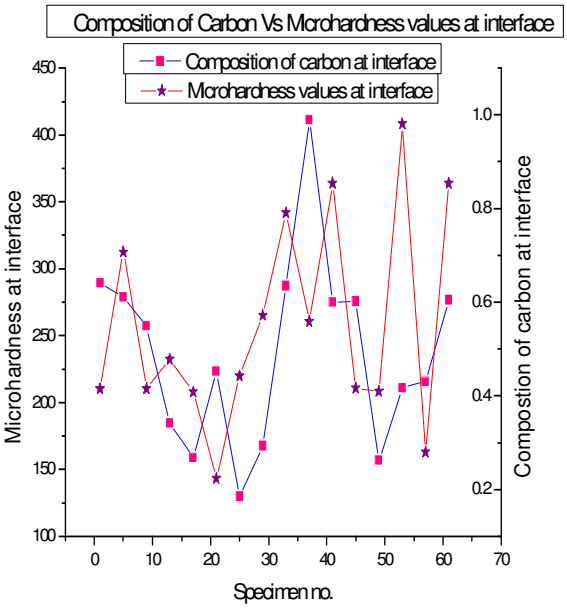

Figure 5.262 Composition of Carbon Vs Micro hardness values at interface

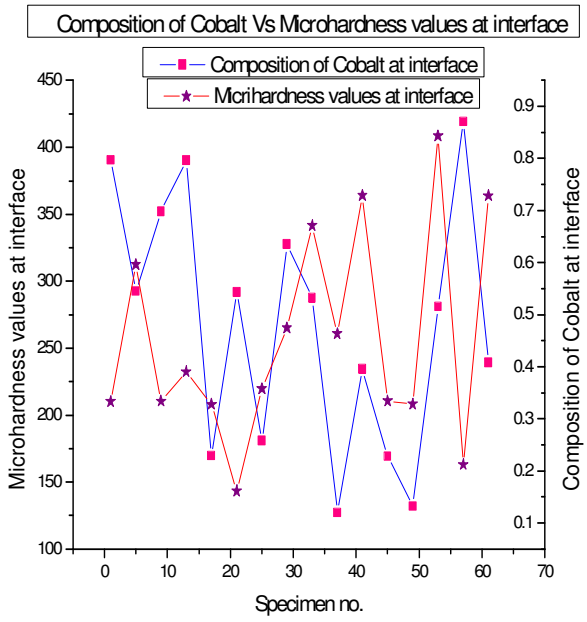

Figure 5.263 Composition of Cobalt Vs Micro hardness values at interface

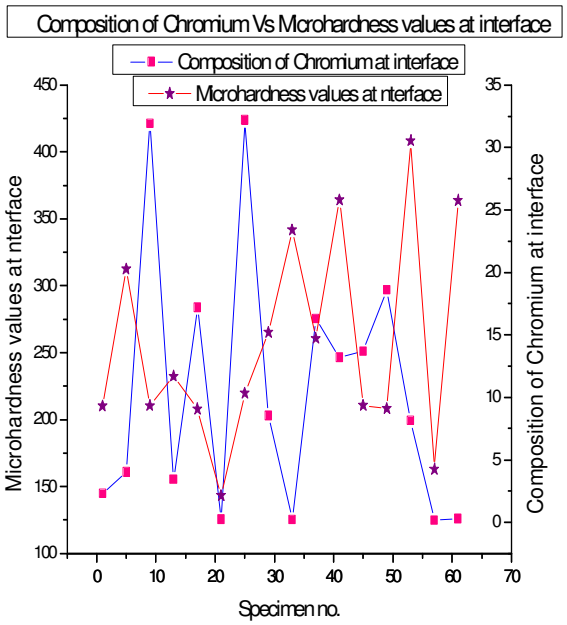

Figure 5.264 Composition of Chromium Vs Micro hardness values at interface

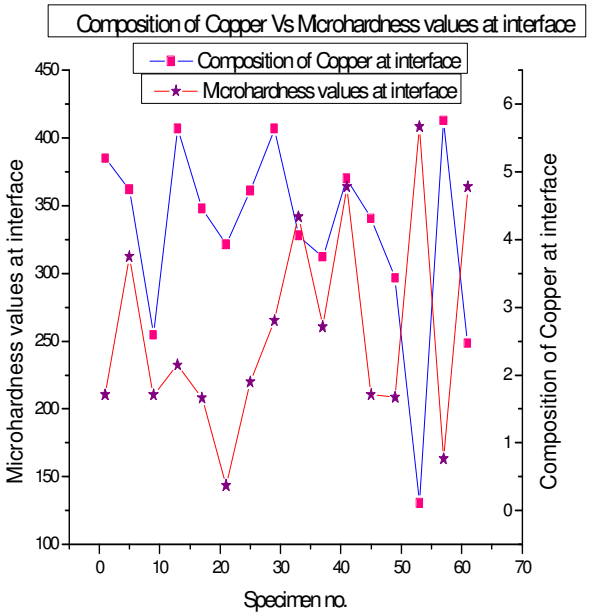

Figure 5.265 Composition of Copper Vs Micro hardness values at interface

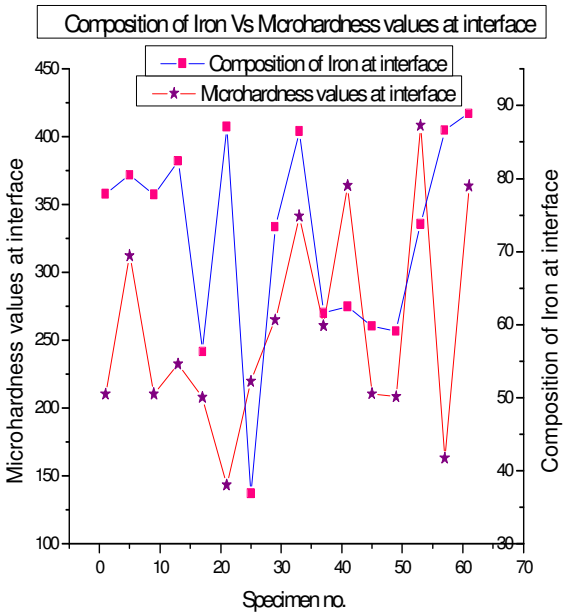

Figure 5.266 Composition of Iron Vs Micro hardness values at interface

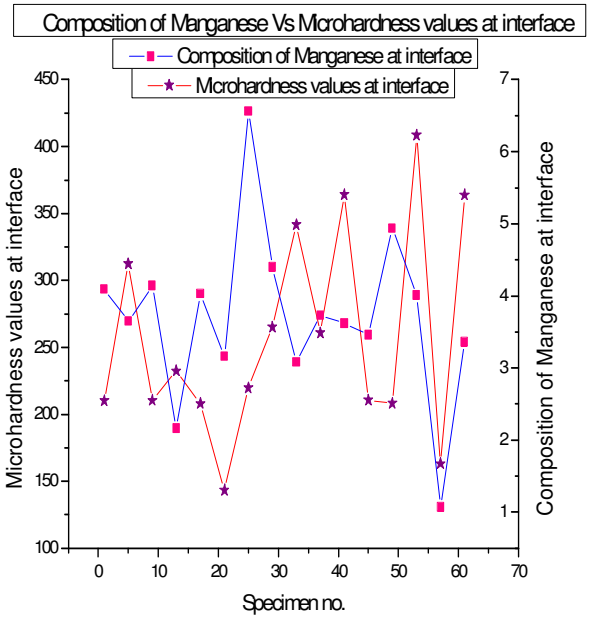

Figure 5.267 Composition of Manganese Vs Micro hardness values at interface

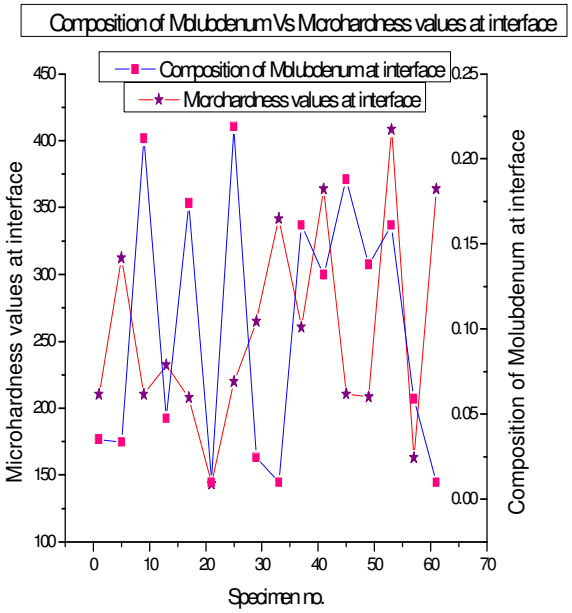

Figure 5.268 Composition of Molybdenum Vs Micro hardness values at interface

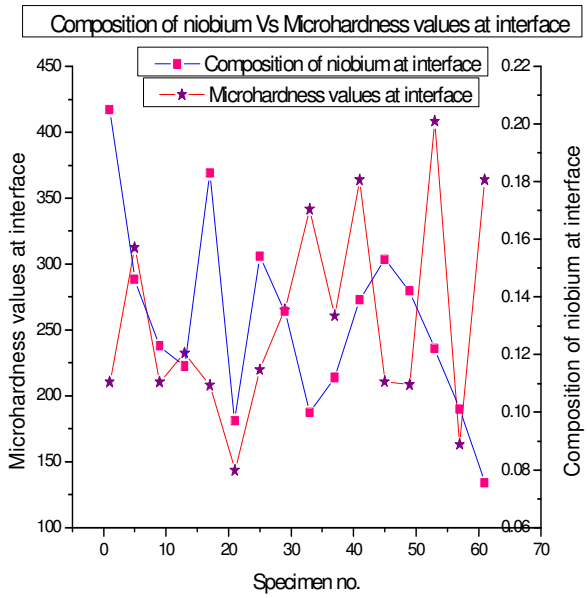

Figure 5.269 Composition of Niobium Vs Micro hardness values at interface

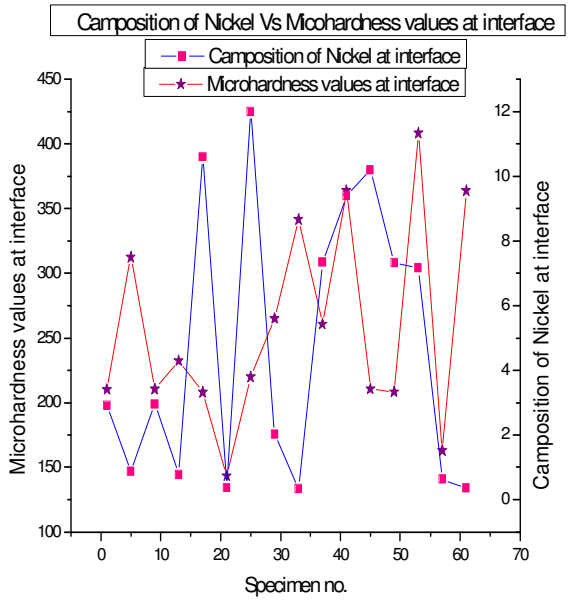

Figure 5.270 Composition of Nickel Vs Micro hardness values at interface

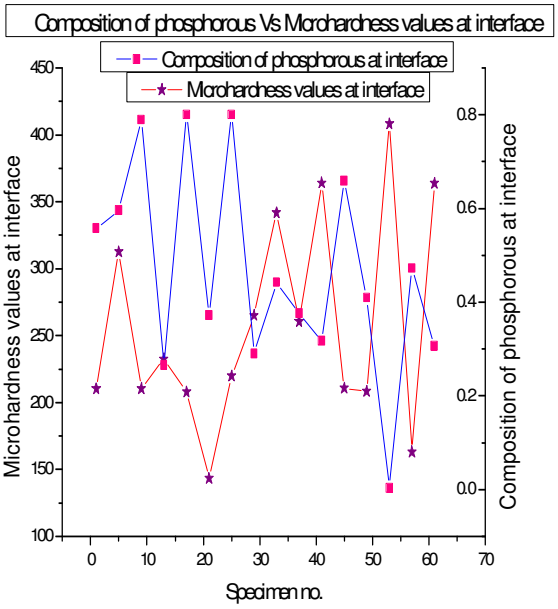

Figure 5.271 Composition of Phosphorous Vs Micro hardness values at interface

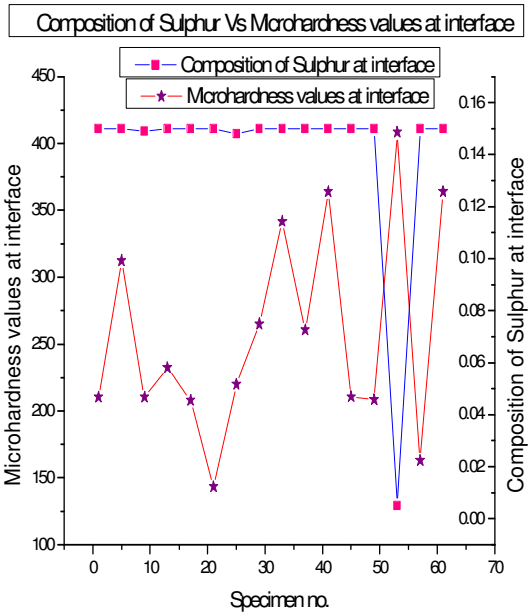

Figure 5.272 Composition of Sulphur Vs Micro hardness values at interface

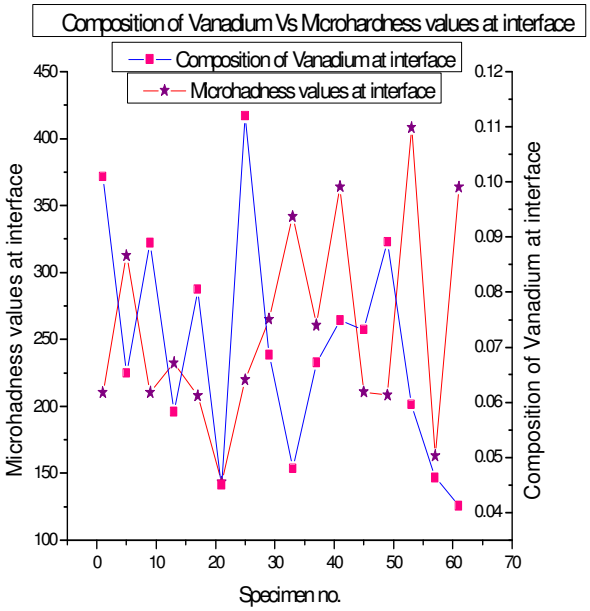

Figure 5.273 Composition of Vanadium Vs Micro hardness values at interface

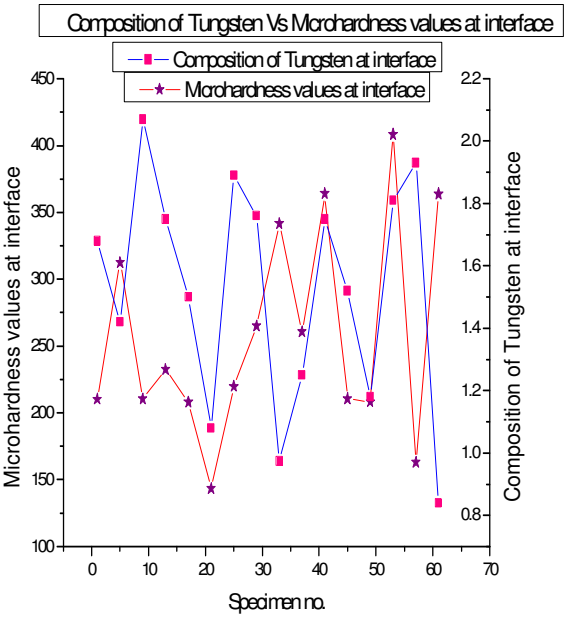

Figure 5.274 Composition of Tungsten Vs Micro hardness values at interface

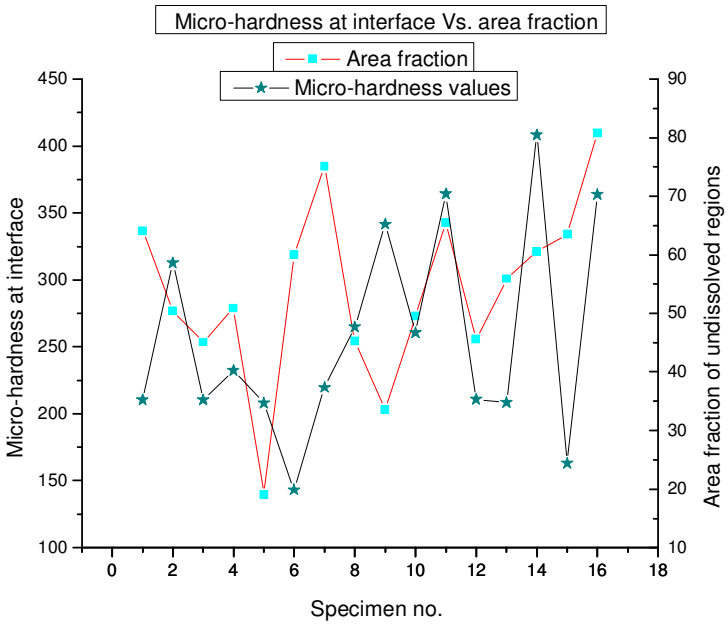

Figure 5.275 Microhardness at interface Vs area fraction of undissolved regions

Discussion on relationship between Macroscopic and Microscopic: Figure 5.259 show relationship between ultimate tensile strength and micro hardness values at interface. In graphs 0 corresponds to specimen no. 1 and 10 corresponds to specimen no. 5 and so on. In some graphs 1 corresponds to specimen no. 1 and 2 corresponds to specimen no. 5 and so on. Graph is showing a strong relationship between Ultimate Tensile Strength and micro hardness. If micro hardness value is increasing, Ultimate Tensile Strength is decreasing, it is reverse relationship. If micro hardness value is increasing with Ultimate Tensile Strength or decreasing with Ultimate Tensile Strength, it is similar relationship. In Figure 5.260 trend is of mixed type, for some specimens it is similar and for some specimens it is of reversed type. In Figure 5.261 there is no relationship between composition of aluminium and micro hardness. Trend in Figure 5.262 is also of mixed type, for some specimens it is similar and for some specimens it is of reversed type. There is a reverse relationship between composition of cobalt and micro hardness values in Figure 5.263. Relationship between composition of chromium and micro hardness values is of mixed type in Figure 5.264. For most of the specimens relationship between composition of copper and micro hardness is similar for most of the specimens and reverse only for few specimens shown in Figure 5.265. In Figure 5.266 the relationship between composition of iron and micro hardness is of similar type. For manganese in Figure 5.267 relationship is of reversed type. For Figure 5.268 and 5.273 relationships is of reversed type. In Figure 5.269, 5.270, 5.274, 5.275 there is a mixed type of relationship between compositions and micro hardness values i.e. for some specimens trend is similar and for others it is of reversed type. There is no relationship between composition of sulphur and micro hardness values.

CHAPTER 6 CLOSURE

6.1 CONCLUSION

1) Friction welding has been successfully employed to weld dissimilar steels. Strength of the joints obtained was good.

2) The Ultimate Tensile Strength values are better when using for lower forge force during friction welding.

3) With increase in friction force, while other parameters are constant, increase in peak temperatures is observed.

4) Microstructure evaluation of the friction welded joints revealed different zones namely, Reheat refined coarse grain region MS HAZ (RC), Dendritic region Interface (D), Reheat refined fine grain region SS HAZ (RF).

5) Highest micro hardness values are formed at the weld interface and SS HAZ regions for welded specimens.

6) At interface and MS HAZ maximum area fraction of undissolved regions is formed through the SEM examination. These undissolved regions results in higher micro hardness values.

7) XRD patterns show the presence of Iron carbide, Iron sulfide, Vanadium oxide and Vanadium sulfide in the friction welded interface regions.

6.2 SCOPE OF FUTURE WORK

In addition to the present work further work can be done in following directions:

1) Different diameters can be used to explore the evaluation of microstructures.

2) Residual stress measurement can be carried out to relate with temperature profiles measured during friction welding.

3) Modeling of friction welding process can be carried out using Finite Element packages.

4) Fatigue and corrosion properties can be measured and correlated with different friction welding parameters.

5) There are lot of parameters (Friction time, Friction force, Forge time, Forge force, Burn off length, RPM, Diameter & Length of the specimens etc.) which can be varied individually to see their individual effects rather than combining these parameters.

6) Modeling of residual stress generation during friction welding can also be carried out.

CHAPTER 7 REFERENCES

1. www.wikipedia.com
2. James R. Huber, President, A.R.D. Industries ltd. - Advanced Friction Welding Techniques For Hydraulic Cylinders [September 7-14, 1988], Presented in 4th Biennial International Machine Tool Technical Conference, U.S.A
3. www.teamafw.com/index.htm
4. www.google.com
5. www.welding-technology-machines.info
6. www.mtiwelding.com
7. www.ardindustries.com
8. www.spinweld.com
9. www.frictionwelding.in

10. **A. A. Essa, A. S. Bahrani,** The friction joining of ceramics to metals, *Journal of Materials Processing Technology,* Volume 26, Pg 133-140, 1991.

11. **Ahmet Hascalik, Nuri Orhan,** Effect of particle size on the friction welding of Al_2O_3 reinforced 6160 Al alloy composite and SAE 1020 steel, *Materials & Design,* Volume 28, pg 313-317, June 2005.

12. **Ahmet Z. Sahin, Bekir S. Yibas, M. Ahmed, J. Nickel,** Analysis of the friction welding process in relation to the welding of copper and steel bars, *Journal of Materials Processing Technology,* Volume 82, Pg 127-136, March 1997.

13. **Antonio A. M. da Silva, Axel Meyer, Jorge F. dos Santos, Carlos Eduardo Fortis Kwietniewski and Telmo R. Strohaecker,** Mechanical & metallurgical properties of friction welded TiC particulate reinforced Ti-6AI-4V, *Composites science & Technology,* Pg 1495-1501, Volume 64, Issues 10-11, August 2004.

14. **A. Vairis, M. Frost,** High frequency linear friction welding of a titanium alloy, *Wear,* Volume 217, Pg 117-131, January 1998.

15. **D. Ananthapadmanaban, V. Seshagiri Rao, Nikhil Abraham and K. Prasad Rao,** A study of mechanical properties of friction welded mild steel to stainless steel joints, *Materials & Design,* Pg 2642-2646, Volume 30, Issue 7, August 2009.

16. **Emel Taban, Jerry E. Gould, John C. lippold,** Dissimilar friction welding of 6061-T6 aluminum and AISI 1018 steel: Properties and micro structural characterization, *Materials & Design,* Volume 31, Pg 2305-2311, December 2009.

17. **F. Rotundo, L. Ceschini, A. Morri, T. S. Jun, A. M. Korsunsky,** Mechanical and micro structural characterization of 2124Al/25 Vol.% SiC_p joints obtained by linear friction welding (LFW), *Composites,* March 2010.

18. **Hakan Ates, Mehmet Turker and Adem Kurt,** Effect of friction pressure on the friction welded MA956 iron-based superalloy, *Materials & Design,* Volume 28, Issue 3, Pg 948-953, September 2007.

19. **Hazman Seli, Ahmad Izani Md. Ismail, Endri Rachman, Zainal Arifin Ahmad,** Mechanical evaluation and thermal modelling of friction welding of mild steel and aluminium, *Journal of Materials Processing Technology,* Volume 210, Pg 1209-1216, March 2010.

20. **H.C. Dey, M. Ashfaq, A.K. Bhaduri and K. Prasad Rao,** Joining of titanium to 304L stainless steel by friction welding, *Journal of Materials Processing Technology,* Volume 209, Issues 18-19, Pg 5862-5870, September 2009.

21. **Hyung-Seop Shin, Jung-Soo Park, Yoon-Chul Jung, Jung-Ho Ahn, Yoshihiko Yokoyama, Akihisa Inoue,** Similar and dissimilar friction welding of Zr-Cu-Al bulk glassy alloys, *Journal of Alloys and Compounds,* Volume 483, Pg 182-185, July 2008.

22. **Hyung-Seop Shin, Young-Jin Jeong, Ho- Yeon Choi, Hidemi, Kato, Akihisa Inoue,** Joining of Zr-based bulk metallic glasses using the friction welding method, *Journal of Alloys and Compounds,* Volume 434-435, Pg 102-105, October 2006.

23. **I. Mitelea, C.M. Craciunescu,** Parameter influence on friction welding of dissimilar surface-carburized/volume-hardened alloyed steels, *Materials and Design,* Volume 31, Pg 2181-2186, October 2009.

24. **J. Luo, Y. H. Ye, J. J. Xu, J. Y. Luo, S. M. Chen, X. C. Wang, K. W. Liu,** A new mixed-integrated approach to control welded flashes forming process of damping-tube-gland in continuous drive friction welding, *Materials and Design,* Volume 30, Pg 353-358, April 2008.

25. **Jolanta Zimmerman, Wladyslaw Wlosinski and Zdzislaw R. Lindemann,** Thermo-mechanical and thermal modelling in the process of ceramic-metal friction welding, *Journal of Materials Processing Technology,* Volume 209, Issue 4, Pg 1644-1653, February 2009.

26. **Koen Faes, Alfred Dhooge, Patrick De Baets, Eric Van Der Donckt and Wim De Waele,** Parameter Optimisation for automatic pipeline girth welding using a new friction welding method, *Materials & Design,* Volume 30, Issue 3, Pg 581-589, March 2009.

27. **L. D'Alvise, E. Massoni and S.J. Walloe,** Finite element modelling of the inertia friction welding process between dissimilar materials, *Journal of Materials Processing Technology,* Volume 125-126, Pg 387-391, September 2002.

28. **Mohamad Zaky Noh, Luay Bakir Hussain, Zainal Arifin Ahmad,** Alumina–mild steel friction welded at lower, *Journal of Materials Processing Technology,* Volume 204, Pg 279-283, November 2007.

29. **M. Maalekian, E. Kozeschnik, H. P. Brantner, H. Ceriak,** Comparative analysis of heat generation in friction welding of steel bars, *Acta Materialia,* Volume 56, Pg 2843-2855, February 2008.

30. **M. N. Ahmad Fauzi, M.B. Uday, H. Zuhailawati and A.B. Ismail,** Microstructure and Mechanical properties of alumina-6061 aluminum alloy joined by friction welding, *Materials & Design,* Volume 31, Issue 2, Pg 670-676, February 2010.

31. **Mumin Sahin,** Joining with friction welding of high speed steel and medium carbon steel, *Journal of Materials Processing Technology,* Volume 168, Issue 2, Pg 202-210, September 2005.

32. **Mumin Sahin,** Evaluation of the joint-interface properties of austenitic-stainless steels (AISI 304) joined by friction welding, *Materials & Design,* Volume 28, Issue 7, Pg 2244-2250, 2007.

33. **Mumin Sahin,** Characterization of properties in plastically deformed austenitic-stainless steels joined by friction welding, *Materials & Design,* Volume 30, Issue 1, Pg 135-144, January 2009.

34. **Mumin Sahin, H. Erol Akata,** Joining with friction welding of plastically deformed steel, *Journal of Materials Processing Technology,* volume 142, Pg 239-246, March 2003.

35. **Mumin Sahin, H. Erol Akata, Kaan Ozel,** An experimental study on joining of severe plastic deformed aluminium materials with friction welding method, *Materials & Design,* Volume 29, Pg 264-274, November 2006.

36. **Mumin Sahin, H. Erol Akata, Turgut Gulmez,** Characterization of mechanical properties in AISI 1040 parts welded by friction welding, *Materials Characterization,* Volume 58, Pg 1033-1038, September 2006.

37. **N. Ozdemir, F. Sarsılmaz and A. Hasçalık,** Effect of rotational speed on the interface properties of friction welded AISI 304L to 4340 steel, *Materials & Design,* Volume 28, Issue 1, Pg 301-307, 2007.

38. **Niyazi Ozdemir and Nuri Orhan,** Microstructure and mechanical properties of friction welded joints of a fine-grained hypereutectoid steel with 4% Al, *Journal of Materials Processing Technology,* Volume 166, Issue 1, Pg 63-70, July 2005.

39. **P.D. Sketchley, P. L. Threadgill, I. G. Wright,** Rotary friction welding of an Fe_3Al based ODS alloy, *Materials Science & Engineering,* Volume A329-331, Pg 756-762, 2002.

40. **P. Sathiya, S. Aravindan and A. Noorul Haq,** Some experimental investigations on friction welded stainless steel joints, *Materials and Design,* Volume 29, Issue 6, Pg 1099-1109, 2008.

41. **R Chhibber, N Arora, S. R. Gupta, B K Dutta,** Use of bimetallic welds in nuclear reactors: associated problems & structural integrity assessment issues, *Journal of Mechanical Engineering Science,* Volume 220, Pg 1121-1133, 2006.

42. **R. E. Craine, A. Francis,** Frictional heat generated in the early stages of an orbital friction welding process, *Wear,* Volume 114, Pg 355-365, June 1986.

43. **S.D. Meshram, T. Mohandas and G. Madhusudhan Reddy,** Friction welding of Dissimilar pure metals, *Journal of Materials Processing Technology,* Volume 184, Issues 1-3, Pg 330-337, April 2007.

44. **V. V. Satyanarayana, G. Madhusudhan Reddy and T. Mohandas,** Dissimilar metal friction welding of austenitic-ferritic stainless steels*, Journal of Materials Processing Technology,* Volume 160, Issue 2, Pg 128-137, March 2005.

45. **Yuanzhi Zhu, Zhe Zhu, Zhidong Xiang, Zhimin Yin, Zhifang Wu, Wenging Yan,** Micro structural evolution in $4Cr_{10}Si_2Mo$ at the $4Cr_{10}Si_2Mo$/Nimonic 80A weld joint by inertia friction welding, *Journal of Alloys and Compounds,* Volume 476, Pg 341-347, August 2008.